Experimental Study on Geocell-Reinforced Flexible Pavements with Recycled Asphalt Pavement (RAP) Bases under Cyclic Loading

By

Bhagaban Acharya
B.E. (Civil Engineering), 2007
Tribhuvan University, Institute of Engineering, Pulchowk Campus, Nepal

Submitted to the Department of Civil, Environmental, and Architectural Engineering and the Graduate Faculty of the University of Kansas in partial fulfillment of the requirements for the degree of Master of Science

_____
Chairperson Dr. Jie Han

Committee members

_____
Dr. Anil Misra

_____
Dr. Robert L. Parsons

Date Defended: December 07, 2011

The Thesis Committee for Bhagaban Acharya certifies that this is the approved version of the following thesis:

Experimental Study on Geocell-Reinforced Flexible Pavements with Recycled Asphalt Pavement (RAP) Bases under Cyclic Loading

_____

Chairperson Dr. Jie Han

Date approved: December 12, 2011

ABSTRACT

The reprocessed old hot mix asphalt (HMA) concrete also called "Recycled Asphalt Pavement (RAP)", if used to build new roads or to maintain existing roads, would have several benefits, such as preservation of natural resources for future generation, protection of environment, and conservation of energy, etc. To use RAP as a granular base in pavement construction as a sustainable solution, it must have enough strength and stiffness to ensure the performance of the pavement. Geocells are three-dimensional honeycombed cellular structures which can provide confinement to compacted infill soil. The literature review of past studies indicated that geocell-reinforced bases provide better lateral and vertical confinement, distribute the load over a wider area, increase the bearing capacity, and reduce the settlement. Use of RAP as a base material with geocell as reinforcement in the HMA pavement can have the combined advantages and can create an attractive solution to pavement reconstruction or rehabilitation.

In this research, the behavior of HMA pavements constructed over unreinforced and geocell-reinforced RAP bases was studied in the geotechnical testing box at the University of Kansas. Pavement sections consisting of subgrade, base, and HMA surface were constructed in the geotechnical testing box and tested under cyclic loading. The subgrade was composed of a mixture of 75% Kansas river sand and 25% Kaolin at 10.4% optimum moisture content, which corresponds to 5% CBR. The RAP base was constructed without or with geocell at 6.6% optimum moisture content to achieve the density requirement. The base thicknesses varied from 15 to 30 cm. The HMA surface above the base was 5 cm thick. Extensive QC/QA tests and instrumentation were included. The test sections were evaluated by vane shear test, light weight deflectometer test, and dynamic cone penetration test for consistency. Earth pressure cells were

placed at the interface between subgrade and base to measure the vertical stresses applied on the subgrade. Tell tales were placed at the interface of subgrade and base and the interface of base and HMA surface to measure their corresponding compression. Strain gauges were placed on geocells and at the bottom of the HMA layer to measure the strains. Large-scale plate load tests with a cyclic load up to 40 kN was applied to the failure criterion of 25 mm permanent deformation.

Six cyclic plate load tests were conducted on unreinforced and geocell-reinforced test sections by varying the thickness of the RAP base. The performance of each test section under cyclic loading was evaluated for a number of passes or number of loading cycles up to the failure of the test section. The test results show better performance of the geocell-reinforced section than the unreinforced section at the same base thickness. The higher stress distribution angle, higher percentage of elastic deformation, lower compression of HMA surface, and lower compression of RAP base were observed in the geocell-reinforced test section as compared with those in the unreinforced test section. The compression of subgrade was high compared to that of RAP base and HMA layers. The geocell-reinforced section with higher stiffness resulted in better compaction of the HMA layer as well. The subgrade and/or RAP base layer with a higher CBR value improved the performance of the pavement section. To obtain consistent test results, it is also important to follow the same procedure to prepare and test the pavement sections.

Dedicated to my parents,

Mr. Hari Prasad Acharya and Mrs. Rudra Kumari Acharya

ACKNOWLEDGEMENT

First of all, my utmost gratitude goes to my thesis supervisor, Professor Jie Han, for giving me the opportunity to join his research team and the support I received from the initial stage to the final level of my Master's Degree study. This thesis would not have been possible without his encouragement, excellent environment, and guidance for doing this research. I would like to thank my graduate advisory committee members, Prof. Anil Misra and Prof. Robert L. Parsons for their valuable advices.

I am grateful to the Mid-American Transportation Center for funding this research project. I am also grateful to PRS Mediterranean, Inc. in Israel for providing the geocell material and R.D. Johnson Excavating, Co., Lawrence, Kansas for providing the RAP material and hot mix asphalt concrete for this research.

The acknowledgement will remain incomplete without thanking my friends, Jitendra Kumar Thakur, Byron Whitted, Brandon W. Basgall, and Guo Jun for their tireless help in my experimental work. I would like to thank Mr. Jim Weaver, Laboratory Manager and Mr. Matthew Maksimowiczat, Laboratory Technician for their technical support throughout the experimental work.

I would like to extend gratitude to my elder brothers (Ramesh Acharya and Narayan Prasad Acharya) and elder sisters (Ganga Acharya Kadel and Laxmi Acharya Bartaula) for their continuous encouragement and support for my study. I am particularly indebted to my parents, Mrs. Rudra Kumari Acharya whose love and inspiration is boundless and Mr. Hari Prasad Acharya who is my role model, is the only reason why I am here today.

TABLE OF CONTENTS

LIST OF TABLES

LIST OF FIGURES

CHAPTER ONE

INTRODUCTION

1.1 Background

The total length of the roads in the United States is over 6.3 million km and is considered one of the largest road systems in the world. According to National Asphalt Pavement Association (NAPA), more than 90 percent of the U.S. roads are paved with hot mix asphalt (HMA) on the surface layer (FHWA-HRT-10-001). Because of many aged roads, rapid growth in traffic volume, and high axle loads etc., the demand for maintaining and rehabilitating existing roads and even constructing new roads is high. This demand leads to the demand for a large amount of construction materials, such as aggregate and asphalt binder from natural resources. The escalating cost as well as scarcity of the materials and their transportation to a desired construction site requires transportation agencies to explore new alternatives of constructing and maintaining roads. The recycling of waste materials can be considered as an alternative for building roads. Old aged Hot Mix Asphalt (HMA) pavement material is the most recyclable product obtained from the roads near or past their design life. The reprocessed old HMA waste is also called "Recycled Asphalt Pavement (RAP)". The use of RAP has several benefits, such as the preservation of natural resources for future generation, the protection of environment, and the conservation of energy. Therefore, the use of RAP is a sustainable approach. RAP has been mostly used in a new HMA mix for pavement surfaces; however, it has been increasingly used as a base course material for construction of new roads or rehabilitation of existing roads.

Geosynthetic materials have been used in road construction to stabilize soft soil all over the world. The concept of strengthening a road using natural materials as reinforcement dates back to 3000 BC (Kerisel, 1985). However, the use of geosynthetic for roadway construction started in 1920s (Becham et al., 1935). Literature review shows that the inclusion of geosynthetics at the subgrade-base interface or even within the base course can improve the service life and performance of paved as well as unpaved roads and reduce the thickness of the base course. The common geosynthetics used for ground improvement in roadway construction are geotextile, geomembrane, geogrid, geocell, geonet, geofoam, and geocomposite, etc. The major functions of geosynthetics include separation, filtration, drainage, reinforcement, protection, barrier etc.

The use of 100% RAP as a base material reinforced by geocell is a new concept developed by Han et al. (2011) and Thakur (2011). The use of RAP is a sustainable approach for constructing new roads and rehabilitating existing roads. The use of geocell improves the mechanical properties of RAP so that it improves the performance of RAP bases and pavements. Due to the three-dimensional configuration of geocell, it can provide better lateral and vertical confinement, distribute the load over a wider area, increase the bearing capacity, and reduce the settlement or rutting. Moreover, a geocell-reinforced pavement system is a composite structure and it has the combined advantages.

1.2 Problem Statement

As a pavement deteriorates, it requires maintenance or even re-construction of the road by removing the old pavement, which results in production of large quantities of old asphalt pavement materials. These pavement materials if not properly treated would causes

environmental problems. On another hand, more virgin aggregate and bituminous materials from natural resources will be used for roadway construction, which is not a wise solution. In the recent years, RAP has been considered as a valuable construction material, which is mostly included in new hot mix asphalt. According to FHWA, the use of RAP to produce new asphalt pavement materials has the following advantages: (1) economic savings, (2) environmental savings, and (3) energy savings (FHWA-HRT-11-021). Recently, RAP has been increasingly used as a base course material for construction of new roads or rehabilitation of existing roads. Due to the strength, stiffness, and creep concerns, RAP is often blended with virgin aggregate. However, blending RAP with aggregate increases material and construction costs and still uses natural materials. The use of 100% RAP with improved performance is a challenge but attractive solution. Han et al. (2011) and Thakur (2011) demonstrated that the use of geocell to confine RAP base courses can increase their strength and stiffness, reduce their creep deformation, and increase the number of loading cycles to failure. However, these studies were conducted on unpaved roads. No research has been conducted so far on the behavior and performance of geocell-reinforced flexible pavements with RAP bases.

1.3 Research Objective

The objective of this research work is to evaluate the behavior and performance of the geocell reinforced RAP bases in the flexible pavement under cyclic loading. The test data obtained from this research would provide the basis for the development of a new design procedure for geocell-reinforced flexible pavements with RAP base courses.

1.4 Research Methodology

The research methodology adopted for this research work includes an extensive literature review on geocell-reinforced RAP bases and large-scale box testing for unreinforced and geocell-reinforced flexible pavements with RAP base courses under cyclic loading. The large-scale cyclic plate load tests were conducted in the large geotechnical testing box in Department of Civil, Environment, and Architecture Engineering at the University of Kansas.

1.5 Organization of Thesis

This thesis is divided into five chapters. Chapter One presents the background, problem statement, research objective, and research methodology. Chapter Two describes the present state of knowledge of geocell and RAP and a detailed literature review on laboratory and field studies of geocell-reinforced RAP unpaved roads. The properties of the materials, equipment, and test procedures used in the large-scale cyclic plate load tests are presented in Chapter Three. Chapter Four presents test results and data analyses. Conclusions and recommendations for future work are given in Chapter Five.

CHAPTER TWO

LITERATURE REVIEW

Recycled Asphalt Pavement (RAP) and geocell have been increasingly used for unpaved and paved road construction in the recent years. This chapter presents a literature review of RAP and geocell materials and their behavior and applications, which are related to this research. This literature review includes the following two components: (1) geosynthetics (especially "geocell") and their applications in the flexible pavement construction; (2) RAP materials and their applications in roadway construction.

2.1 Geosynthetics

A geosynthetic can be defined as "a planer product manufactured from polymeric material used with soil, rock, earth, or other geotechnical engineering related material as a integral part of a man-made project, structure or system" (ASTM D 4439). The main objective of using the geosynthetic is to improve the physical, mechanical, and hydraulic properties of the soils. The geosynthetics that are frequently used in construction industries are geotextile, geogrid, geomembrane, geonet, geocell, geosynthetic clay liner, geofoam, and geocomposites. Geosynthetics have been continuously used in several areas of civil engineering including roadways, airports, railroads, embankments, retaining structures, reservoirs, dams, landfills, etc.

2.1.1 History

The use of geosynthetic as a reinforcing material, when construction is carried out in soft soil, has been increasing all over the world in the past 40 years. The concept of reinforcing soils

is not new. Non-soil materials have been used for thousands of years to improve the performance of soils. The examples in nature include the nests of certain insects and birds as well as beaver dams. Tree roots can be quite effective as slope reinforcement. Large temples ("Ziggurates") up to 57 m high were constructed in Mesopotamia with soils reinforced with woven reed mats 3,000 years ago (Kerisel, 1985). The Great Wall of China (built in 200 B.C.) contains sections that were constructed by mixtures of clay and gravel reinforced with tree branches. The reinforcement of earthen revetments and fortifications has been done in Europe since the Roman times, perhaps even earlier (Jones, 1985). Some ancient levees and roads were constructed directly on brush fascines, logs or timbers, and bamboo fascines in soft soil areas (Holtz, 1978; Broms, 1979).

The method of reinforcing embankment dams with steel rods and plates was mentioned by Professor A. Cassagrande in his lectures at Harvard University (Holtd, 1990). This idea resulted from an understanding of the earth pressure developed within embankments constructed on compressible soils, but it was rejected as being too costly for dams. Wager at the Swedish Geotechnical Institute developed a system consisting of two rows of short sheet piles or steel channel sections under each crests of embankments connected by steel tie rods to increase the stability of the embankments constructed on soft foundations (Wager 1968; Wager and Holtz, 1976). The Wager system has been used more than 30 times in Sweden and Denmark for both highway and railway embankments where no other foundation treatment alternative is feasible., because it is expensive In 1971, Wager initiated the first use of a woven geotextile for

reinforcement of an embankment constructed on soft foundation (Holtz, 1975; Holtz and Massarsch, 1976).

Literature shows that the state of South Carolina used a cotton textile to reinforce the underlying soft soil in a road in 1920s (Becham and Mills, 1935). The evaluation of the road after several years found the textile in a good workable condition. The concept and application of woven filter fabrics in different kinds of erosion control systems, such as revetments, seawalls, jetties, channel linings, breakwater etc, was developed by Barret with the US Army Corps of Engineers (Source: www.geosyntheticsmagazine.com/materials/geocells).

2.1.2 Basic Functions

The basic functions of geosynthetics in civil engineering projects are: separation, filtration, drainage, reinforcement, protection, barrier, etc.

Separation: Separation is the introduction of a flexible geosynthetic between two dissimilar materials so that the functions of both materials are maintained. The geosynthetic works as a separator which prevents the intermixing of dissimilar materials thus maintain the design thickness and roadway integrity of two different layers like sub-base and subgrade in roadways. The separator prevents granular particles in bases from penetrating into subgrade and fines in subgrade from migrating into permeable granular road bases. Geotextile and geomembrane are commonly used as a function of separation in roadways.

Filtration: The function of geosynthetic as a filtration consists of movement of liquid through the geosynthetic and retains the fine particles of soil. Geotextiles are the geosynthetic products commonly used for filtration purposes. Geotextiles are used to prevent the movement of fine particles from soft subgrade to the granular base thus maintain the design thickness and roadway

integrity as the same as the separation function. Geosynthetics have been used for the filtration function roadways, landfills, retaining walls, and slopes, etc.

Drainage: Geosynthetics perform a drainage function by transmitting the liquid within the plane of the structure. The geosynthetics generally used for drainage purposes are geocomposites and textiles. The geotextiles are used to dissipate pore water pressures at the base of road embankments, expopsed soil or rock surfaces, retaining walls, dams, and reservoirs etc.

Reinforcement: Geosynthetics can be used as a reinforcing element within a soil mass to produce a composite that has improved strength and deformation properties over the unreinforced soil. The geogrid, woven geotextile, and geocell are the geosynthetic products commonly used for reinforcement of soil to their provide tensile strength and stiffness and lateral confinement.

Protection: Geosynthetics are sometimes used to protect the other geosynthetic against damage during placement and construction, such as tearing by sharp edged rock, penetration of roots of the trees, damage due to sun, and other localized damage. Geomembrane is sometimes used with a geotextile as protection in roadway and embankment construction in expansive soils, which is called the membrane encapsulated soil layer.

Barrier: The function of geosynthetic as a barrier is the isolation of two different layers. Geomembrane is often used as a impermeable barrier to moisture movement from subgrade and surrounding soil to a granular base layer. This barrier prevents the change in moisture content of subgrade and maintain its strength almost the same throughout the life of the pavement thus increase the life of the pavement.

2.1.3 Geosynthetics in Roadways

The use of geosynhetics to improve the performance of flexible pavements has been increasing significantly in the past three decades. Among various geosynthetics available in the market, nonwoven geotextile is commonly used as a separator between subgrade and aggregate base. Geogrid has been commonly used for subgrade improvement and base reinforcement by interlocking with granular bases.

An earlier research on goegrid-reinforced granular base courses under flexible pavements was carried out at the University of Waterloo in 1984 (Haas et al. 1988). The variables investigated in this research included subgrade strength (CBR values of 1, 3.5, and 8%), aggregate base thickness (150, 200, and 300 mm), asphalt concrete thickness (75 and 100 mm), and reinforcement location (bottom, middle, and top of the aggregate base course). One of the purpose of this study was to determine the Traffic Benefit Ratio (TBR, i.e., the ratio of the number of load cycles of a stiff geogriod-reinforced section to that of the unreinforced section), after incorporating a stiff biaxial geogrid in the granular base. The experimental result found a TBR value of approximately 3 when the stiff biaxial geogrid was placed at the bottom of the base course. For thick aggregate base courses, the geogrid provided better performance when it was located at the mid-height of the base course rather than at the bottom of the base course. The geogrid placed at the top of the aggregate base course provided no improvement.

A full-scale field study conducted at the US Army Corps of Engineers demonstrated that under a large moving wheel load (130 kN), a remarkable improvement in the pavement performance was observed when the pavement was reinforced with the stiff biaxial geogrid (Webster 1992). The test results showed that the flexible pavements with geogrid-reinforced base courses on subgrade at CBR of 1.5 to 5.0% carried approximately 3.5 times more traffic repetitions than equivalent unreinforced sections based on a rut depth criterion of 38 mm.

The experimental study conducted at the University of Alaska (Collin et al., 1988) with flexible pavements constructed on subgrade with a CBR of 3% and the base course thickness between 175 and 300 mm resulted in reasonable agreement with those by Haas et al. (1998) and Webster (1992). They concluded that the geogrid-reinforced flexible pavements increased the pavement life by approximately 2 to 4 times with respect to that of the unreinforced pavements.

2.1.4 Geocell and Its Application in Road Construction

Geocells are three-dimensional honeycombed cellular structures and provide confinement to compacted infill soil. Their confinement reduces the lateral movement of the soil particles and forms a stiffened mattress or slab to distribute applied loads over a wider area. Geocells have been used for slope protection, retaining wall, channel protection, road and railway construction.

In the late 1970s, the U.S. Army Corps of Engineers first developed the concept of a cellular confinement system over a grid confinement system to construct roads in soft terrain and wet weather conditions. Webster and Bach developed a method to weld polyethylene strips to form a cellular structure that became known as "Sandgrid" (Source: www.geosyntheticsmagazine.com/materials/geocells). They produced the first cellular confinement system with high density polyethylene (HDPE) primarily for military road

applications. This cellular confinement system was used first for load support applications like road constructions in the United States in the early 1980s, used second for slope erosion control and channel lining in the United States in 1984 and used third for earth retention in Canada in 1986. The new type of geocell is made of novel polymeric alloy that is characterized by flexibility at low temperatures similar to HDPE and an elastic behavior similar to engineering thermoplastic (Pokharel, 2010; Yang, 2010).

Geocell has been increasingly used to confine base course materials in roadway construction. The main mechanisms of the confinement include active earth pressure within loaded cells, soil resistance in the adjacent cells, and hoop stresses in the cell walls. Under vertical loading, hoop stresses within the cell walls and soil resistance in the adjacent cells are mobilized and increase the strength and stiffness of the soil. The geocell-reinforced base layer acts as a stiff mattress or slab to distribute the vertical traffic load over a wider area of the subgrade. As a result, the vertical stresses applied on the subgrade are reduced and the bearing capacity is increased.

Field trafficking tests and falling weight deflectometer measurements showed that the vertical stresses beneath the geocell layer were reduced by approximately 30%, the deflections on the flexible pavement surface were reduced by approximately 15%, and the back-calculated layer modulus was increased by approximately 10% compared to an unreinforced section (Emersleben and Meyer, 2008, 2010). Al Qadi and Hughes (2000) reported that geocell confinement increased the resilient modulus of the aggregate layer in a flexible pavement by approximately two times.

Pokharel et al. (2009a) conducted an experimental study to evaluate the behavior of geocell-reinforced bases under static and repeated loading. Two base course materials, Kansas River sand and quarry waste were used as the infill materials. The test results showed that geocell confinement increased the bearing capacity and stiffness of the Kansas River sand by improvement factors of 1.75 and 1.5 respectively, under static loading. However, geocell confinement had a minor effect on the stiffness of the quarry waste under static loading due to the existence of apparent cohesion. The single geocell reduced the permanent deformation of the quarry waste base by a factor of approximately 1.5 compared to the unreinforced base. The Kansas River sand had a lower percentage of elastic deformation as compared with the unreinforced and reinforced quarry waste due to the poor gradation, sub-rounded particles, and no apparent cohesion of the sand. The reinforced quarry waste had a higher percentage of elastic deformation than the unreinforced quarry waste due to the contribution of the geocell. Pokharel et al. (2009b) conducted another similar experimental study to evaluate the influence factors for single geocell-reinforced sand. This study found that the geocell placed in a circular shape had a higher bearing capacity and stiffness of the reinforced base than that placed in an elliptical shape. The performance of the geocell with a higher elastic modulus had a higher bearing capacity and stiffness of the reinforced section. The improvement factor for a geocell-reinforced base over its corresponding unreinforced base ranged from 1.5 to 2.5 in terms of bearing capacity and 1.3 to 2.0 in terms of stiffness. The geocell with a higher elastic modulus had a higher improvement factor.

Due to poor subgrade condition in a desert area, it is difficult to construct roads of good quality. Ta-teh et al. (2009) conducted static and dynamic loading tests to determine the bearing capacity and dynamic properties of sandy soil confined with geocells. They concluded that

desert subgrade can be improved in terms of bearing capacity and settlement compared to the unreinforced sandy subgrade.

Keif and Rajagopal (2008) conducted a field study to examine the benefit of the geocell reinforcement of the base layer in a flexible pavement. The field test demonstrated that the vertical stress underneath the geocell-reinforced granular layer due to traffic loading was reduced by more than 50% as compared with the unreinforced case. The finite element analysis of the test sections revealed that the bearing capacity of the subgrade layer was increased by approximately 2.5 times.

Dash et al. (2003) conducted model studies on a circular footing supported on geocell-reinforced sand underlain by a soft clay bed. The test section was subjected to monotonic loading by a rigid circular footing. Footing load, footing settlement, and surface deformations on the fill were measured during the test. The test results show that geocell confinement of the sand layer substantially increased the bearing capacity and reduced in surface heaving of the foundation bed. An additional layer of geogrid placed at the base of the geocell mattress further enhanced the bearing capacity and stiffness of the foundation bed.

Singh et al. (2007) found that the ultimate bearing capacity of a square footing was appreciably increased by geocell confinement under the axial load as well as under the eccentric-inclined load. It was observed that the confinement of soil under the footing resisted the lateral displacement of the infilled material leading to a significant decrease in the settlement and an increase of the ultimate bearing capacity.

Sitharam et al. (2006) conducted a numerical study using FLAC3D to evaluate the influence of geocell confinement on the bearing capacity of a circular footing supported on a

sand bed subjected to vertical loading. The numerical analysis demonstrated that the footing pressure was well distributed within the geocell mattress and was transferred to a wider area of the subsoil when compared to the unreinforced sand bed.

Latha et al. (2006) conducted laboratory model tests to investigate the benefit of geocell reinforcement on the performance of earth embankments constructed over weak foundation soil. They evaluated the influence of several factors, tensile stiffness of geocell material, height and length of geocell layer, pocket size of the cell, pattern of formation of geocells, and type of fill material inside the cells, on the behavior of the embankment. Geocell reinforcement was found to be beneficial in increasing the bearing capacity and reducing the deformation of the embankment.

2.2 Recycled Asphalt Pavement Materials

2.2.1 Sources and Applications

Recycled Asphalt Pavement (RAP) is a removed or reprocessed material from existing aged asphalt pavements or plant hot mix asphalt (HMA) waste containing asphalt and aggregate. Generally asphalt pavements are removed either by milling using a milling machine or full depth removal using a bulldozer or pneumatic pavement breaker. The removed asphalt material is processed using the series of operations, including crushing, screening, conveying, and stacking etc. The RAP is processed either at the central processing plant or in place. According to the National Asphalt Pavement Associationthe NAPA, it is estimated that U. S. production of asphalt pavement materials is around 500 million tons per years, including about 60 million tons of RAP - which transportation agencies reuse or recycle directly into pavements. In addition, agencies reuse or recycle about 40 million ton of RAP into other pavement related applications every year.

Thus, about 100 million ton of RAP is used in 2011, compared to 72 million tons used annually in the early 1990s (FHWA-HRT-11-021). High-quality and well graded aggregates coated with asphalt binder can be obtained when RAP is crushed and screened properly.

The use of RAP in pavement construction has become more popular since the mid-1970s although it was practiced as early as 1915. The earlier sustained efforts to recover and reuse old asphalt paving materials in road construction were made in Nevada and Texas in 1974. RAP has been mostly used in hot or cold mix asphalt with virgin asphalt binder and aggregate. In addition, RAP has been used as granular bases or subbases, recycled asphalt paving i, stabilized base aggregate, and embankment fill. RAP has been used for constructing roadways, roadbeds, shoulders, and embankments (AASHTO Center for Environmental Excellence 2003). According to the FHWA Pavement Recycling Guidelines (FHWA-HRT-11-021), the recycling or reuse of RAP for pavement construction has the following advantages: (a) reduced cost of construction, (b) preservation of aggregate and binder resources, (c) preservation of the environment, and (d) preservation of energy.

According to the National Asphalt Pavement Association (NAPA), more than 90% of U.S. roads are paved with HMA. As the roads become old, the transportation agencies face increasing demand for raw materials required to maintain and rehabilitate these roads. Because of the growing demand, scarcity and rising cost of aggregate and binder, environmental and energy saving considerations, RAP is considered as an alternative to virgin aggregate materials in roadway construction. According to a Federal Highway Administration (FHWA) survey (FHWA-HRT-10-001), as of 2007, the average amount of RAP incorporated into HMA mixtures by state DOTs was 12% by weight. State DOT specifications have set restriction on the

maximum amount of RAP in HMA. If more than 15% RAP is used in a new mix, the required performance grade of the virgin binder should be adjusted.

In 2007, the North Carolina Department of Transportation (NCDOT) conducted a survey on behalf of FHWA and AASHTO to determine the level of RAP use across the country as well as in Ontario, Canada. The survey revealed the potential for the increasing use of RAP across the nation. Figure 2.1 and 2.2 shows the number of state Departments of Transportation that used and permitted a given amount of RAP in intermediate and surface pavement layers in 2007. The data indicated that the maximum permitted amount of RAP was not being used on a nationwide basis. NCDOT conducted the survey again in 2009, and approximately half of the states reported more RAP use after 2007 (Figure 2.3) (FHWA-HRT-11-021).

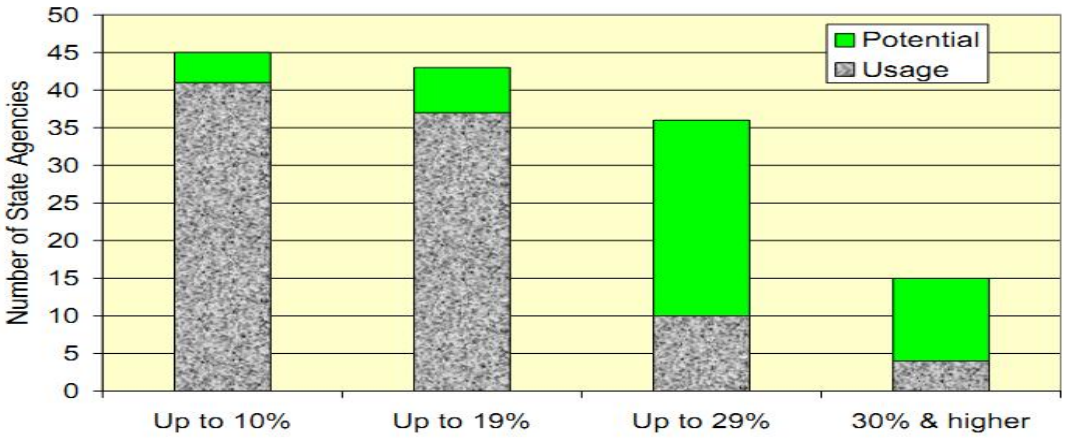

Figure 2.1 Usage and potential of various RAP percentages in the intermediate layer (Source: FHWA-HRT-11-021).

Recent Surveys (AASHTO, 2010) have reported that across the U.S., the average RAP content in new asphalt mixes is around 12% to 15%. A goal established by the NAPA is to increase the average RAP content to 25% by the end of 2013. Table 2.1 gives the summary of

survey conducted by the AASHTO regarding the usage of RAP in asphalt bound base and HMA surface for the construction of pavements by the state DOTs in the U.S.

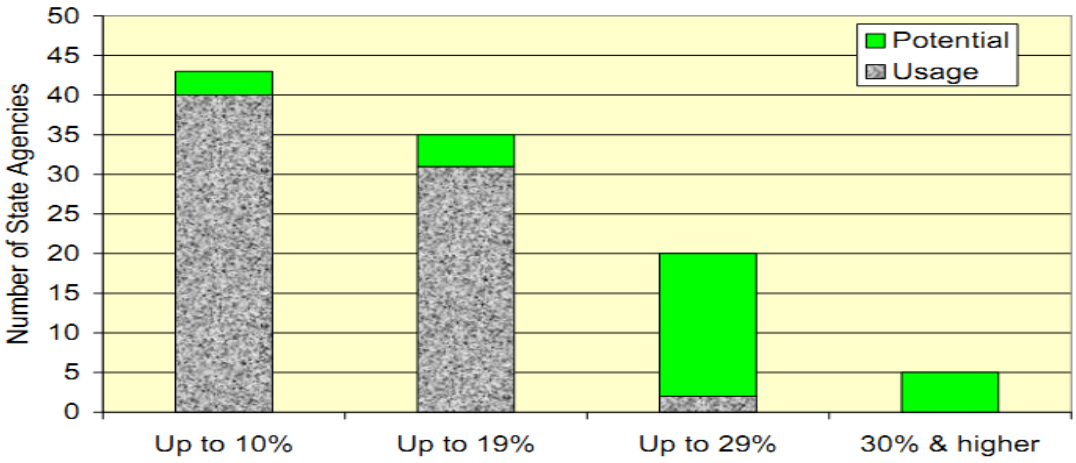

Figure 2.2 Usage and potential of various RAP percentages in the surface layer (Source: FHWA-HRT-11-021).

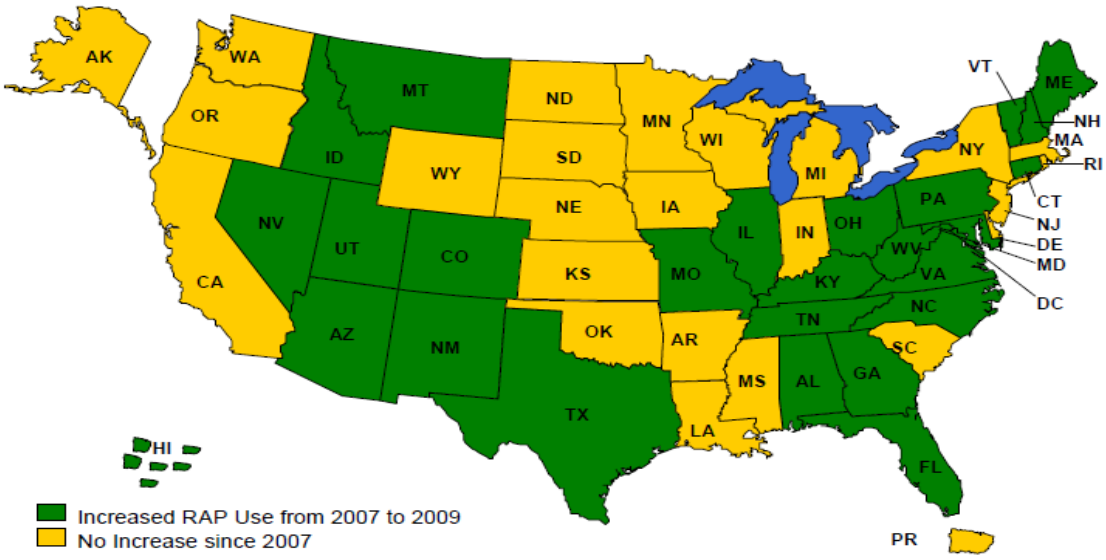

Figure 2.3 States with increased RAP use since 2007 (source: FHWA-HRT-11-021).

Table 2.1 Percentage use of RAP in pavement construction by the U.S. DOTs

State	% Limit of RAP	State	% Limit of RAP	State	% Limit of RAP
Alaska	20 - Base, None in surface	Maine	15-Surface (unknown source), (20-25) - Surface (known source) (30-35) - Base	Tennessee	20 - Surface,35 - Base
Arizona	20 - Surface, 25 - Base			Texas	10 and 20 for un-fractionated and fractionated mixture for surface. 15 and 30 for un-fractionated and fractionated mixture for less than 8 inch from the final riding surface for base. 20 and 40 for un-fractionated and fractionated mixture for more than 8 inch from the final riding surface for base.
California	15 - Surface	Michigan	17 - Surface, (18-27) - Base		
Colorado	20 - Surface, 15 - Base				
		Mississippi	15 - Surface, 30 - Base		
Delaware	35 - Surface				
DC	15 - Surface, 25 - Base	Montana	10 - Surface, (25-50) - Base		
Florida	20 - Surface, 40-45 Base	New Mexico	35 - Surface		
		North Dakota	20 - Surface		
Illinois	30 - Surface	Ohio	(10-25)-Surface, (30-40) - Base		
Iowa	20 - Base				
Kansas	15 - Surface, 30 - 40 Base	Oklahoma	15 - Base, 30 - Base		
				Utah	30 - Surface
Louisiana	15 - Surface, 30 - Base	Oregon	15 - Base, 30 - Base	Wisconsin	25 - Surface, 35 - Base
				Wyoming	30 - Surface

(Source: AASHTO survey regarding the usage of RAP in road construction, October 2010)

2.2.2 General Characteristics of RAP

The characteristics of RAP are largely dependent on the characteristics of the constituent materials and the type of the asphalt concrete (wearing course, base course) used in old pavements. The aggregates used in the asphalt wearing course and base course have different requirements, such as the aggregate quality and size. The aggregate used in the asphalt surface course requires sufficient resistance to abrasion. However, the aggregate in the asphalt base

course is not required for abrasion resistance. This difference leads to the use of higher-quality aggregate in the surface layer rather than in the asphalt base layer. The composition of RAP is influenced by several factors, such as the number of times of pavement resurfacing, the amount of patching and/or crack sealing, possible presence of prior seal coat applications, and percent of asphalt cement used in each maintenance activity.

The quality of aggregate may degrade to some extent after a milling or crushing process. In addition to the original gradation, the gradation of RAP depends on the milling or crushing process, the type of equipment used for removal, the type of aggregate used in pavement construction, and mixing with underlying base or subbase aggregate during the removal. The gradation of a milled RAP is generally finer than its original gradation. A crushed RAP is generally not as fine as the milled RAP, but is finer than the original gradation of the virgin aggregate crushed with the same type of equipment. In other words, crushing does not cause so much degradation as milling during RAP production. Table 2.2 shows the typical range of particle size distribution of RAP.

The physical and mechanical properties of RAP depend on the properties of aggregate, asphalt binder, pavement type, amount of time of the original pavement in service, method of recover in place, and method of processing. Table 2.3 shows the typical range of the physical and mechanical properties of RAP.

Table 2.2 Typical range of particle size distribution for RAP

Screen Size (mesh)	Percent Finer After Processing or Milling
37.5 mm (1.5 in)	100
25 mm (1.0 in)	95 - 100
19 mm (3/4 in)	84 - 100
12.5 mm (1/2 in)	70 - 100
9.5 mm (3/8 in)	58 - 95
7.5 mm (no. 4)	38 - 75
2.36 mm (no. 8)	25 - 60
1.18 mm (no. 16)	17 - 40
0.60 mm (no. 30)	10 -35 a
0.30 mm (no. 50)	5 - 25 b
0.15 mm (no. 100)	3 - 20 c
0.075 mm (no. 200)	2 - 15 d
a. Usually less than 30%	
b. Usually less than 20%	
c. Usually less than 15%	
d. Usually less than 10%	

(Source: U. S. Department of Transportation, FHWA-RD-97-148).

Table 2.3 Typical physical and mechanical properties of RAP

Type of Property	RAP Properties	Typical Range of values
Physical Properties	Unit Weight	1940 - 2300 kg/m^3
	Moisture Content	Normal: up to 5%
		Maximum: 7-8 %
	Asphalt Content	Normal: 4.5-6%
		Maximum Range: 3-7%
	Asphalt Penetration	Normal: 10-80 at 25˚C
	Absolute Viscosity or Recovered Asphalt Cement	Normal: 4,000 - 25,000 poises at 60˚C (140˚F)
Mechanical Properties	Compacted Unit Weight	1600 - 2000 kg/ m^3
	California Bearing Ratio (CBR)	100% RAP: 20-25%
		40% RAP and 60% natural aggregate: 150% or higher

(Source: U. S. Department of Transportation, FHWA-RD-97-148).

2.2.3 Performance of RAP Base Materials

Due to the scarcity of high-quality aggregate as well as the high demand for aggregate for roadway construction, RAP has been increasingly used as subbase and base courses. Berthelot et al. (2010) demonstrated that the use of RAP and PCC rubble materials for road construction is a technically and environmentally sustainable solution.

However, 100% RAP is often too weak and soft as a base course material; therefore, it is blended with virgin aggregate to increase the strength and stiffness. To evaluate the suitability of using RAP blended with crushed angular aggregate or pit run gravel, the State of Montana Department of Transportation conducted a laboratory study including grain size analysis, specific gravity tests, modified Proctor compaction tests, shear strength tests, permeability tests, R-value tests, and x-ray CT scan tests (Mokwa and Peebles, 2005). The specific gravity of RAP blended

samples decreased as the percentage of RAP was increased. Results from the Proctor compaction tests indicated that the maximum dry unit weight and optimum water content decreased with the addition of RAP. The shear strength tests showed that the blending of RAP with to aggregate resulted in a more ductile and softer response than that of the virgin (unblended) soil. The secant modulus of the blend at low strain decreased as the percentage of RAP in the sample was increased. Unblended, crushed aggregate provided a much stiffer response to loading than the unblended pit run because of their particle shape difference. As the RAP content was increased, the stiffness of the blend decreased and approached to that of the blend with 75% RAP content. The large direct shear tests showed that the shear strength of the blend decreased with an increase of RAP up to 20%, and appeared to level off with no significant change as the RAP content was increased to 75%. Constant head permeability tests indicated that the permeability of the blend increased as the percentage of RAP increased. The addition of RAP to the crushed angular aggregate had a minor effect on the R-value while the addition of RAP to the natural pit run soil resulted in an increase of the R-value. Mokwa and Peebles (2005) concluded that the R-value was primarily dependent upon the properties of the virgin aggregate, and was only secondarily influenced by the percent of RAP. In contrast, Bennert and Maher (2005) found that as the percentage of RAP in the blend of base courses increased, both the CBR and permeability values decreased, but the permanent deformation increased.

To evaluate the potential use of recycled asphalt pavement (RAP) and recycled concrete aggregate (RCA) as base and subbase materials, New Jersey Department of Transportation conducted the following performance tests: permeability (falling head and constant head tests), triaxial shear strength, cyclic triaxial loading, California Bearing Ratio (CBR), and resilient modulus tests. The tests showed that an increase of the percent of RAP in the blend reduced

both the CBR and permeability values. The addition of RAP also caused larger permanent deformations during the cyclic triaxial testing.

Mechanistic-Empirical Pavement Design Guide (MEPDG) requires resilient moduli of unbound layers for pavement design. The laboratory tests showed that as the RAP content was increased, the resilient modulus of the blend increased (Alam et al., 2009). RAP has a potential to be used in high percentage in pavement base layer applications which may help alleviate a growing environmental problem while providing a strong pavement foundation.

Kim et al. (2005) carried out resilient modulus tests on specimens with different ratios of RAP to aggregate. The test results show that the specimens at 65% optimum moisture content (OMC) were stiffer than the specimens at 100% OMC at all confining pressures. The 50% aggregate-50% RAP specimens had the stiffness equivalent to 100% aggregate specimens at lower confining pressures. At higher confining pressure, the blended RAP specimens were even stiffer. However, the test results indicated that the specimens with RAP exhibited larger permanent deformation than those with 100% aggregate.

The effect of moisture content on the resilient modulus of RAP base layer was similar to its effect on virgin aggregate base course. The modulus of resistance of the RAP base layer decreased with an increase in the moisture content (Mohamed et al., 2010).

2.3 Summary of the Past Studies

The findings from the past studies on geosynthetics and RAP are summarized as follows:

i. The inclusion of geosynthetics in a pavement reduces required base thickness, increases bearing capacity, and increases the life of the pavement.

ii. Geocell-reinforced granular bases behave as stiffened mattresses or slabs and distribute traffic loads over a wider area of subgrade thus increase the bearing capacity and reduce the deformation.

iii. The properties, height, location of placement of geocell in base courses, the thickness of base courses, and strength of subgrade, etc. affect the overall performance of geocell-reinforced granular bases.

iv. Recycled Asphalt Pavement (RAP) is a reclaimed waste material from existing flexible pavements. It can be used in hot mix asphalt or as a base course material to provide a sustainable solution.

v. RAP is often blended with virgin aggregate to attain sufficient strength and stiffness as a base course material. The variation of RAP content in the blend affects the properties and behavior of the blend.

CHAPTER THREE

MATERIAL PROPEERTIES AND EXPERIMENTAL SET-UP

The chapter presents the characteristics of the materials as well as the experimental set-up of the large-scale cyclic plate load tests used in this study. The cyclic plate load tests were conducted in a large geotechnical test box equipped with a servo hydraulic MTS loading system available at the University of Kansas.

3.1 Subgrade and Characteristics

The subgrade material used in the experiment was made in the laboratory by mixing 25 % Kaolin and 75 % Kansas River (KR) Sand with water. This subgrade material was also used by Pokharel (2010). Kaolin is a soft and white clayey mineral produced by the chemical weathering of aluminum silicate. The most common constituent of Kaolin is the mineral Kaolinite which has low shrinkage and swelling characteristics. The KR sand was poorly-graded and sub-rounded and had specific gravity of 2.62, mean particle size (d_{50}) of 0.54 mm, coefficient of uniformity (C_u) of 3.1, and coefficient of curvature (C_c) of 0.95, respectively (Pokharel, 2010). The gradation curve of the KR sand is given in Figure 3.1. Standard Proctor compaction tests following ASTM D698 – 00a were conducted and determined the maximum dry density of 2.01 g/cm^3 and the optimum moisture content of 10.4 %. Unsoaked CBR tests were performed in the laboratory at different moisture contents. The standard Proctor compaction and CBR curves are shown in Figure 3.2. Unconfined compression strength tests and vane shear tests were carried out on this subgrade material. A correlation between the CBR

value and the undrained shear strength (c_u) was established as follows: c_u = 20.5 × CBR kPa, CBR in % (Pokharel, 2010).

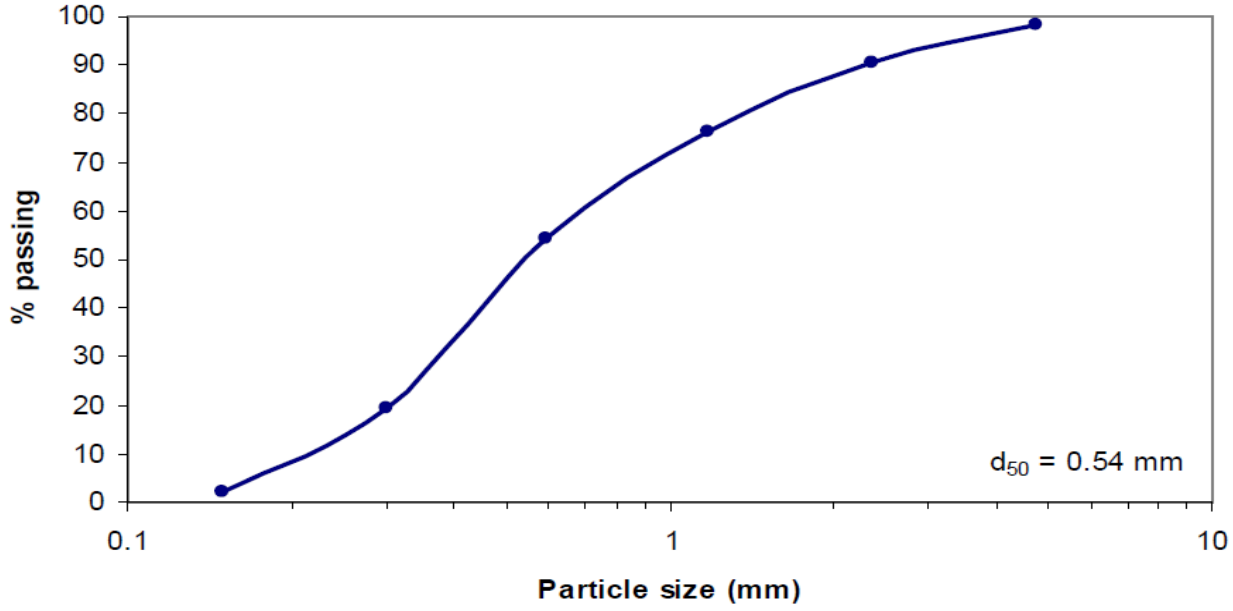

Figure 3.1 Grain size distribution of Kansas River (KS) sand (after Pokharel, 2010)

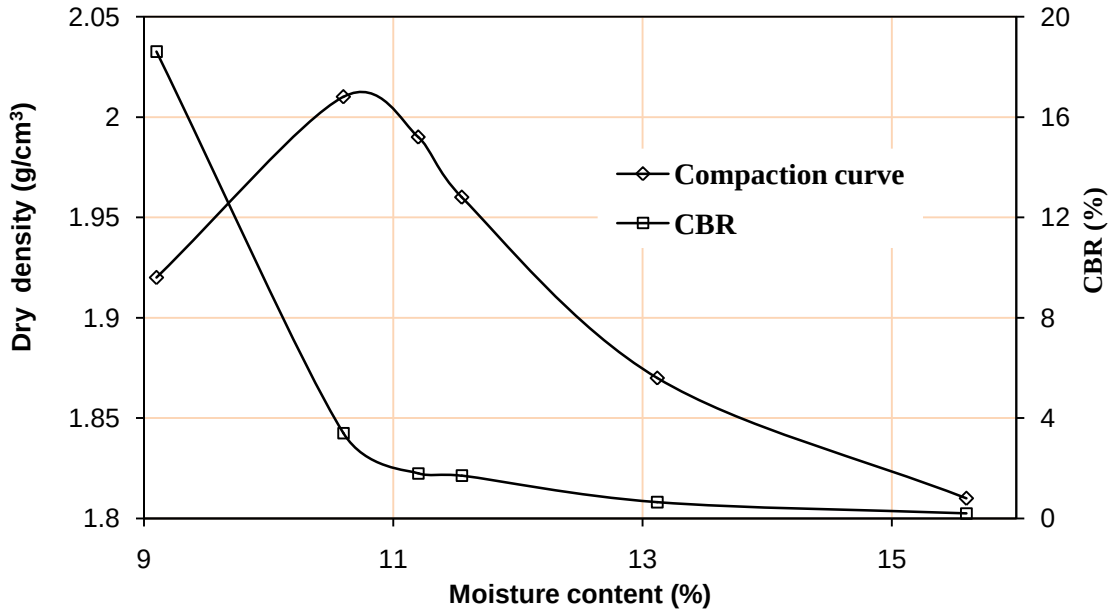

Figure 3.2 Standard Proctor compaction and CBR curves of the subgrade (modified from Pokharel, 2010)

3.2 Base Course Material and Characteristics

The base course material used in this study was RAP, which was provided by R.D. Johnson Excavating, Co. in Lawrence, Kansas. The RAP was milled off from a city street in Lawrence, Kansas. The binder content of the RAP was determined by the ignition method (ASTM D6307) and the centrifuge method (ASTM D2172). The gradation of the RAP aggregate was determined for the sample extracted by the ignition method before and after compaction tests. The gradation curves (Figure 3.3) of the RAP aggregates before and after compaction show that the compaction did not affect the gradation of the RAP aggregate.

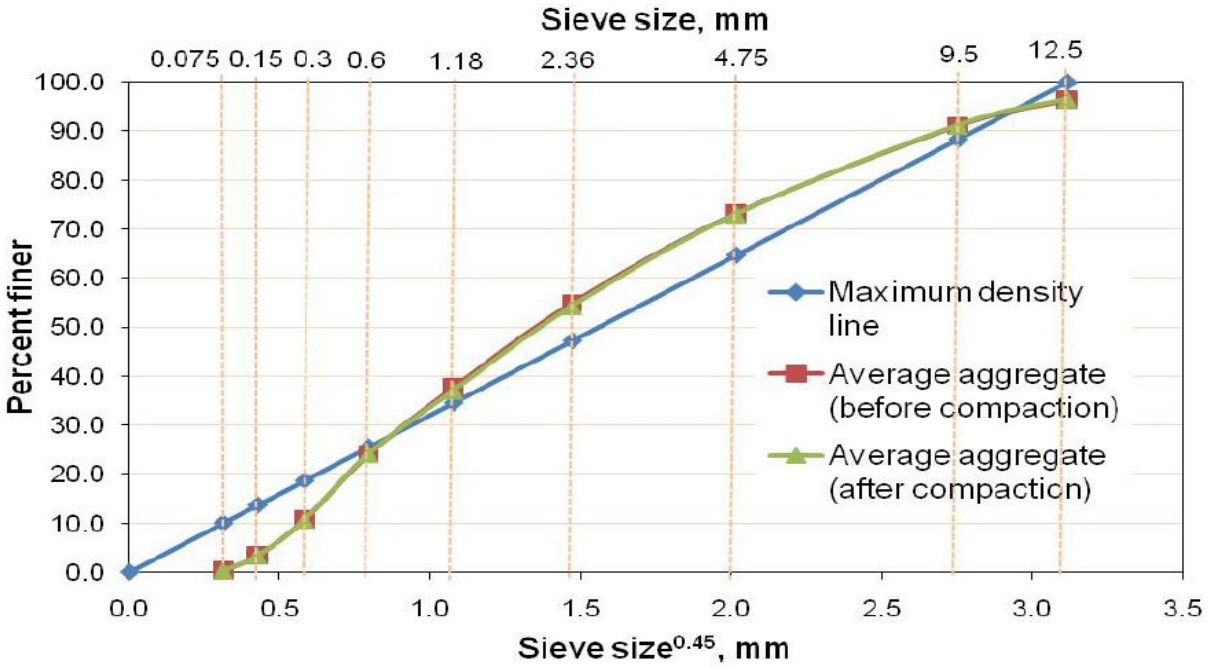

Figure 3.3 Power gradation curve of the aggregate extracted by the ignition method before and after compaction (from Thakur, 2011).

Standard Proctor compaction tests (ASTM D1557-09) of the RAP resulted in the compaction curve as shown in Fig. 3.4 and determined the maximum dry density of 1.95 g/cm^3 and the optimum moisture content of 6.6 %. Unsoaked CBR tests (ASTM D1188-07) were

performed in the laboratory at different moisture contents. The dry density and CBR vs. moisture content curves are shown in Figure 3.4.

The specific gravity and angularity (uncompacted void content) of coarse and fine aggregates angularity were determined from the aggregates extracted by the ignition method. Other material properties, such as viscosity of asphalt binder, maximum and minimum densities of RAP, cohesion and friction angle of RAP, and cohesion and friction angle of geocell-RAP interface, were also determined in the laboratory. Table 3.1 presents the properties of RAP found in the laboratory:

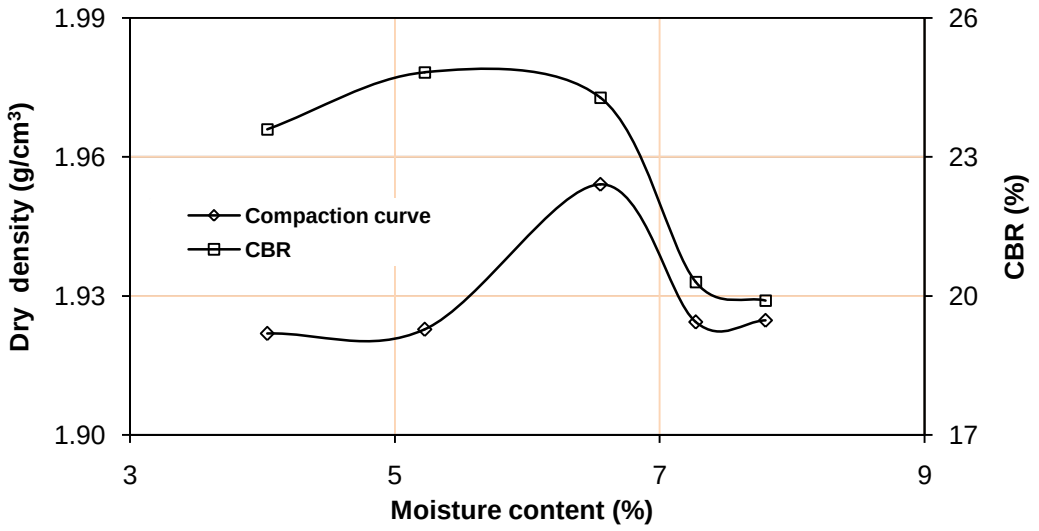

Figure 3.4 Standard Proctor compaction and CBR curves of RAP (modified from Pokharel, 2010)

Table 3.1 Properties of the RAP base material (from Thakur, 2011)

Description	Measured Values	
Binder content		
Ignition method	6.71 %	
Centrifuge method	6.87 %	
Gradation properties of RAP aggregate		
Maximum size	12.5 mm	
Mean size (d_{50})	2 mm	
Coefficient of uniformity (C_u)	8.33	
Coefficient of curvature (C_c)	0.85	
Specific gravity of RAP aggregate	Coarse	Fine
Bulk specific gravity	2.39	2.484
SSD Bulk specific gravity	2.487	2.557
Apparent specific gravity	2.585	2.592
Uncompacted void content of fine aggregate	39.15 %	
Kinematic viscosity of asphalt binder at 135℃	1.408 Pa-s	
Maximum and minimum densities of RAP	1.740 gm/cm^3 and 1.415 gm/cm^3	
Cohesion and friction angle of RAP	30.68 kPa and 12.90˚	
Cohesion and friction angle of geocell-RAP interface	8.95 kPa and 11.06˚	

3.3 Asphalt Concrete and Characteristics

Hot mix asphalt (HMA) concrete used in this research was provided by the R.D. Johnson Excavating, Co. in Lawrence, Kansas. The HMA material was prepared in the plant, hauled by the truck to the University of Kansas, and placed in the test box. The HMA is a Superpave mix – SM9.5 with the asphalt content of approximately 5.5 %. The asphalt binder was PG 64 – 22.

3.4 Geocell

The geocell used in this study was made of NEOLOY^{TM} polymeric alloy (referred as NPA geocell in this thesis). The NPA is a nano-composite alloy of polyester or polyamide nano-fibers, which is dispersed in polyethylene matrix. The geocell had a tensile strength of 19.1 MPa, an elastic modulus at 2% strain of 355 MPa, three perforations of 100 mm^2 area on each

pallet, and wall thickness of 1.1 mm. Geocells with heights of 100 and 150 mm were used as a single or double layer system depending on the base thickness adopted for the experimental propose. The basic properties of the NPA geocell and its creep resistance properties are presented in Table 3.2 and 3.3 respectively (Pokharel, 2010). Figure 3.5 shows the picture of a bundled NPA geocell before placed in the test box.

Figure 3.5 The bundled NPA Geocell used in this research

Table 3.2 Basic properties of NPA geocell (from PRS Mediterranean, Inc., Israel)

Properties		Description	Unit	Test method
Tensile strength		>20	N/mm	PRS method
Allowed strength for design of 50 yrs		>5.7	N/mm	ASTM D6992
Creep reduction factor		<3.5	N/mm	ASTM D6992
Coefficient of thermal expansion (CTE)		≤80	ppm/˚C	ISO 11359-2 ASTM E831
Flexural Storage Modulus at	30˚C	>750	MPa	ISO 6721-1
	45˚C	>650		ASTM E2254
	60˚C	>550		
	80˚C	>300		
Oxidation Induction time (OTI)		≥100	minutes	ISO 11375-6, ASTM D3895 (OTI @ 200˚C, 35 kPa)
Durability to UV Degradation		>400	minutes	ASTM D5885 (HPOIT @ 150˚C, 3500 kPa)

Table 3.3 Creep resistance properties of the NPA geocell (from PRS Mediterranean, Inc., Israel)

Stress to create 10% strain at	NPA
23℃ for (Years)	**(N/mm)**
25	5.82
50	5.65
75	5.56

3.5 Geotextile

A 3.5 oz (99.65 g) non-woven geotextile was used as a separator between subgrade and RAP base in case of all geocell-reinforced sections in the large geotechnical test box. Figure 3.6 shows the picture of the non-woven geotextile roll used in this research.

Figure 3.6 Non-woven geotextile used in this research

3.6 Test Devices and Instrumentation

To ensure the consistency of test sections and evaluate the performance of the pavements, series of test devices and instrumentation were used in this research.

Vane shear tests were carried out in the subgrade to check the approximate CBR value of the subgrade for the quality control proposes during the preparation of the test sections. Dynamic cone penetration tests were carried out from the top of the base course to a depth of 30 cm into the subgrade to obtain the CBR profile of each test section. Light weight deflectometer tests were carried out on the top of subgrade, base course, and HMA surface to check the quality of work of each test section in terms of average surface deformation, degree of compactibility, and dynamic modulus.

Earth pressure cells were installed at the interface between subgrade and base course. Strain gauges were placed on the geocell and at the bottom of the HMA surface. Tell-tales were installed at the interface between subgrade and base and the interface between HMA surface and base. Data acquisition software was configured to record the above mentioned information on full time-history of response for prescribed maximum load cycles and maximum surface deformations.

3.6.1 Earth Pressure Cells

The earth pressure cells used in this research were strain gauge-type soil pressure gauges, which were manufactured by Tokyo Sokki Kenkyujo Co., Ltd. in Japan. They had two capacity ranges: 200 (Model: KDE-200KPA) and 500 kPa (Model: KDE-500KPA). These pressure cells are made of stainless steel and suitable for measuring earth pressure under dynamic loading. Each cell had an external diameter of 50 mm, a diameter of the sensing area of 46 mm, a thickness of 11.3 mm, and a total weight of 160 g. This type of pressure cell can work at a temperature range from -20˚C to 60˚C.

In this research, the earth pressure cells were used to measure the vertical stresses at the interface between subgrade and base course. Five earth pressure cells were installed on the subgrade before the RAP base course was placed. They were installed at five distances from the center of the loading plate at 0, 12.5, 25, 50, and 75 cm. The earth pressure cells with the capacity of 500 kPa were installed at the distances of 0, 12.5, 25, and 50 cm because higher vertical stresses were expected. The earth pressure cell with the capacity of 200 kPa was installed at the farthest distance of 75 cm from the center. Figure 3.7 shows a picture of two earth pressure cells placed on the top of the subgrade.

Figure 3.7 Earth pressure cells on the top of the subgrade

3.6.2 Strain Gauge

Strain gauges were used to measure the strains developed at different locations of the geocell and at the bottom of the HMA surface during dynamic loading. The strain gauges used in this research were C2A-series general purpose strain gauges, which were manufactured by the Micro-Measurements, Vishay Precision Group , USA. The strain gauges had grid resistance of 120 ± 0.6% in ohms, a gauge factor at 24˚C of 2.1 ± 0.5%, and a grid length and width of 6.35 and 3.18 mm, respectively. The strain gauges were rated for a maximum temperature of 82˚C.

Prior to the placement of strain gauges on geocell, the surface of the geocell wall at which the strain gauge was fixed was smoothened by a sand paper and cleaned by isoropyl alcohol. A strain gauge was then attached to the smoothened surface by the N-1 (VH10L) coating material manufactured by Tokyo Sokki Kenkyujo, Co., Ltd., Japan. Six strain gauges were attached on three pockets of the geocell: three on the central pocket just under the loading plate (at top, middle, and bottom of the wall), two at the top and middle of the wall next to the

central pocket, and one at the top of the wall next to the second pocket. Strain gauges at top and bottom were placed horizontally and strain gauges at middle were placed vertical direction. All geocell pockets with strain gauges were oriented in the line same as the width of the test box at the distances of 0, 25, and 50 cm from the center. Figure 3.8 shows a picture of strain gauges affixed on the geocell at different locations.

The same C2A series strain gauges were used to measure the strains developed at the bottom of the HMA surface during cyclic loading. For easy installation, a rectangular shape aluminum plate of 80 long mm × 7 mm wide × 1.0 mm thick was smoothened by a sand paper and cleaned by isopropyl alcohol. A strain gauge was attached to the aluminum plate and M-Coat C was applied to cover the strain gauge. The coating was cured for 24 hours for hardening. After 24 hours, 3145 RTV silicon rubber coating was applied and allowed for curing for another 24 hours before the aluminum plate with the strain gauge was placed at the bottom of the HMA surface. The aluminum plate with the strain gauge is referred as the pavement strain gauge in this thesis. The main purpose of applying M-Coat C and 3145 RTV silicon rubber coating was to protect the strain gauge and its wire from high temperature (approximately 135˚C) in HMA. A typical strain gauge without any protection can survive up to a maximum temperature of about 82˚C. Figure 3.9 shows a picture of prepared pavement strain gauges.

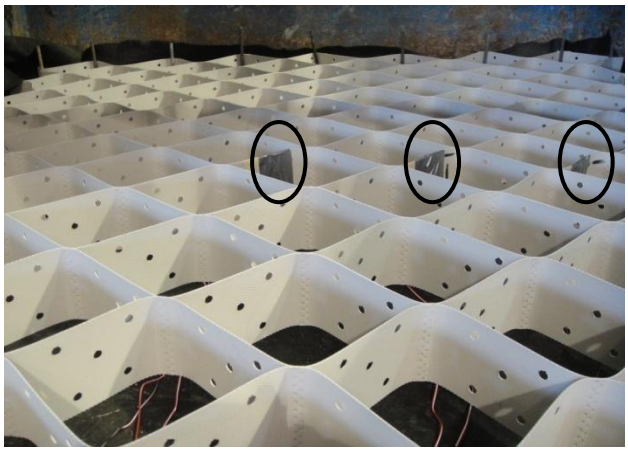

Figure 3.8 Strain gauge affixed on geocell

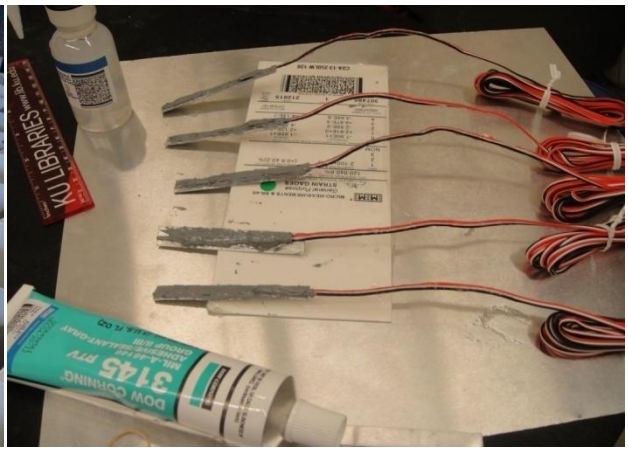

Figure 3.9 Pavement strain gauge

3.6.3 Displacement Transducer and Tell Tales

The displacement transducers used in this research were strain gauge-type sensors manufactured by Tokyo Sokki Kenkyujo, Co., Ltd., Japan. They had two displacement ranges: 0 to 100 mm (Model: CDP-100) and 0 to 50 mm (Model: CDP-50). Two displacement transducers of 100 mm limit were fixed on the loading plate. One displacement transducer of 100 mm limit was fixed at a distance 25 cm away from the center of the plate. Moreover, two displacement transducers of 50 mm limit each were fixed at the distances of 50 and 75 cm away from the center of the loading plate. All of the displacement transducers were suspended from the reference beam fastened on the top of the box. The displacement transducers were rested on the loading plate or the metal plates on the HMA surface.

Moreover, displacement transducers were also used to measure the vertical displacements at the interface of HMA surface and RAP base and the interface of RAP base and subgrade through pre-installed tell-tales. Each tell-tale included a hollow metal tube of 6.3 mm in diameter and 0.40 mm in wall thickness, inside which there was a steel rod of 3.15 mm in

diameter connected to a steel plate of 15 mm in diameter at the bottom and a steel plate on the top for measurement. Two small holes of 8 mm in diameter were drilled on the loading plate and the tell tales were ran through these pre-drilled holes. Figure 3.10 shows a picture of displacement transducers as well as tell tales.

Figure 3.10 Displacement transducers and tell tales through the loading plate

3.6.4 Data Acquisition

Smart Dynamic Strain Recorder DC-204R manufactured by Tokyo Sokki Kenkyujo, Co., Ltd., Japan was used to record the data from earth pressure cells, strain gauges, and displacement transducers. There were four recorders used during the tests. One data recorder served as a master recorder and the remaining three served as slaves, which were synchronized with the master recorder during connections. Each recorder had four connection ports to strain gauge sensors. A manual data recorder was also used in some experiment when the number of sensors

was more than the capacity of the four Smart Dynamic Strain Recorders. In this case, a connection was made between DC-204R and a manual data recorder and the corresponding data through the manual data recorder was noted manually.

Figure 3.11 Smart Dynamic Strain Recorders and software for data acquisition

3.6.5 MTS Loading System

A servo hydraulic MTS loading system was used to apply cyclic loads on test sections in the large geotechnical testing box. The MTS loading system consists of a steel loading frame, a hydraulic actuator, and a servo-control unit connected to both software and a hydraulic control valve. The Multi Purpose Test Ware (MPT) software was used to apply a load, design a loading pattern, and set the maximum number of loading cycles and maximum displacement limit in the test. The MPT software was found to be flexible for the MTS servo-hydraulic control systems.

A steel loading plate of 304 mm in diameter and 30 mm in thickness was used to apply cyclic loading on the test sections. A 10 mm thick rubber base was affixed at the bottom of the

loading plate to simulate the rubber tire contact to the HMA surface. Figure 3.12 shows the experimental set up of a typical test section in the large geotechnical test box.

The cyclic loads having a peak value of 40 kN and a trough value of 0.5 kN were applied on the loading plate at a loading wave frequency of 0.77 Hz. The peak value of the load was selected to simulate the single wheel load of 40 kN, which corresponds to a tire pressure of 550 kPa. Figure 3.13 shows the cyclic loading wave form of the MTS load system.

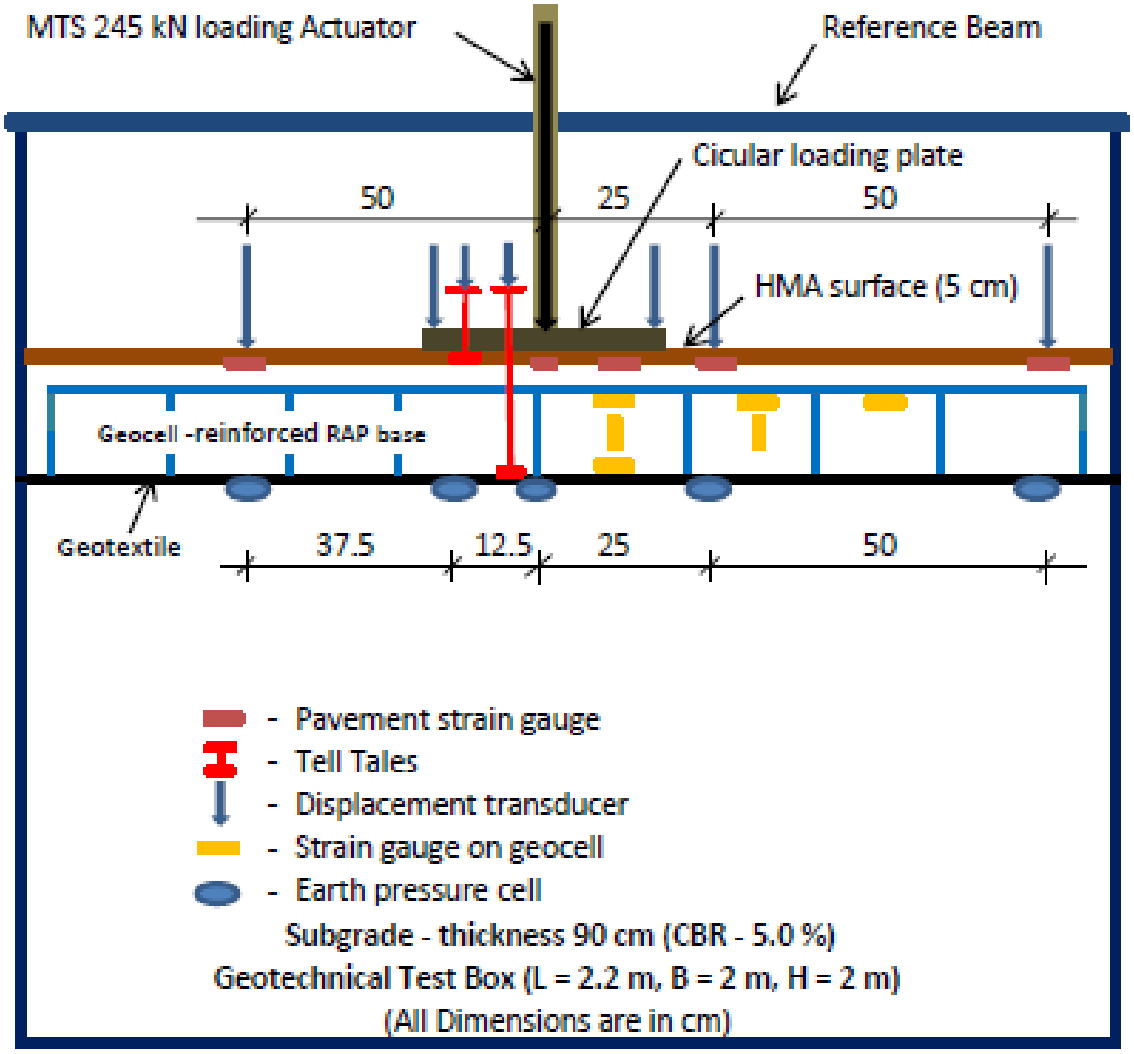

Figure 3.12 Experimental set up of a typical test section in the large geotechnical test box

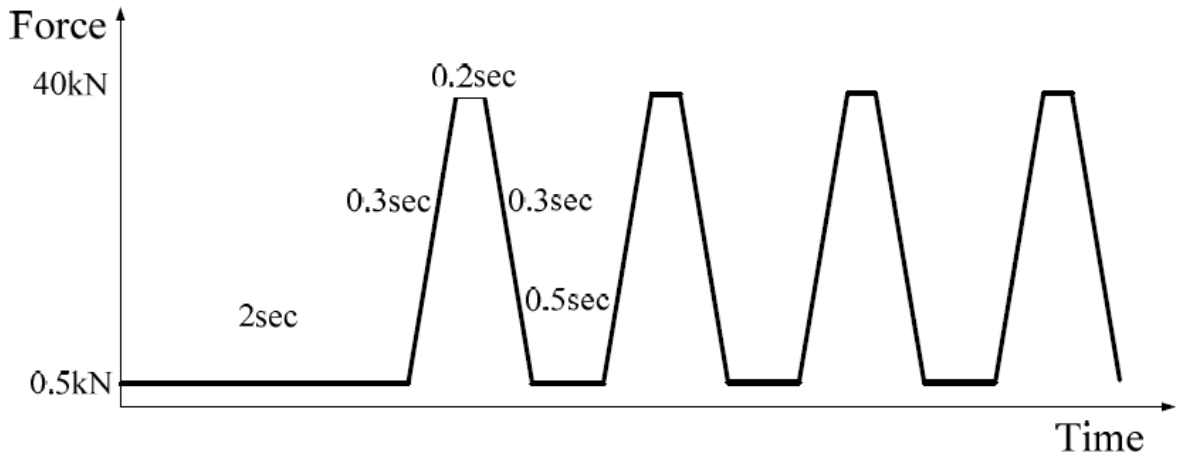

Figure 3.13 Cyclic loading wave form (from Pokharel, 2010)

3.6.6 Vane Shear Test

Vane shear tests (ASTM D2573-08) were carried out to check the undrained shear strength and CBR value during the preparation of subgrade for test sections. The size of the vane was 18.8 mm in diameter and 28.5 mm in length. The vane shear test, as shown in Fig. 3.14 was used to evaluate the undrained shear strengths (C_u) at different depths of 10 cm, 18 cm, and 25 cm from the top of the prepared subgrade section at 5 different locations and ensure the quality and consistency of the prepared subgrade to attain the desired strength or CBR value. The obtained undrained shear strength by the vane shear test was used to estimate the CBR value of the prepared subgrade. If the desired value of strength was not met, the subgrade would be re-prepared until the desired strength was reached. The following relationship established by Pokharel (2010) was used to estimate the subgrade CBR value using the undrained shear strength (C_u) by the vane shear test:

$$CBR(\%) = \frac{C_u}{20.5} \qquad \textbf{(3.1)}$$

Figure 3.14 Vane shear test apparatus

3.6.7 Dynamic Cone Penetration Test

Dynamic Cone Penetration (DCP) tests (ASTM D6951-03) were carried out at four different locations at approximately 24 hours after the placement of the RAP base course. The objective of this test was to determine the CBR profile of subgrade and base course in each test section. The following relationship established by Webster et al. (1992, 1994) was used to estimate the CBR value.

$$CBR(\%) = \frac{292}{(DPI)^{1.12}} \qquad \textbf{(3.2)}$$

Where, DPI = dynamic cone penetration index (mm/blow).

3.6.8 Light Weight Deflectometer Test

Light Weight Deflectometer (LWD) tests, as shown in Fig. 3.15, were carried out on each pavement layer of the prepared test section including subgrade, base, and HMA surface. ZFG 3000 LWD manufactured by Zorn Instruments, Germany was used. This test is a nondestructive method which measures the deflection of the plate under an impact load by a falling weight. There is an acceleration sensor on the loading plate. When the falling weight drops on the loading plate, the acceleration signal captured by the sensor can be used to calculate the deflection of the plate and the dynamic deformation modulus (E_{vd}) of the soil. The mass of the falling weight was 10 kg and the falling distance was 73 cm. The test has three different loading plate diameters of 15, 20, and 30 cm. The large diameter loading plate is suitable for fine grained soil while the small diameter plate is suitable for coarse grained soil or even HMA surface.

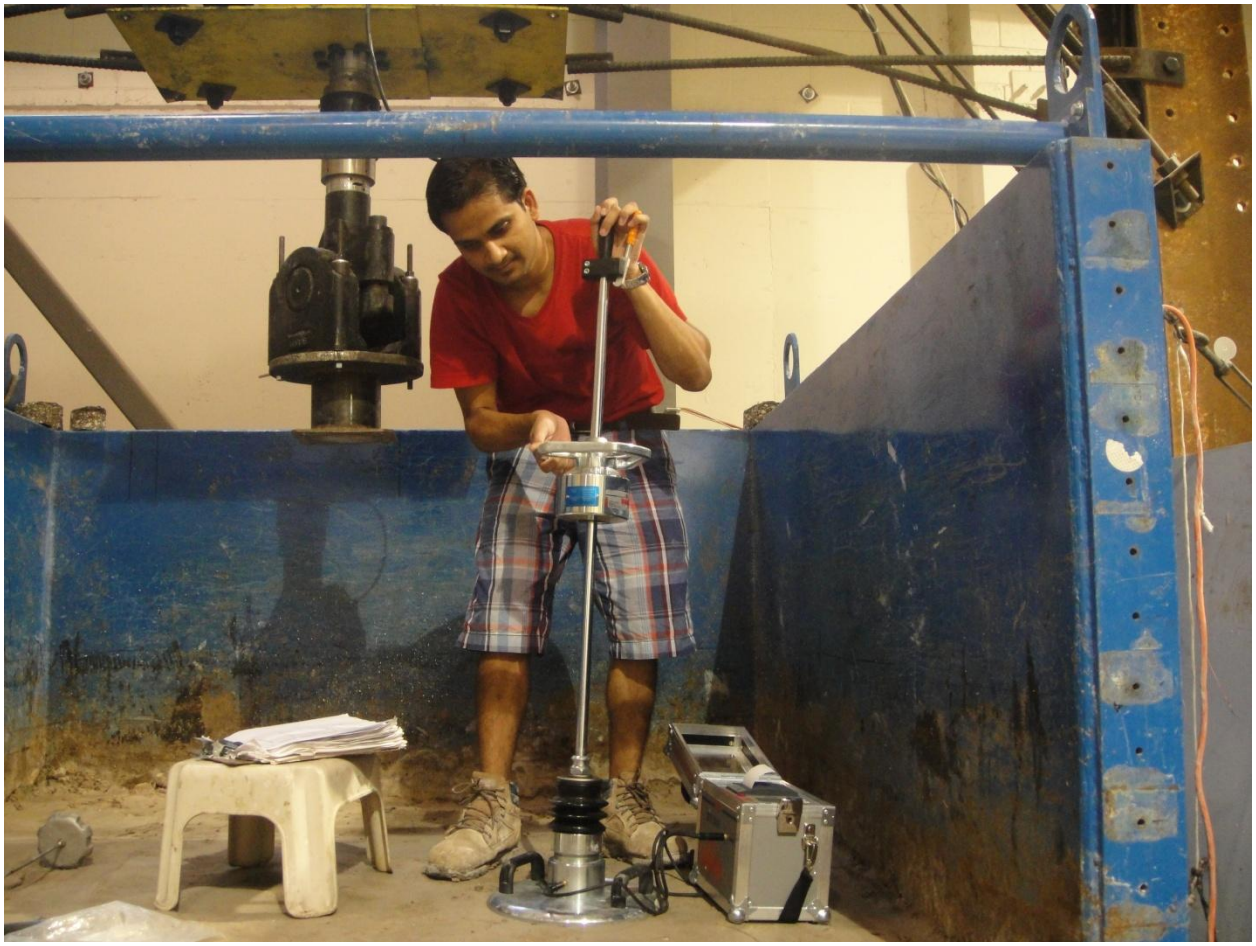

Figure 3.15 Light Weight Deflectometer Test on the prepared test section

3.7 Vibratory Plate Compactor

A vibratory plate compactor, as shown in Fig. 3.16, was used to compact the subgrade, base, and HMA surface during the preparation of test sections. The vibratory plate compactor was not used to compact the geocell-reinforced RAP base because it could not densify the infill material well. Therefore, manual compaction using the modified Proctor compaction hammer was done for the infill material in the geocell-reinforced RAP base.

Figure 3.16 Vibratory plate compactor

3.8 Core Cutter

After the completion of each test, a core cutter was used to take samples from the HMA surface as shown in Fig. 3.17. The HMA sample was used to find the air void of the HMA surface. The diameter of the core cutter was 3 or 4 in. depending on its availability in the laboratory. Sampling was done at different locations to have a better representation of the quality of the HMA surface. The bulk specific gravity (G_{BS}) and theoretical maximum specific gravity (G_{MS}) of the core samples were determined and the air void (V_a) was calculated following ASTM D3203 as follows:

Figure 3.17 Samples taken by the core cutter at different locations

$$V_a = \left(1 - \frac{G_{BS}}{G_{MS}}\right) \times 100\% \qquad \textbf{(3.3)}$$

The materials and equipment discussed above were used in all the experimental tests in this research. The data collected from the experiment are presented in the next chapter.

CHAPTER FOUR

EXPERIMENTAL DATA ANALYSIS

The chapter presents the analysis of the data of the experiments carried out in the large-scale geotechnical test box. In the first part, the chapter explains the preparation of test sections. In the second part, the data obtained from the tests are presented in a graphical form. At the end of this chapter, the comparison of the results from different test sections is presented.

4.1 Preparation of Test Sections

4.1.1 Subgrade

The subgrade consisted of a mixture of 75% Kansas River (KR-I) sand and 25% Kaoline. The target CBR value of the subgrade was 5%, which represents an intermediate stiff subrade for pavement applications. The earlier discussion in Chapter 3 showed that the CBR of 5% occurred at the moisture content close to the optimum moisture content (OMC) of 10.4%. These two materials were mixed in proportion manually on a platform to get a homogeneous dry mixture. The water was added to the mixture and mixed again with water to achieve the water content slightly higher than the OMC of 10.4%. The prepared mixture was set for more than 24 hours to allow uniform distribution of moisture in the mass.

The total thickness of the subgrade was 90 cm. The prepared mixture was placed inside the large box in a lift thickness of 15 cm for six lifts and its moisture content was checked for each lift. If the moisture content was different than the required one, the moisture content of the subgrade was adjusted by adding more water or by allowing it to dry. The placed subgrade soil

was then compacted by a vibratory plate compactor for several passes until the average vane shear strength reached the desired value. The vane shear tests were conducted at five different locations. The average undrained shear strength obtained from the vane shear tests was used to estimate the subgrade CBR value based on the correlation described in Section 3.6.6.

Light weight deflectometer tests were carried out at six different locations over the prepared subgrade using three different loading plates of 10, 20, and 30 cm in diameter as described in Section 3.6.8. These tests were carried out to determine the dynamic deformation modulus of the subgrade in each test section.

After the preparation of subgrade, a geotextile layer was placed at the interface between the subgrade and the base course in the geocell-reinforced RAP base sections. In the unreinforced RAP base sections, no geotextile was placed at the interface between the subgrade and the base.

4.1.2 RAP Base Course

The base material used in the experiments was RAP for all of the tests. The nominal thicknesses of the RAP base courses adopted in the tests were 15, 23, and 30 cm, respectively. No test was done for a 23 cm thick unreinforced base section. In the geocell-reinforced test sections, the geocell was installed over the geotextile placed on the top of the subgrade. The plan view and actual installation of the geocell over the subgrade with the geotextile are shown in Figures 4.1 and 4.2, respectively. In the 15 cm thick geocell-reinforced RAP base section, one layer of 10 cm high geocell was installed with a 5 cm thick RAP cover. In the 30 cm thick geocell-reinforced RAP base section, two layers of geocells (10 cm high geocell each) were

installed and the RAP covers on the bottom and upper geocells were 3 and 7 cm thick, respectively. In the 23 cm thick geocell-reinforced RAP base section, one layer of 15 cm high geocell was installed with an 8 cm thick RAP cover. The total numbers of strain gauges fixed on the wall of the geocell were 6, 6 and 12 (6 on each layer) for the 15 cm, 23 cm, and 30 cm thick RAP base courses, respectively.

The quantity of RAP placed in each lift was calculated by multiplying the volume of that lift by the density of RAP. The RAP was compacted at the moisture content of 5.5%, which corresponded to 95 % of the maximum dry density. The lift thickness depended on the base thickness. The 15 cm thick unreinforced RAP base was compacted in two lifts (8 cm for the first lift and 7 cm for the second lift). The 30 cm thick unreinforced RAP base was compacted in three lifts (10 cm each lift). Both unreinforced base courses were compacted by the vibratory plate compactor. For the 15 cm and 23 cm thick geocell-reinforced RAP base courses, the infill RAP in one layer of geocell was placed and compacted by hand tamping using the Proctor hammer and the RAP cover was compacted by the vibratory plate compactor. For the 30 cm thick geocell-reinforced RAP base course, RAP was placed and compacted in four lifts, which included the bottom 10 cm thick geocell-reinforced RAP layer, the 3 cm thick RAP cover, the upper 10 cm thick geocell-reinforced RAP layer, and the 7 cm RAP. The infill RAP inside the geocell was placed and compacted by hand tamping using the Proctor hammer and the RAP cover was compacted by the vibratory plate compactor. The symbols, orientations, and locations of strain gauges affixed on geocell wall is as shown in Figure 4.3.

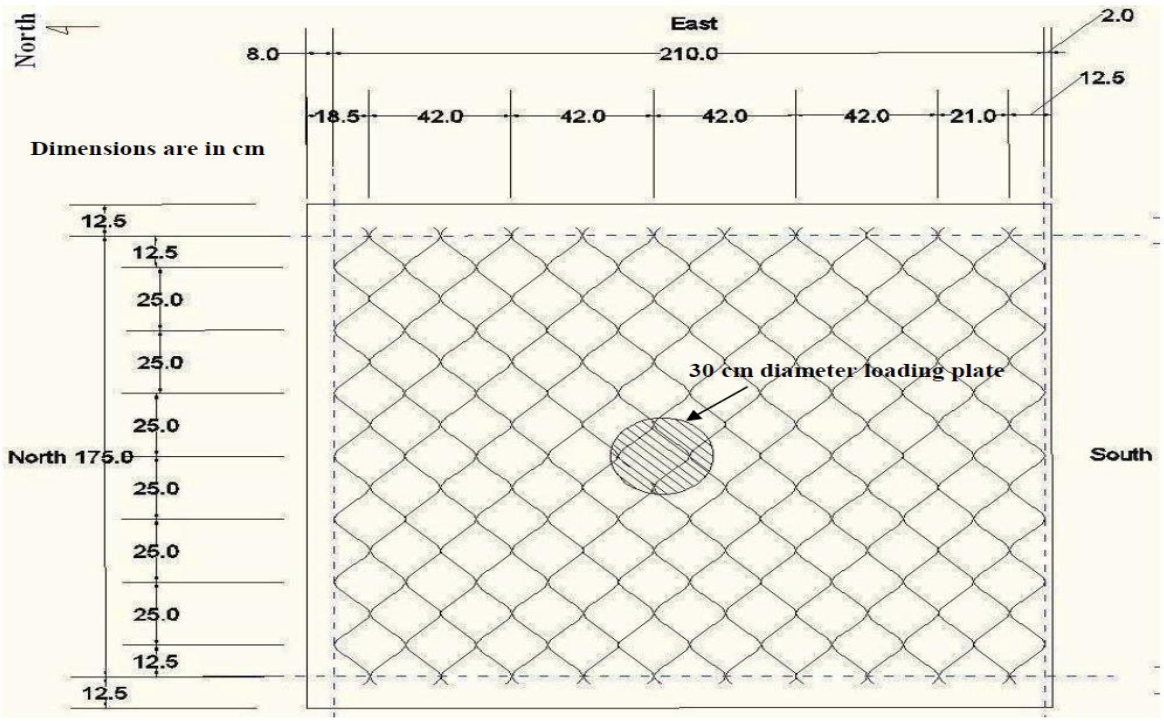

Figure 4.1 Plan view of the geocell layout in the large test box (from Pokharel, 2011)

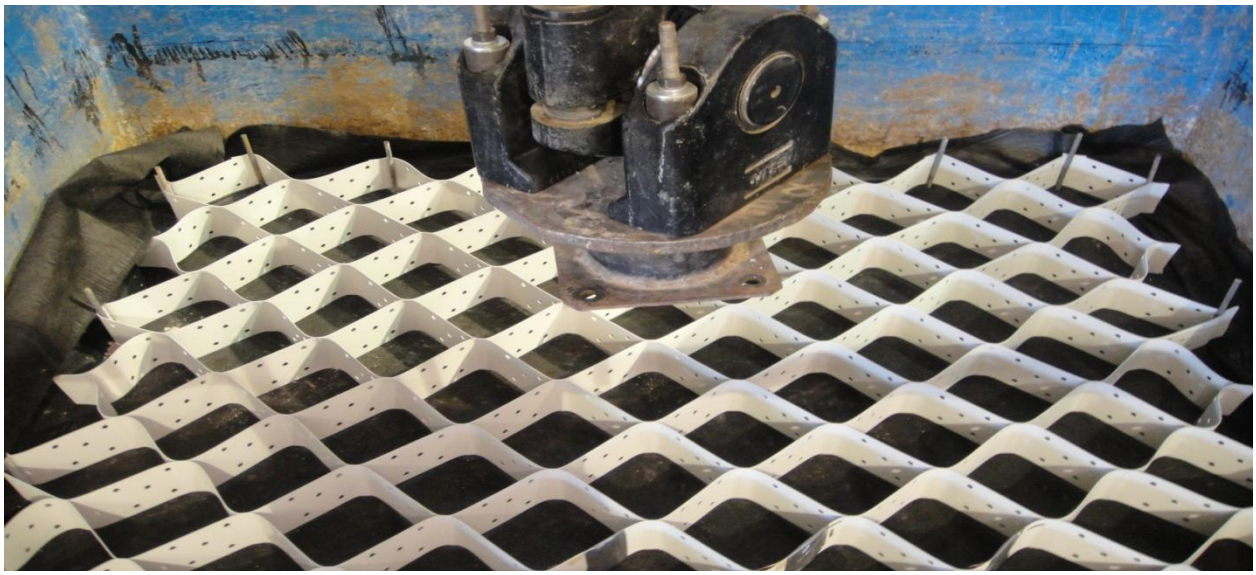

Figure 4.2 Geocell installed on the geotextile over the subgrade

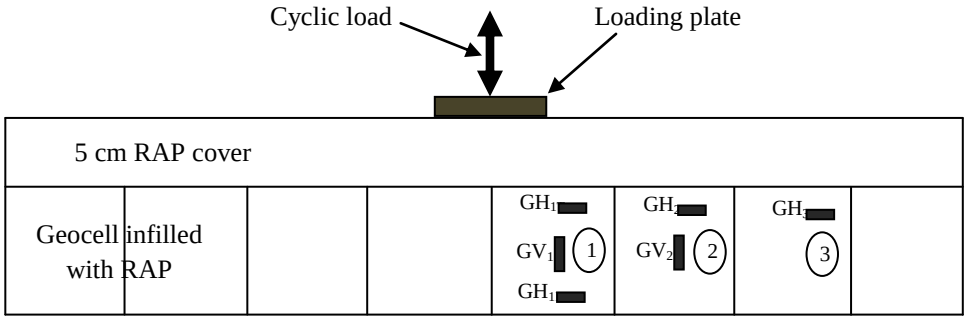

(a) 15 cm thick reinforced RAP section

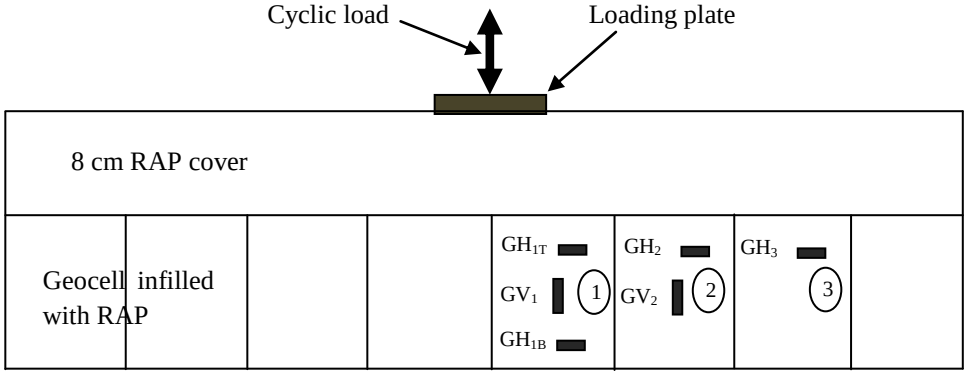

(b) 23 cm thick reinforced RAP section

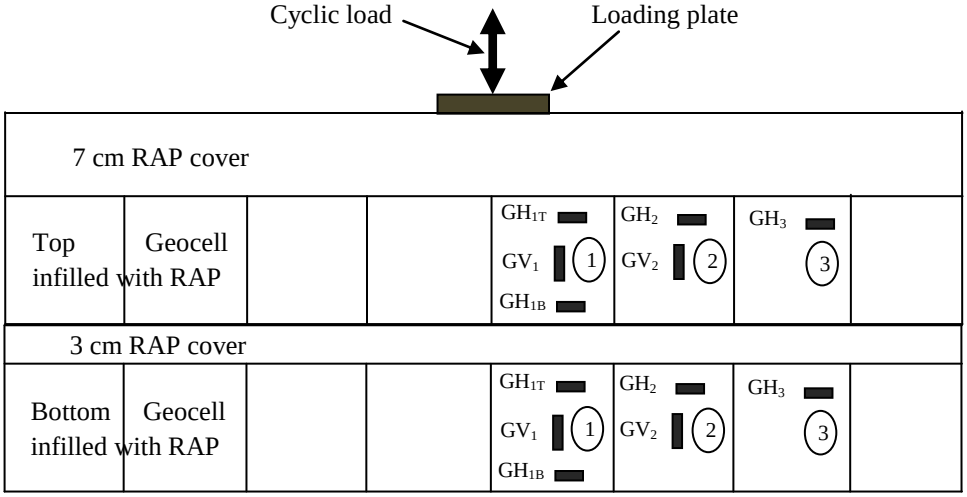

(c) 30 cm thick reinforced RAP section

Figure 4.3 Symbols, orientations, and location of strain gauges

The light weight deflectometer tests were carried out over the prepared RAP base course at six different locations using three different loading plates as described in Section 3.6.8. The objective of this test was to determine the dynamic deformation modulus of the prepared base.

To obtain the CBR profile of the test section including the subgrade and the base course, the dynamic cone penetration tests were carried out at four different locations. The tests were carried out from the top of the RAP base down to the subgrade for at least 30 cm deep. The CBR values of the prepared test sections were determined using Equation 3.2.

4.1.3 Hot Mix Asphalt Surface

The prime coat was applied on the surface of the base course to create a proper bond between the RAP base and the HMA concrete surface. The prime coat liquid was heated in the oven and was applied on the surface of the RAP base. The second tell-tale was fixed on the top of the base course as shown in Figure 4.4. In addition, the pavement strain gauges were placed on the top of the base course (i.e., at the bottom of the HMA surface to measure the strains developed at the bottom of the HMA layer). The pavement strain gauges were covered by cold mix asphalt and its wires were taken to the side of the test box through a small trench on the surface of the RAP base, which was cover by the same RAP base material. This measure was adopted to protect the pavement strain gauges from being damaged by the high-temperature HMA during its placement. Figure 4.4 shows the pavement strain gauges on the top of the base course.

Figure 4.4 Prime coat on the RAP base with the tell-tale and pavement strain gauges

The HMA surface was placed on the top of the RAP base after 24 hours of application of the prime coat. The HMA was prepared by the nearby asphalt plant and transported to the laboratory within 30 minutes. The thickness of the HMA surface after compaction by the vibratory plate compactor was 5 cm and the density was controlled by the volume and mass. Figure 4.5 shows the compaction of the HMA surface on the large box. The LWD tests were carried out on the HMA surface after its placement for 72 hours.

Figure 4.5 Compaction of the HMA surface by the vibratory plate compactor

4.1.4 Test Setup

A reference beam was set up on the top of the large box and the profile of the HMA surface was measured from the reference beam. Five displacement transducers were fixed on the reference beam to measure the vertical displacements at different locations of the HMA surface as well as the displacements of the two tell tales. The tell tales were run through the holes on the loading plate and two small horizontal metal strips was fixed on the tell-tales for the displacement transducers to sit on as shown in Figure 4.6. All of the cables of the pressure cells, displacement transducers, strain gauges on the geocell, and pavement strain gauges were connected to the DC-204R data recorders as mentioned in Section 3.6.4. Some of the strain

gauge wires were connected to the manual data recorder in the case when the channels of the DC-204R data recorders were not sufficient for all the data recordings.

Figure 4.6 Setup of the tell tales and the displacement transducers

4.2 Cyclic Plate Load Tests

The cyclic plate load tests were carried out using the MTS loading system with the MPT software. The cyclic load started from the valley value of 0.5 kN to the peak value of 40 kN at the frequency of 0.77 Hz.

Six cyclic plate load tests were conducted following the same testing procedure:

1. 15 cm thick unreinforced RAP base section
2. 15 cm thick geocell-reinforced RAP base section (harder subgrade)
3. 15 cm thick geocell-reinforced RAP base section

4. 23 cm thick geocell-reinforced RAP base section
5. 30 cm thick unreinforced RAP base section
6. 30 cm thick geocell-reinforced RAP base section.

The subgrade CBR was maintained at approximately 5% in all the tests except Test No. 2, in which the subgrade became harder due to the delay in the delivery of HMA.

The profile of the HMA surface after each test was measured from the same reference beam. Figure 4.7 shows the deformation of the HMA surface under the loading plate after the test. This figure also shows the two tell-tales extended above the HMA surface. To determine the percent of air void in the HMA surface, samples were taken at different locations by the core cutter as mentioned in Section 3.8.

Figure 4.7 Surface deformation of the HMA surface under the loading plate after the test

4.3 Test Results

4.3.1 Format of presentation

The results from each test are presented in a tabular or graphical form, which include CBR values from vane shear tests, average CBR values and CBR profiles from on DCP tests, dynamic deformation moduli from LWD tests, surface profiles before and after the tests, surface permanent and elastic deformations at the center, permanent deformations of bases and subgrade, strains in geocell and pavement strain gauges, maximum vertical stresses at the interface between subgrade and base, and stress distribution angles.

The applied load is distributed through the pavement structure to the subgrade. The stress distribution angle method is a simple and approximate method to estimate the maximum stress at the top of the subgrade. This method has been used by Giroud and Han (2004) to develop their design method for geosynthetic-reinforced unpaved roads. The stress distribution angle from the HMA surface to the base course (α_1) is generally higher than that from the base course to the subgrade (α_2) due to the higher modulus of the HMA surface as shown in Fig. 4.8. The earth pressure cells at the interface between subgrade and RAP base measured the vertical stresses at the bottom of the RAP base. The combined stress distribution angle (α) for the test section can be calculated based on the vertical stress at the center as follows:

$$P = \pi \times p(r + h.\tan\alpha)^2 \qquad \textbf{(4.1.5)}$$

Where, P = applied load (40 kN);

p = vertical stress at the interface between subgrade and base course;

r = radius of the loading plate (15.2 cm);

h = combined thickness of the HMA surface and RAP base;

α = combined stress distribution angle.

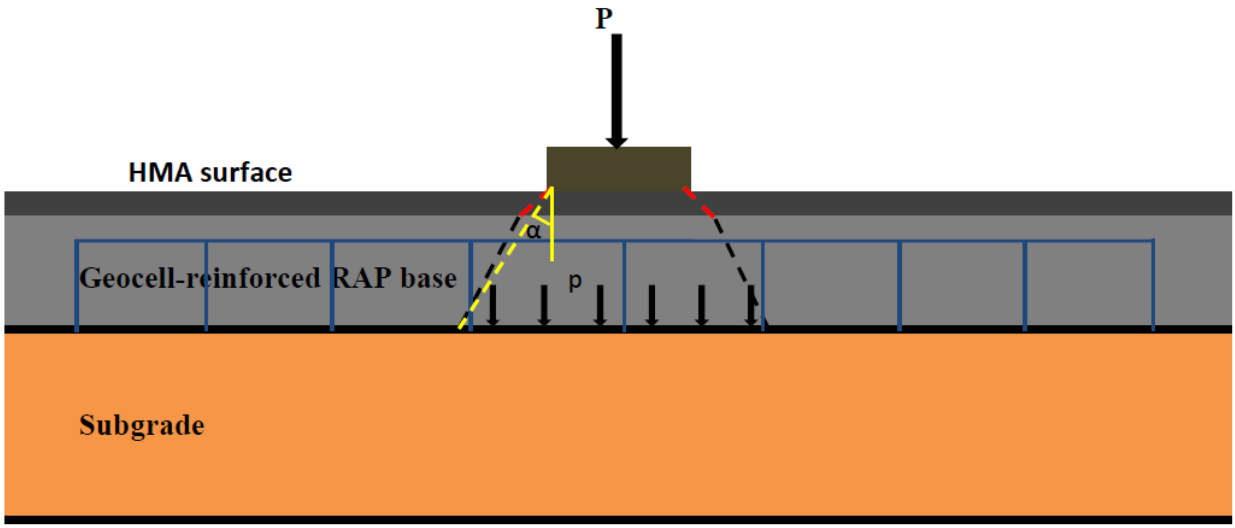

Figure 4.8 Stress distribution through the pavement structure under an applied load

4.3.2 15 cm thick unreinforced RAP base section

The CBR profile of the test section obtained from the DCP tests is shown in Figure 4.9. The locations of the DCP tests, L1, L2, L3, and L4, were randomly distributed inside the test box. The average CBR profile was obtained by averaging the CBR values from the four curves at the same depth. The average CBR values of the subgrade and base estimated by the vane shear tests and DCP tests are presented in Table 4.1. The average CBR value of the subgrade obtained from the vane shear tests was 4.9 %. Similarly, the average CBR values of the subgrade and the RAP base obtained from the DCP tests were 5.7 % and 10.5 % respectively.

The test results indicated that the CBR value of the subgrade from the DCP tests is higher than that by the vane shear tests.

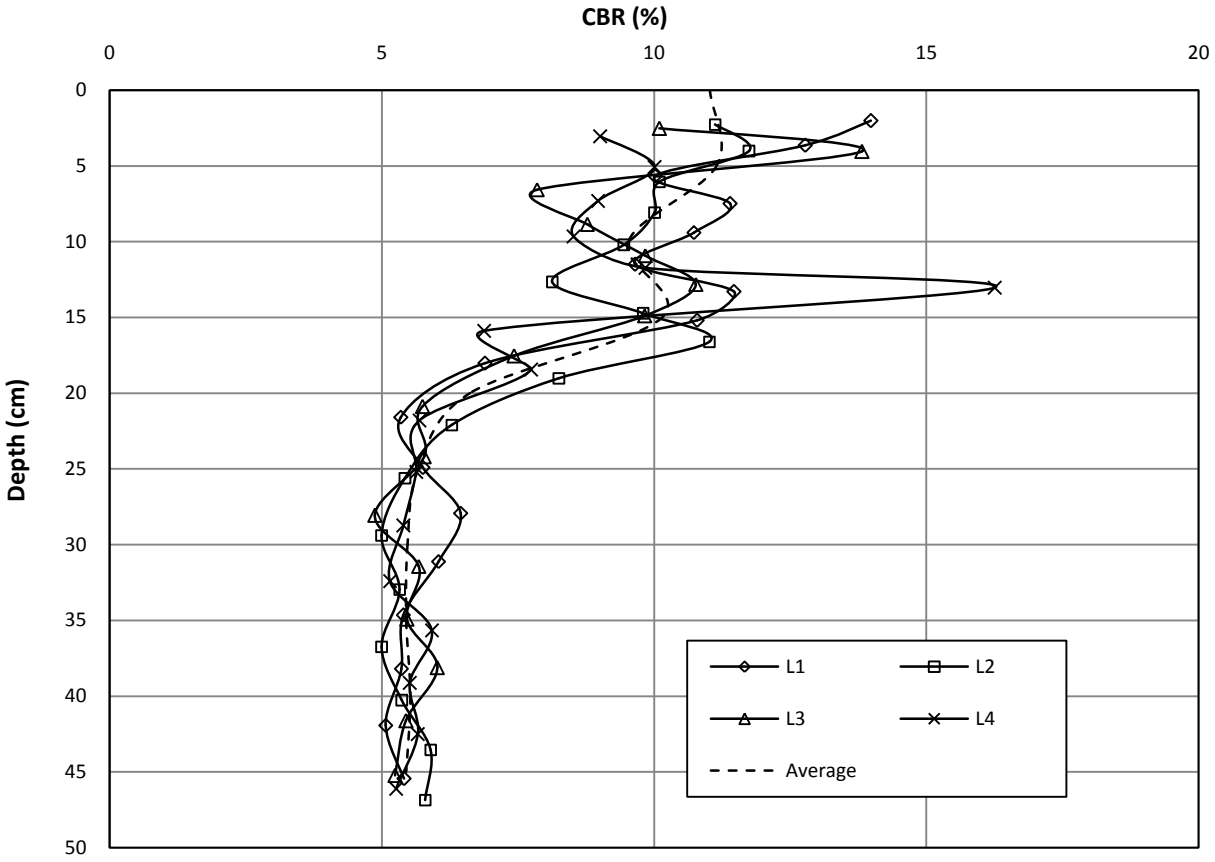

Figure 4.9 The CBR profile obtained from the DCP tests for the 15 cm thick unreinforced RAP base section

Table 4.1 The average CBR values of subgrade and base from the vane shear tests and DCP tests

Test method	CBR value (%)						
	Subgrade at different locations						Base
Vane shear test	1	2	3	4	5	Average	
	4.9	4.7	5.2	4.7	5	4.9	-
DCP test	5.7						10.5

The calculated dynamic deformation moduli (E_{vd}) of the subgrade, base and HMA surface versus the size of the loading plate of the instrument from the LWD tests result are

shown in Figure 4.10. The test results show that the E_{vd} values decreased from the HMA surface, the RAP base to the subgrade.

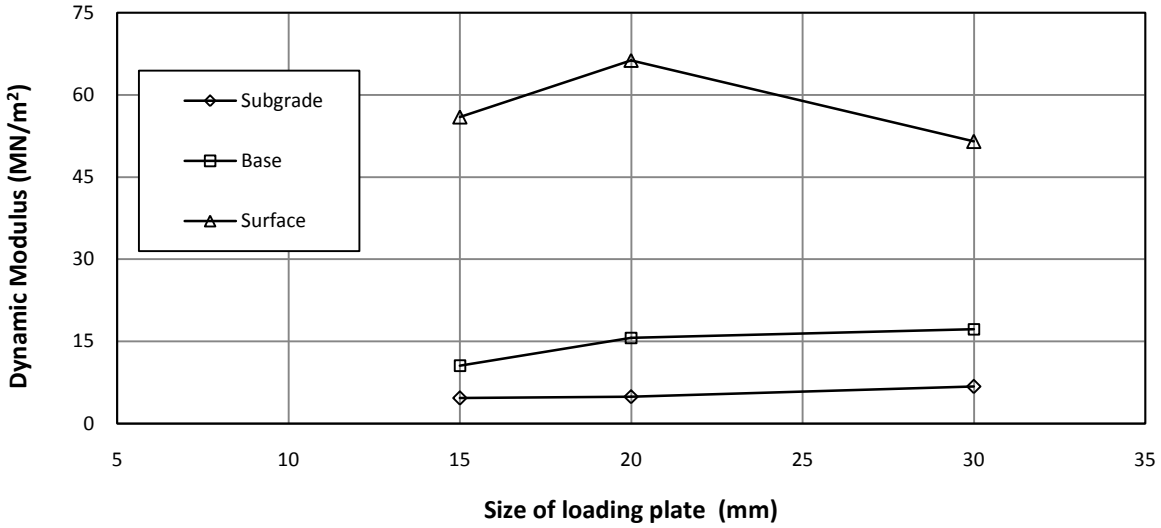

Figure 4.10 The calculated dynamic deformation modulus versus the size of loading plate for the 15 cm thick unreinforced RAP base section

The profiles of the HMA surfaces as shown in Fig. 4.11 were measured from the reference beam before and after the cyclic plate load test. It shows that a depression (equivalent to rutting under traffic) developed under the loading plate and some heaving occurred away from the loading plate after the test.

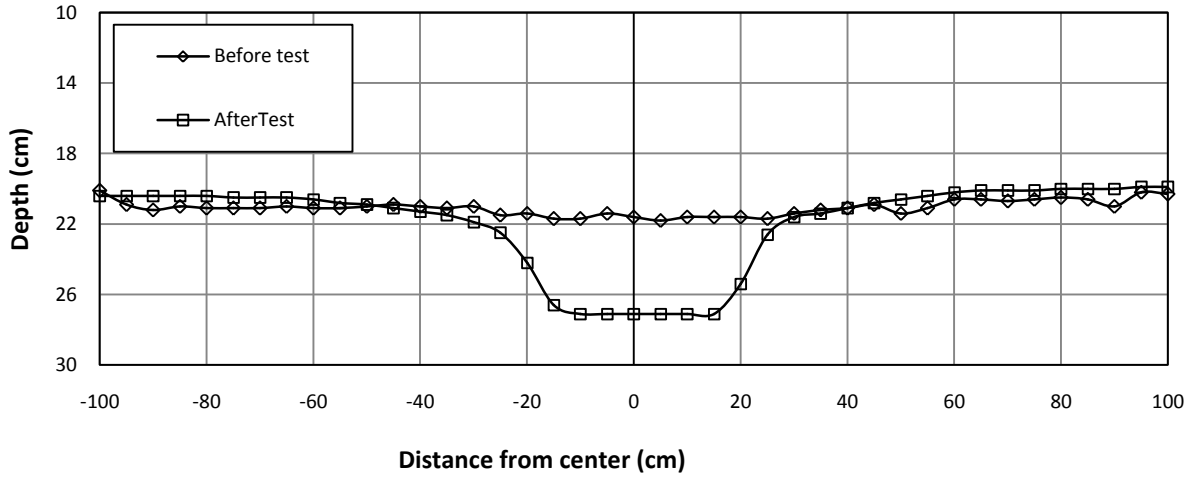

Figure 4.11 Profiles of the HMA surface before and after the test for the 15 cm thick unreinforced RAP base section

The permanent deformation was obtained after unloading of each cycle. Figure 4.12 presents the measured permanent deformations of the pavement at the surface, at the top of the base, and at the top of the subgrade. The difference in the permanent deformations between the HMA surface and the base is the compression of the HMA surface while that between the base and the subgrade is the compression of the base course. At the end of the test, the permanent deformation of the subgrade was approximately 50% of the total permanent deformation. The surface deformations at different distances from the center were obtained by the displacement transducers while the deformations at the top of the base and subgrade were obtained by the tell tales. It is shown that the surface permanent deformation was higher at the center and decreased at the distances of 25, and 50 cm away from the center. The elastic deformation (i.e., the rebound during the unloading of each cycle) as shown in Fig. 4.13 increased up to 40 cycles of loading and then decreased slightly at a small rate until the end of the test. The elastic deformation was much smaller than the permanent deformation and was less than 10% of the permanent deformation at the end of the test.

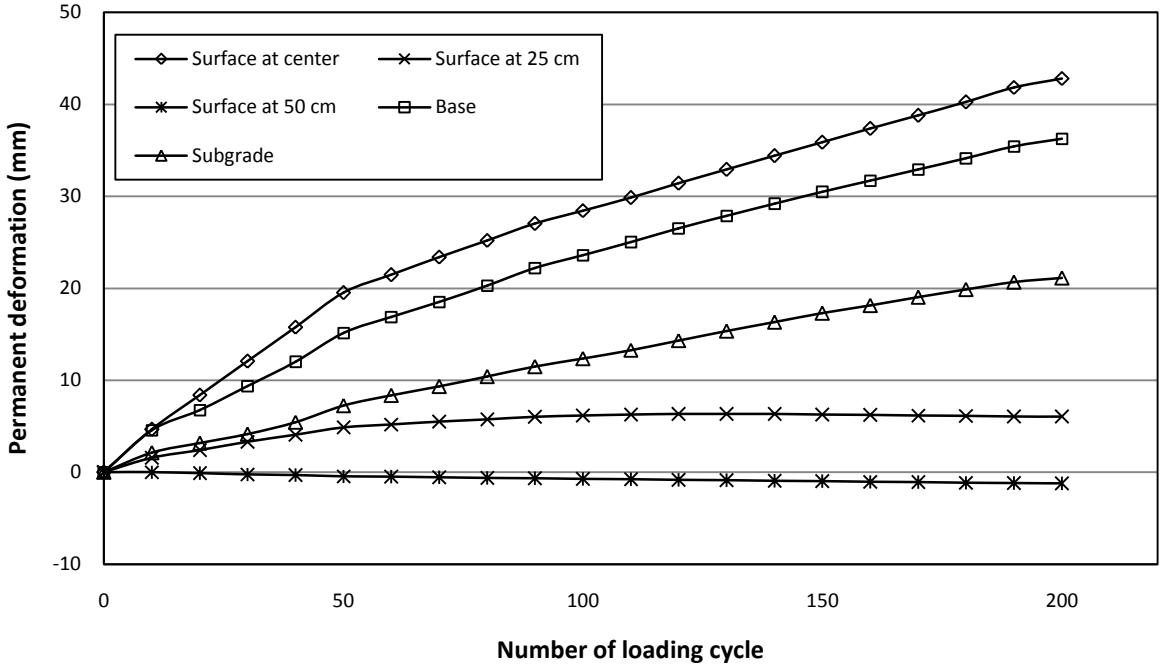

Figure 4.12 The permanent deformation versus the number of loading cycle for the 15 cm thick unreinforced RAP base section

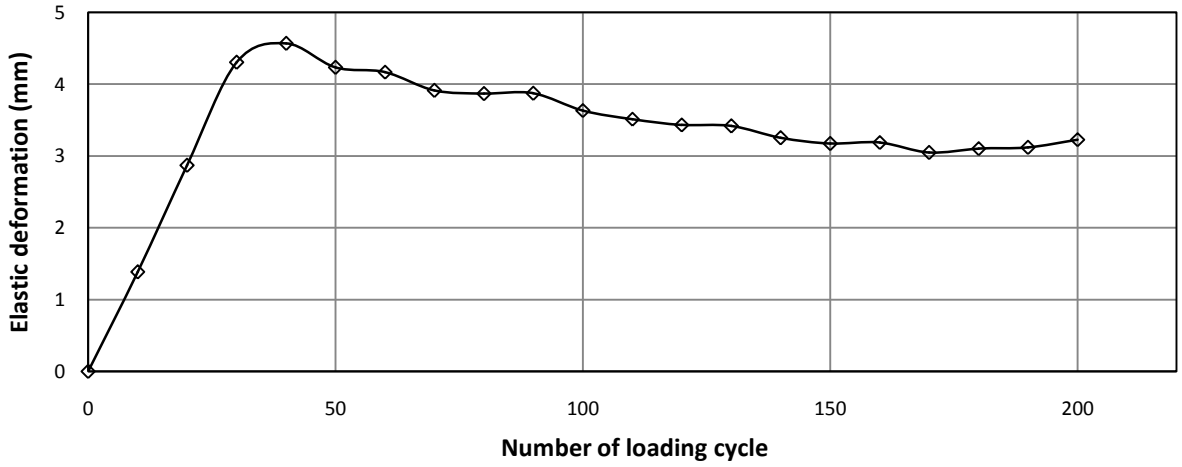

Figure 4.13 The elastic deformation versus the number of loading cycle for the 15 cm thick unreinforced RAP base section

The strains at the bottom of the HMA surface were measured by the pavement strain gauges at the center and 12.5 cm away from the center as shown in Fig. 4.14. In this research,

the strain is positive under tension and negative at compression. The bottom of the HMA surface at the center was under tension from the beginning up to 120 cycles and then became under compression up to the end of the test even though the magnitude of the strain was small. However, the tensile strain developed at the bottom of the HMA surface at the distance of 12.5 cm away from the center.

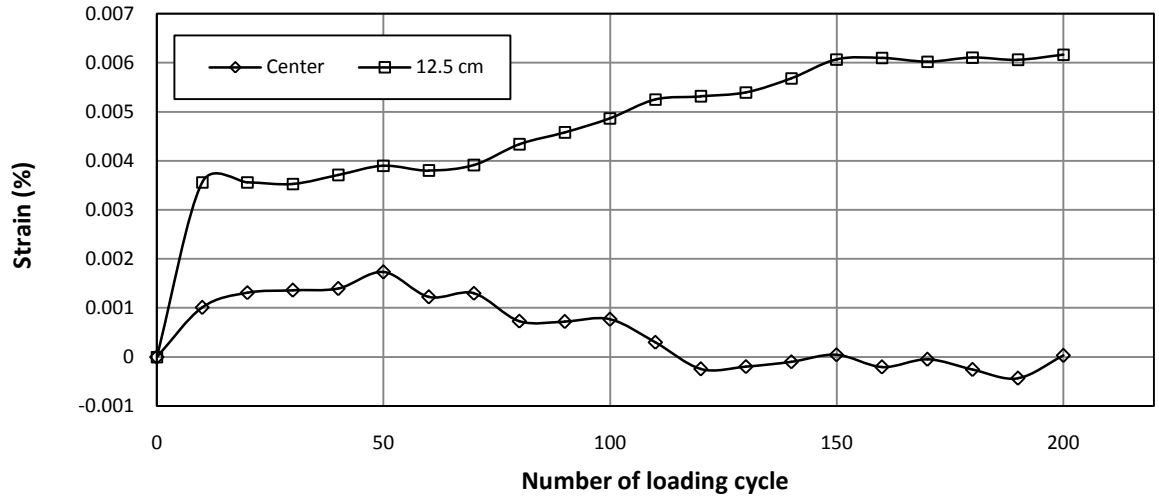

Figure 4.14 The strain at the bottom of the HMA surface versus the number of loading cycle for the 15 cm thick unreinforced RAP base section

Figure 4.15 shows the measured vertical stresses at the interface between subgrade and base at five locations (center, 12.5, 25, 50, and 75 cm away from the center) versus the number of loading cycles. It is shown that the vertical stresses at the center or close to the center were much higher than those away from the center. The vertical stress at the distance of 75 cm away from the center is almost zero. As discussed earlier, the vertical stress at the center was used to calculate the stress distribution angle. The stress distribution angle versus the number of loading cycle is shown in Fig. 4.16. The stress distribution angle decreased with an increase of the load cycle and remained almost the same after 50 loading cycles.

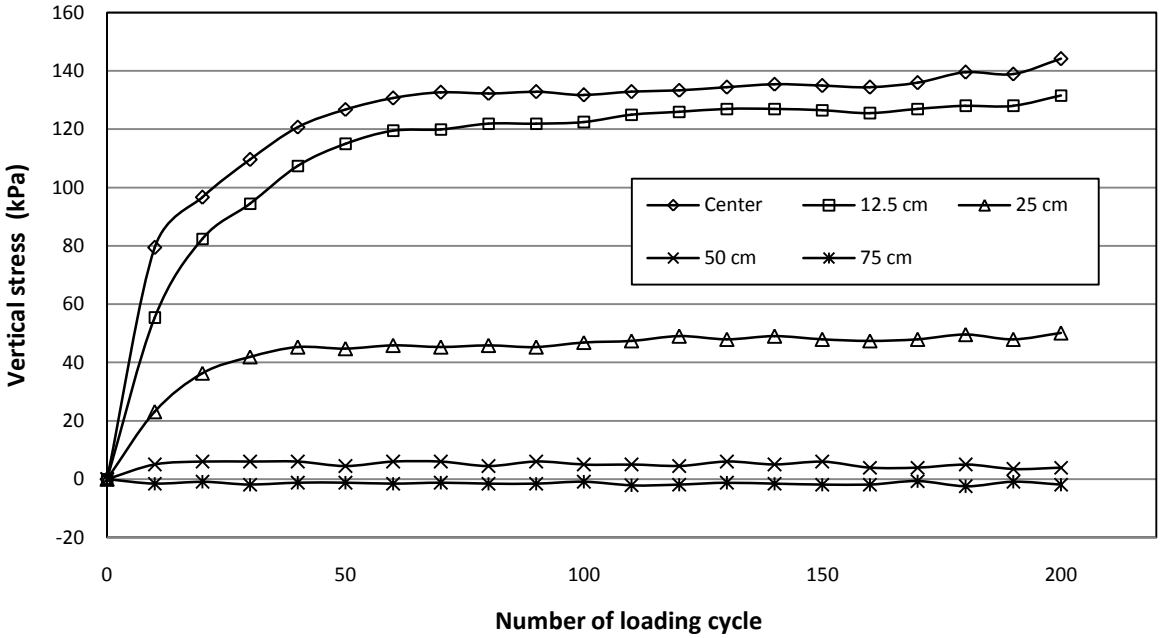

Figure 4.15 The vertical stress at the interface between subgrade and base versus the number of loading cycle for the 15 cm thick unreinforced RAP base section

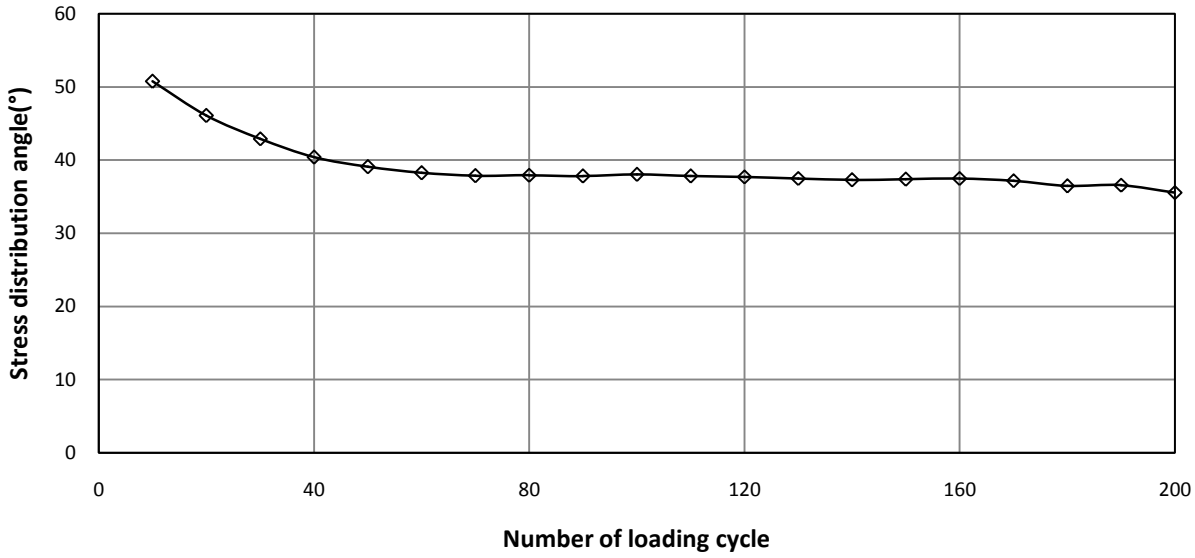

Figure 4.16 The stress distribution angle versus the number of loading cycle for the 15 cm thick unreinforced RAP base section

4.3.3 15 cm thick geocell-reinforced RAP base section (hard subgrade)

The CBR profile of the test section obtained from the DCP tests is shown in Figure 4.17. The locations of the DCP tests, L1, L2, L3, and L4, were randomly distributed inside the test box. The average CBR profile was obtained by averaging the CBR values from the four curves at the same depth. The average CBR values of the subgrade and base estimated by the vane shear tests and DCP tests are presented in Table 4.2. The average CBR value of the subgrade obtained from the vane shear tests was 5.5 %. Similarly, the average CBR values of the subgrade and the RAP base obtained from the DCP tests were 5.9 % and 10.2 % respectively. The test results indicated that the CBR value of the subgrade from the DCP tests is higher than that by the vane shear tests.

The scheduled placement of the HMA surface over the RAP base was 24 hours after the preparation of the base course. In this test, however, there was a long delay (seven days of the preparation of RAP base) in the delivery of the HMA from the local asphalt plant. The actual CBR values of the test section were re-evaluated after the cyclic plate load test and removal of the HMA surface. Figure 4.18 shows the CBR profiles from the DCP tests after the cyclic plate load test. The average CBR values of the subgrade and RAP base were 9.0 % and 13.8 % respectively, which are higher than those determined at seven days earlier. The increase of the CBR values resulted from the loss of moisture in the RAP base and the subgrade during the 7-days waiting period. The harder subgrade and base course resulted in a much stronger response of this test section, which will be discussed below. This test was repeated and the repeated test will be discussed in Section 4.3.4.

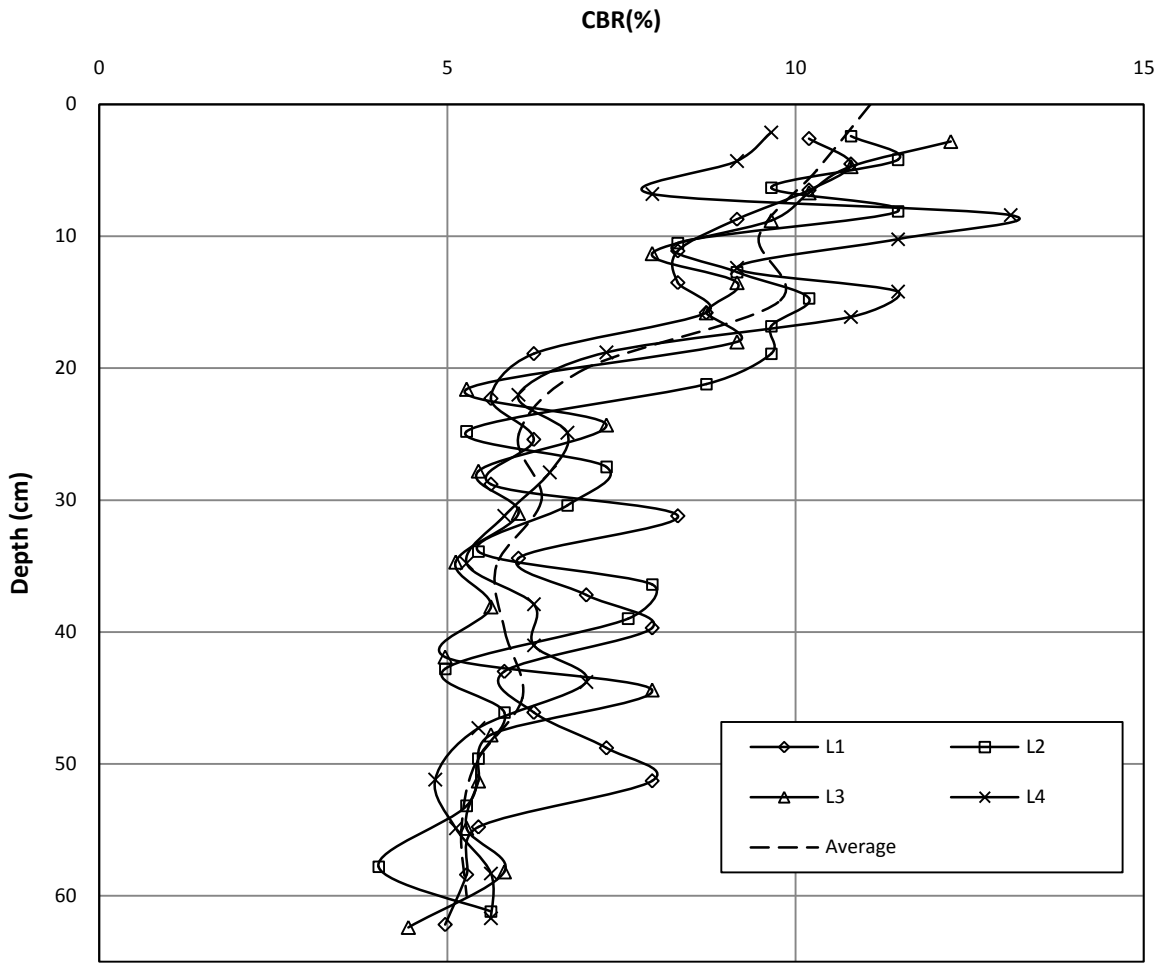

Figure 4.17 CBR profile obtained from DCP tests for the 15 cm thick geocell-reinforced RAP base section before the test (hard subgrade).

The calculated dynamic deformation moduli (E_{vd}) of the subgrade, base and HMA surface versus the size of the loading plate of the instrument from the LWD tests result are shown in Figure 4.19. The test results show that the E_{vd} values decreased from the HMA surface, the RAP base to the subgrade.

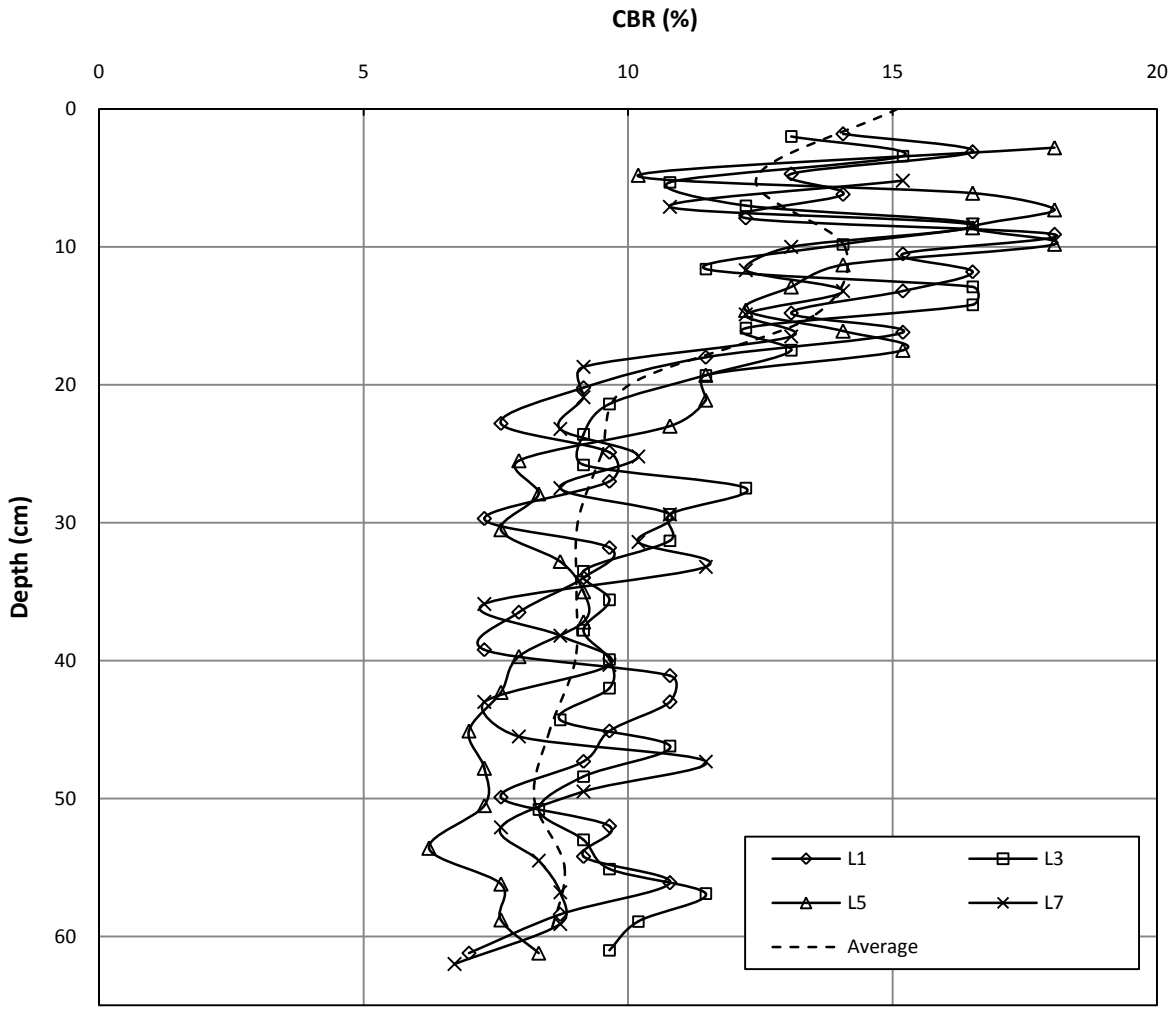

Figure 4.18 CBR profile obtained from DCP tests for 15 cm thick geocell-reinforced RAP base section after the test (hard subgrade)

Table 4.2 The average CBR values of subgrade and base from vane shear tests and DCP tests

Test method	CBR Value (%)						
	Subgrade at different locations						Base Layer
Vane Shear Test	1	2	3	4	5	Average	-
	5.9	5.6	5.4	5	5.4	5.5	
DCP Test (before)	5.9						10.2
DCP Test (after)	9						13.8

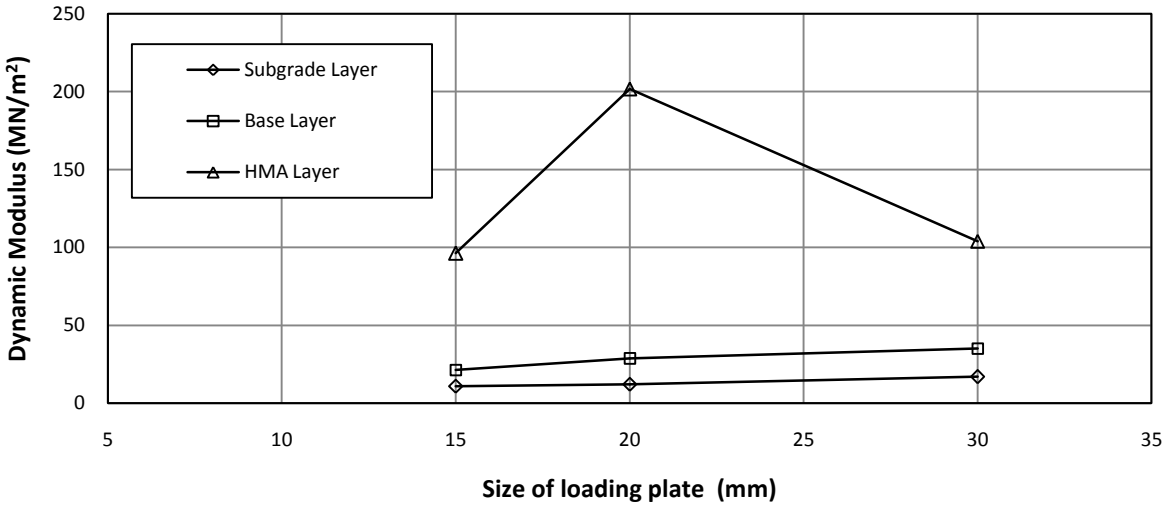

Figure 4.19 The calculated dynamic deformation modulus versus size of loading plate for the 15 cm thick geocell-reinforced RAP base section (hard subgrade)**.**

The profiles of the HMA surfaces as shown in Fig. 4.20 were measured from the reference beam before and after the cyclic plate load test. It shows that a depression (equivalent to rutting under traffic) developed under the loading plate and some heaving occurred away from the loading plate after the test.

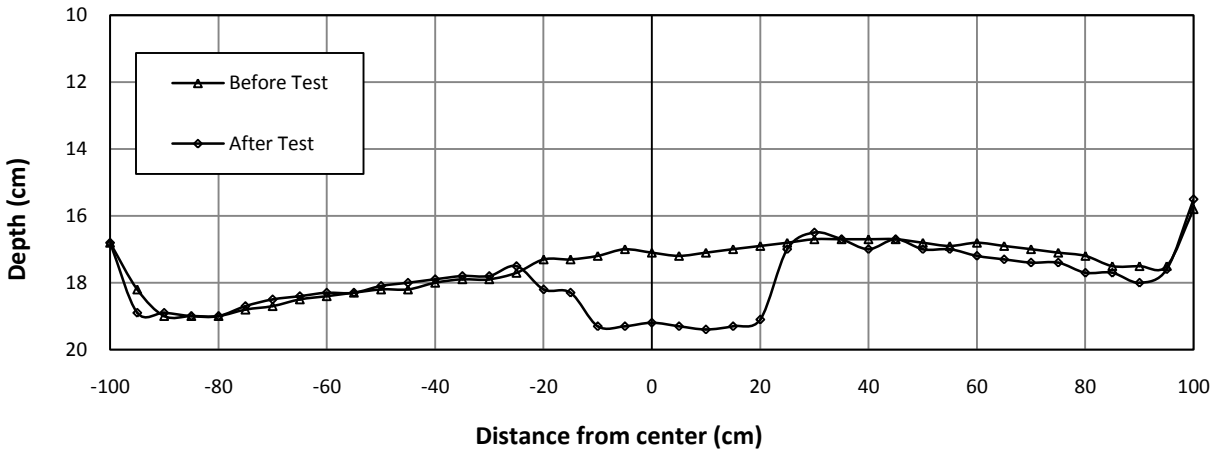

Figure 4.20 Profiles of the HMA surface before and after the test for the 15 cm thick geocell-reinforced RAP base section (hard subgrade)

The permanent deformation was obtained after unloading of each cycle. Figure 4.21 presents the measured permanent deformations of the pavement at the surface, at the top of the base, and at the top of the subgrade. The surface deformations at different distances from the center were obtained by the displacement transducers. It is shown that the surface permanent deformation was higher at the center and decreased at the distances of 25, and 50 cm away from the center. The elastic deformation (i.e., the rebound during the unloading of each cycle) is higher at the beginning of loading and then decreased slightly at a small rate until the end of the test as shown in Figure 4.22. The elastic deformation was much smaller than the permanent deformation and was less than 10% of the permanent deformation at the end of the test.

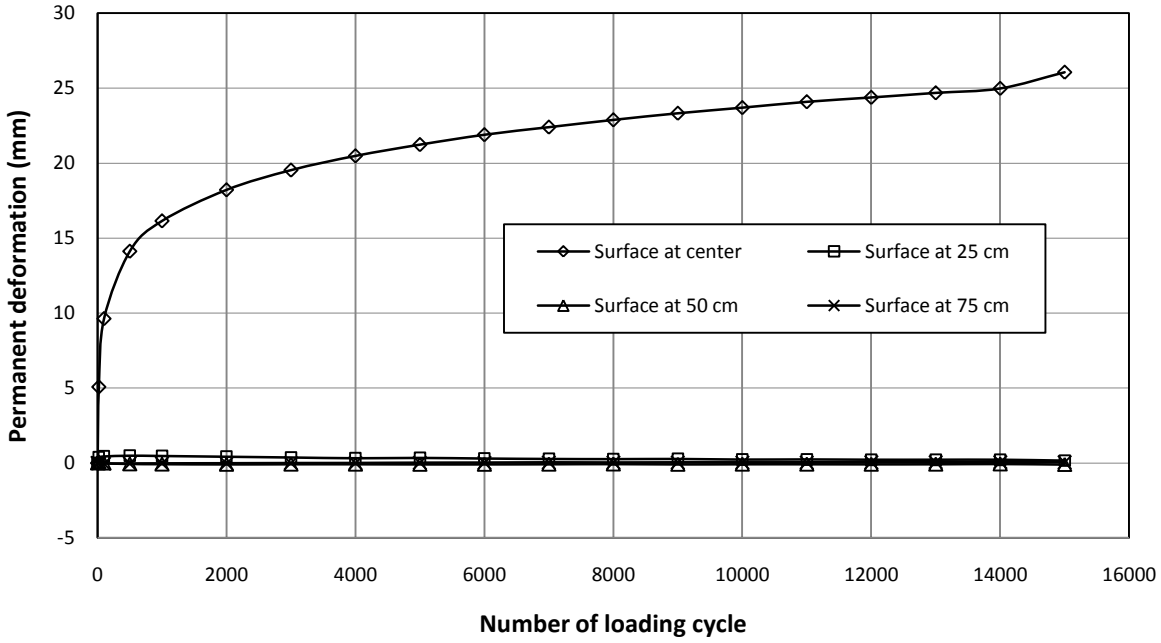

Figure 4.21 The permanent deformation versus number of loading cycle for the 15 cm thick geocell-reinforced RAP base section (hard subgrade)

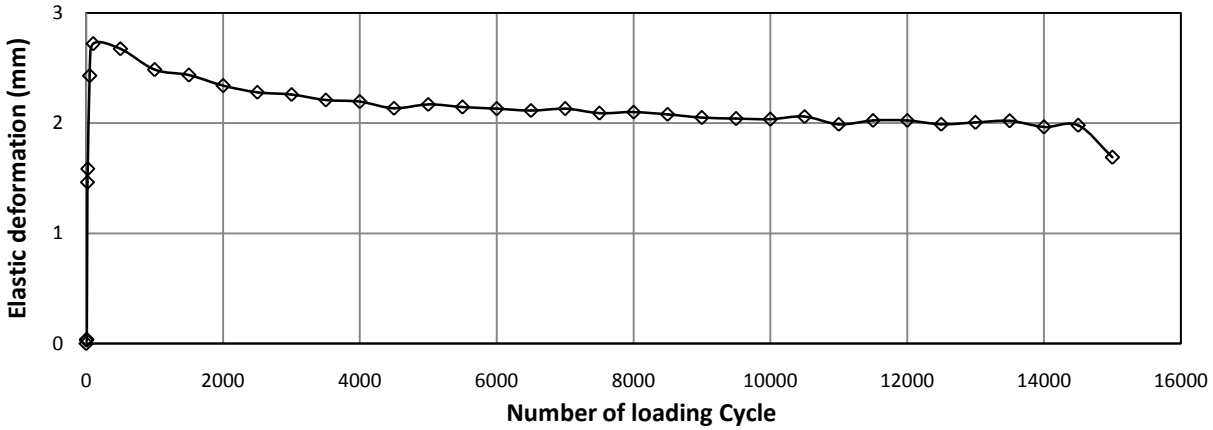

Figure 4.22 The elastic deformation versus number of loading cycle for the 15 cm thick geocell-reinforced RAP base section (hard subgrade)

Figure 4.23 shows the measured maximum strains on the geocell wall at different locations during the cyclic plate load test. The maximum strains were recorded manually during the test. It is shown that the tensile strains developed at all of the top gages while the compressive strains occurred at the middle gauges. The higher strains occurred at the central geocell under the loading plate. The strain at the bottom of the central geocell could not measure as it broke down during construction of base layer.

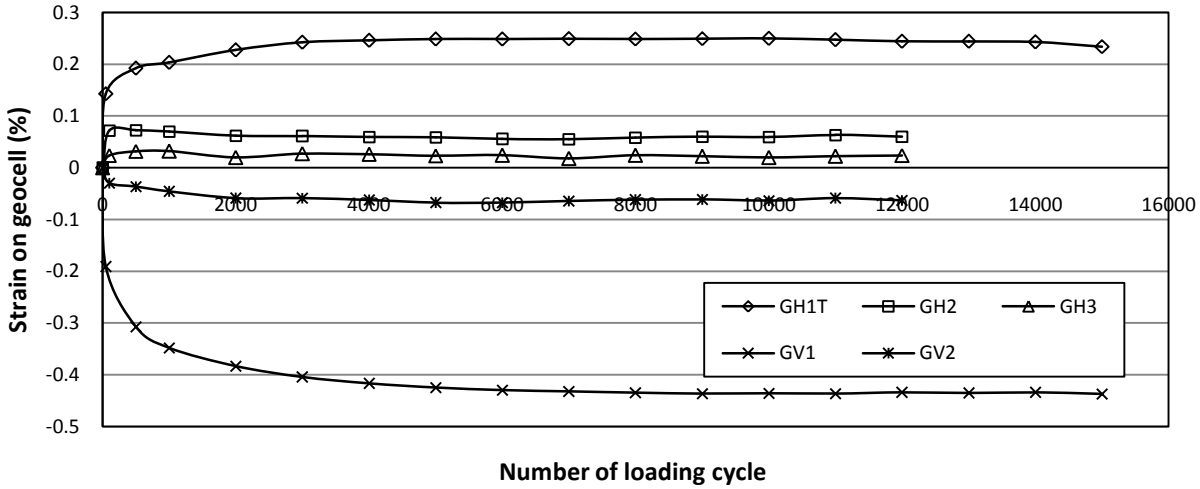

Figure 4.23 The measured strains on the geocell wall in different locations for the 15 cm thick geocell-reinforced RAP base section (hard subgrade)

The strains at the bottom of the HMA surface were measured by the pavement strain gauges at distances 0, 12.5, 25, 50, and 75 cm away from center as shown in Fig. 4.24. In this research, the strain is positive under tension and negative at compression. The bottom of the HMA surface at 0, 12.5, 50, and 75 cm from the center were under tension and 25 cm from center was under compression up to the end of the test.

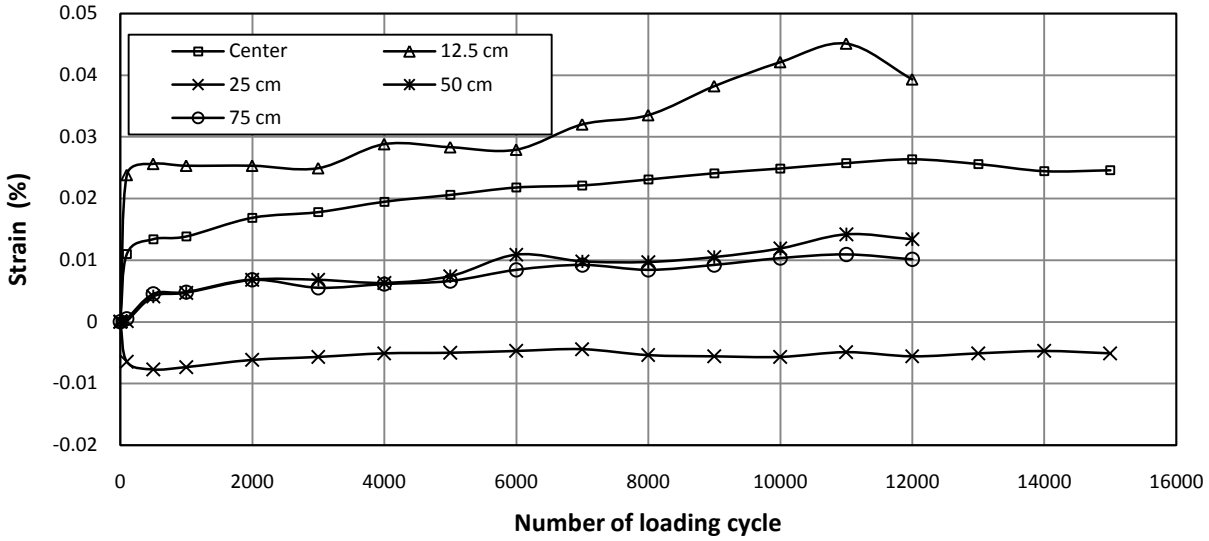

Figure 4.24 The strain at the bottom of the HMA surface versus the number of loading cycle for the 15 cm thick geocell-reinforced RAP base section (hard subgrade)

Figure 4.25 shows the measured vertical stresses at the interface between subgrade and base at five locations (center, 12.5, 25, 50, and 75 cm away from the center) versus the number of loading cycles. It is shown that vertical stress is higher at a distance 12.5 cm than at the center and decrease at the distances 25 cm, and 50 cm away from the center. The vertical stress at the distance of 75 cm away from the center is almost zero. As discussed earlier, the vertical stress at the center was used to calculate the stress distribution angle. The stress distribution angle versus the number of loading cycle is shown in Fig. 4.26. The stress distribution angle decreased with an increase of the load cycle in small rate up to the end of the test.

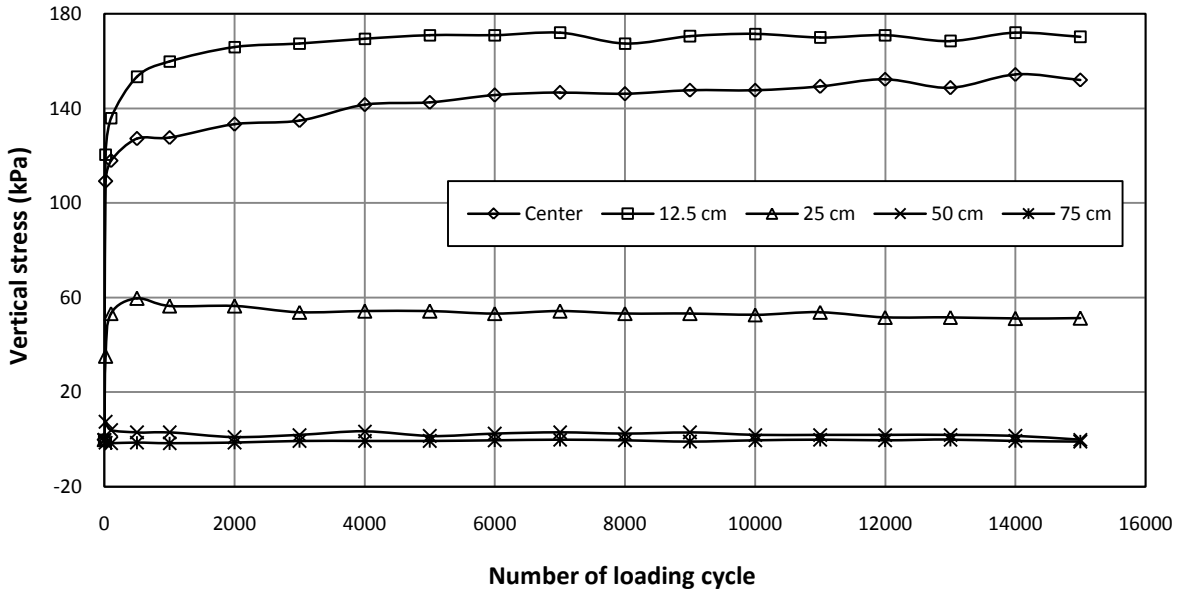

Figure 4.25 The vertical stress at the interface between subgrade and base versus the number of loading cycle for the 15 cm thick geocell-reinforced RAP base section (hard subgrade)

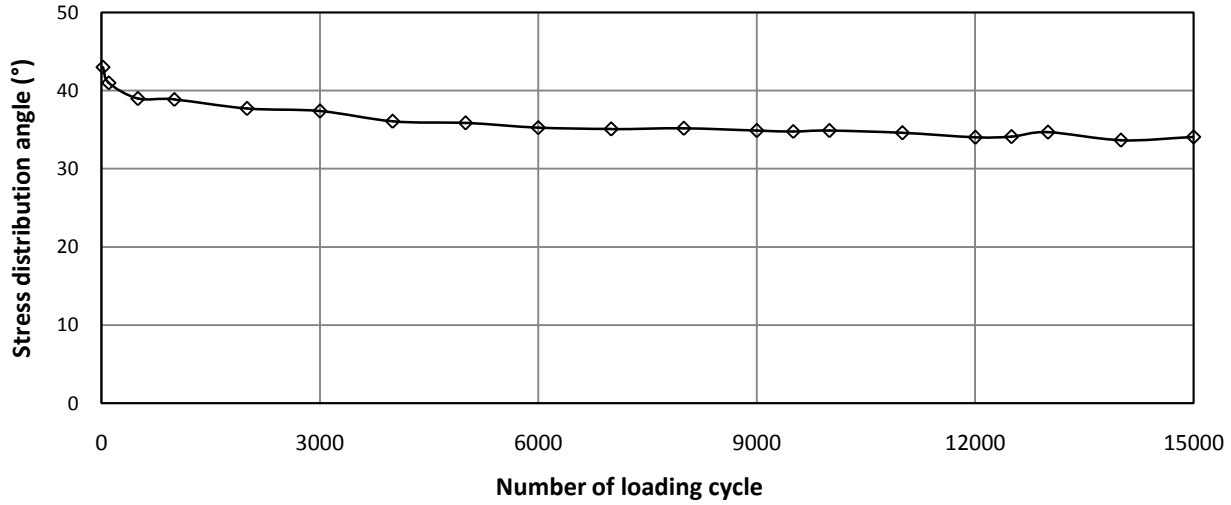

Figure 4.26 The stress distribution angle versus number of loading cycle for 15 cm thick geocell-reinforced RAP base section (hard subgrade)

4.3.4 15 cm thick geocell-reinforced RAP base section

The CBR profile of the test section obtained from the DCP tests is shown in Figure 4.27. The locations of the DCP tests, L1, L2, L3, and L4, were randomly distributed inside the test box. The average CBR profile was obtained by averaging the CBR values from the four curves at the same depth. The average CBR values of the subgrade and base estimated by the vane shear tests and DCP tests are presented in Table 4.3. The average CBR value of the subgrade obtained from the vane shear tests was 5.1 %. Similarly, the average CBR values of the subgrade and the RAP base obtained from the DCP tests were 5.7 % and 10.9 % respectively. The test results indicated that the CBR value of the subgrade from the DCP tests is higher than that by the vane shear tests.

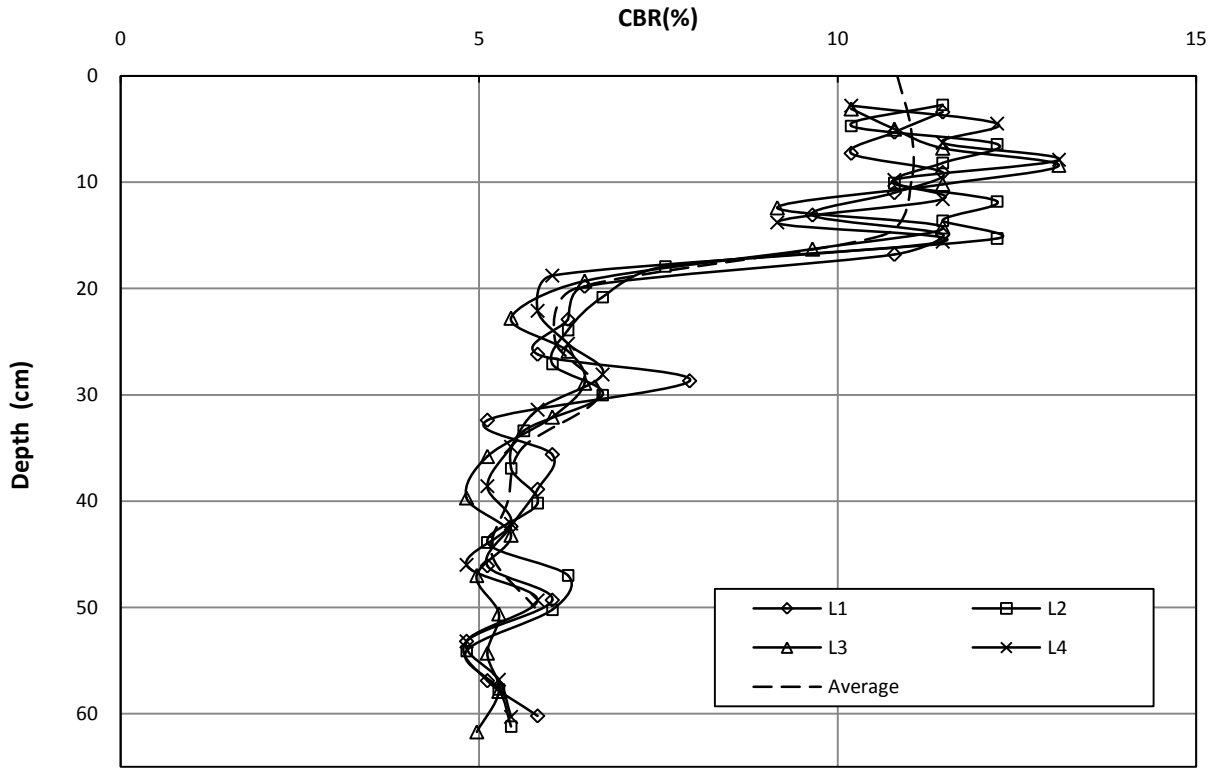

Figure 4.27 CBR profile obtained from DCP tests for the 15 cm thick geocell-reinforced RAP base section before the test

Table 4.3 The average CBR values of subgrade and base from vane shear test and DCP tests

Test method	CBR Value (%)						
	Subgrade at different locations						Base Layer
Vane Shear Test	1	2	3	4	5	Average	-
	5.9	5	5	5.1	4.8	5.1	
DCP Test	5.7						10.9

The calculated dynamic deformation moduli (E_{vd}) of the subgrade, base and HMA surface versus the size of the loading plate of the instrument from the LWD tests result are shown in Figure 4.28. The test results show that the E_{vd} values decreased from the HMA surface, the RAP base to the subgrade.

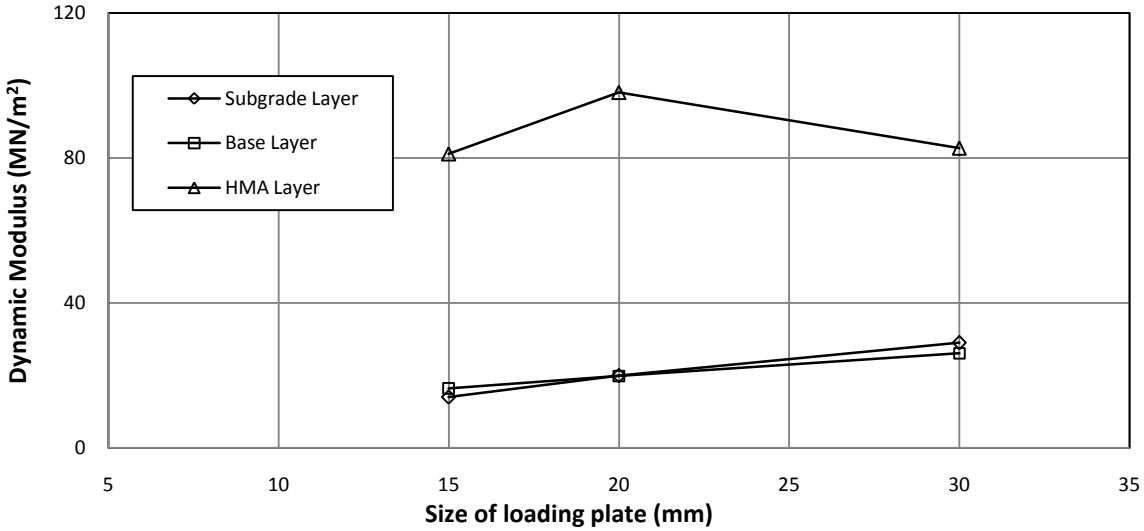

Figure 4.28 The calculated dynamic deformation modulus versus size of loading plate for the 15 cm thick geocell-reinforced RAP base section

The profiles of the HMA surfaces as shown in Fig. 4.29 were measured from the reference beam before and after the cyclic plate load test. It shows that a depression (equivalent to rutting under traffic) developed under the loading plate and some heaving occurred away from the loading plate after the test.

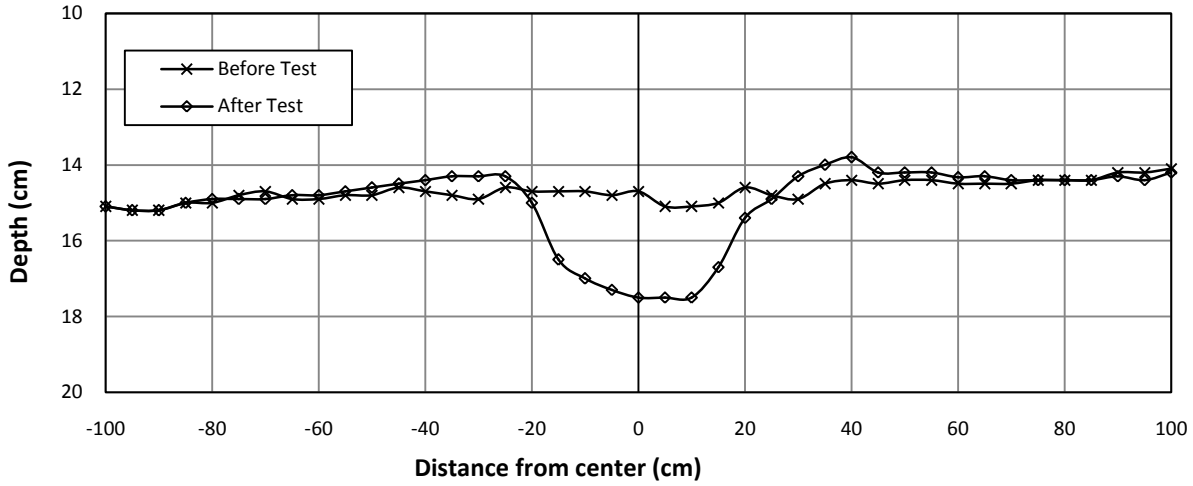

Figure 4.29 Profiles of the HMA surface before and after the test for the 15 cm thick geocell-reinforced RAP base section

The permanent deformation was obtained after unloading of each cycle. Figure 4.30 presents the measured permanent deformations of the pavement at the surface, at the top of the base, and at the top of the subgrade. The difference in the permanent deformations between the HMA surface and the base is the compression of the HMA surface while that between the base and the subgrade is the compression of the base course. The surface deformations at different distances from the center were obtained by the displacement transducers. It is shown that the surface permanent deformation was higher at the center and decreased at the distances of 25, and 50 cm away from the center. The elastic deformation (i.e., the rebound during the unloading of each cycle) is higher at the beginning of loading and then decreased slightly at a small rate until the end of the test as shown in Figure 4.31. The elastic deformation was much smaller than the permanent deformation and was less than 10% of the permanent deformation at the end of the test.

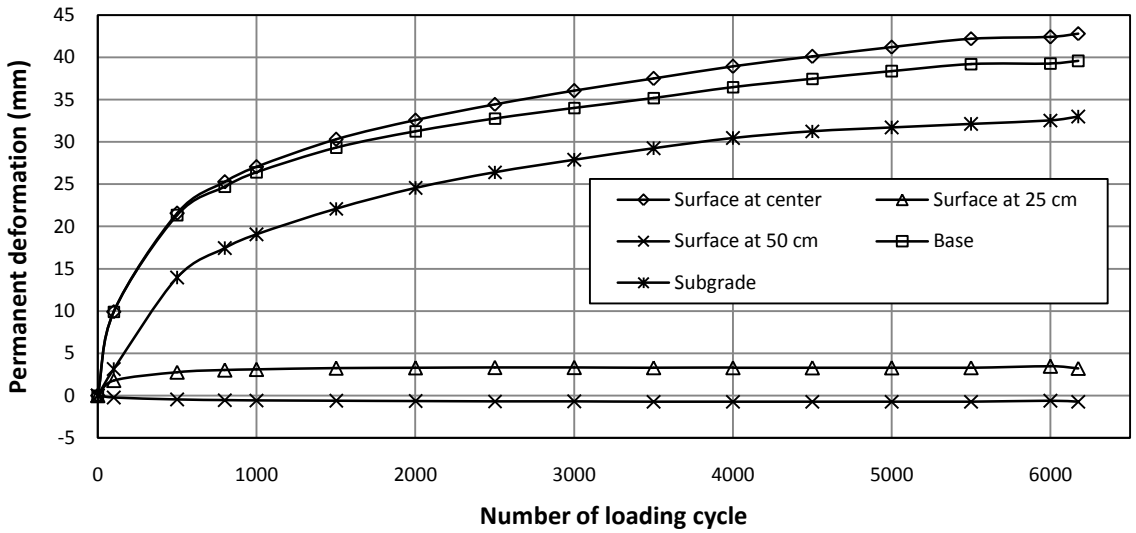

Figure 4.30 The permanent deformation versus number of loading cycle for the 15 cm thick geocell-reinforced RAP base section

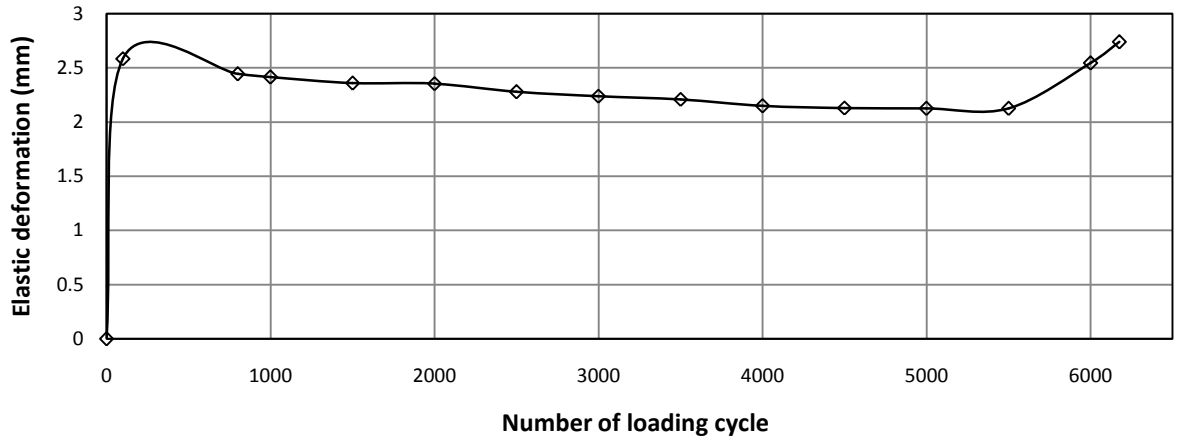

Figure 4.31 The elastic deformation versus number of loading cycle for the 15 cm thick geocell-reinforced RAP base section

Figure 4.32 shows the measured maximum strains on the geocell wall at different locations during the cyclic plate load test. The maximum strains were recorded manually during the test. It is shown that the tensile strains developed at all of the top gages while the compressive strains occurred at the middle gauges. The strain at the bottom gauge of the central

geocell and top gauge of third geocell could not measure as they broke down during construction of base layer.

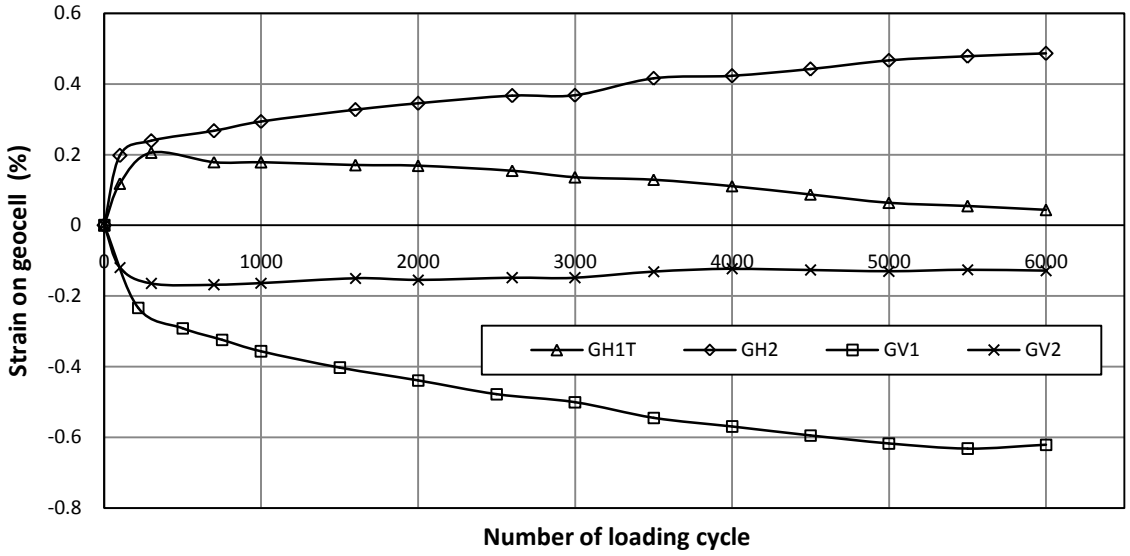

Figure 4.32 The measured strains on the geocell wall in different locations for the 15 cm thick geocell-reinforced RAP base section

The strains at the bottom of the HMA surface were measured by the pavement strain gauges at distances 0, 12.5, 25, 50, and 75 cm away from center as shown in Fig. 4.33. In this research, the strain is positive under tension and negative at compression. The bottom of the HMA surface at 0 and 25 cm from the center were under tension while 50 and 75 cm from center was under compression up to the end of the test. However, there was compression up to 2200 cycle and changed to tension up to the end of the test at a distance 12.5 cm from center.

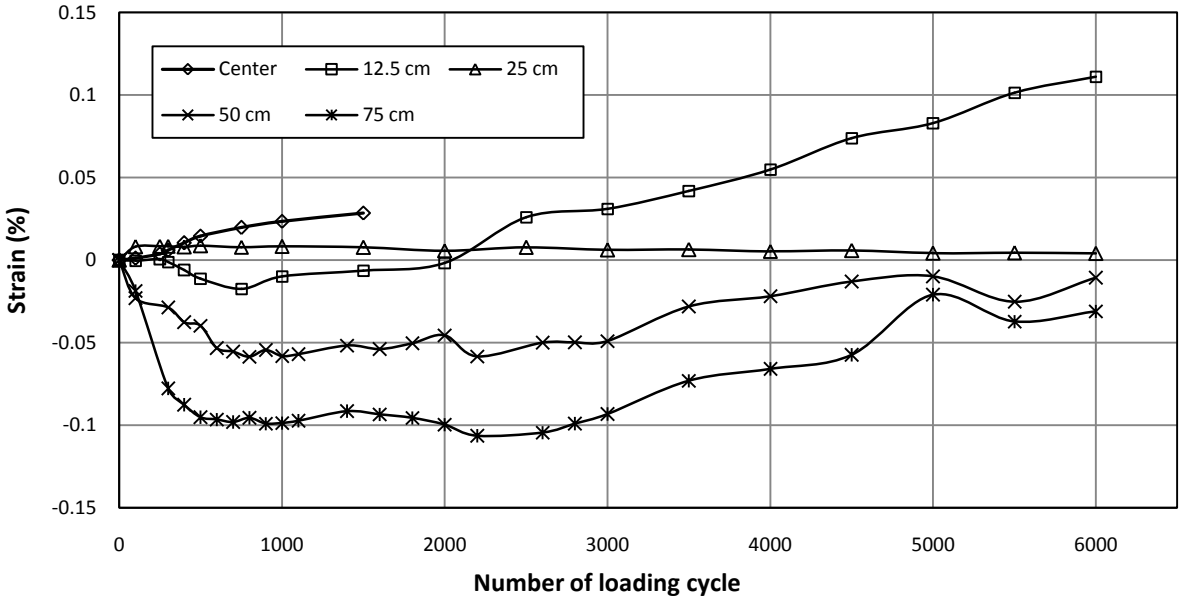

Figure 4.33 The strain at the bottom of the HMA surface versus the number of loading cycle for the 15 cm thick geocell-reinforced RAP base section

Figure 4.34 shows the measured vertical stresses at the interface between subgrade and base at five locations (center, 12.5, 25, 50, and 75 cm away from the center) versus the number of loading cycles. It is shown that vertical stresses at the center or close to the center were much higher than those away from center. The vertical stress at the distance of 75 cm away from the center is almost zero. As discussed earlier, the vertical stress at the center was used to calculate the stress distribution angle. The stress distribution angle versus the number of loading cycle is shown in Fig. 4.35. The stress distribution angle decreased with an increase of the load cycle in small rate up to the end of the test.

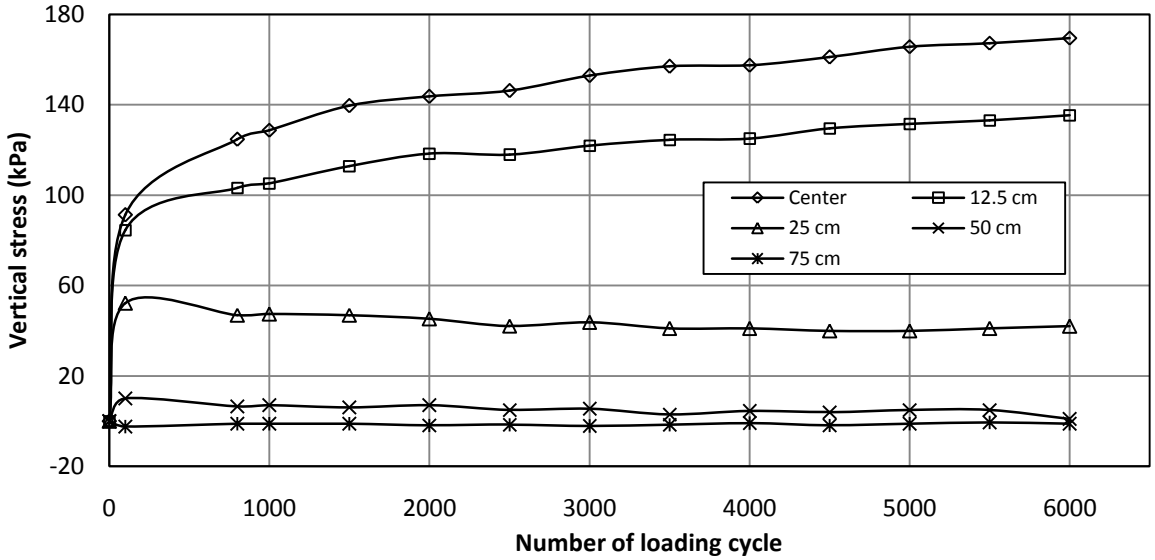

Figure 4.34 The vertical stress at the interface between subgrade and base versus the number of loading cycle for the 15 cm thick geocell-reinforced RAP base section

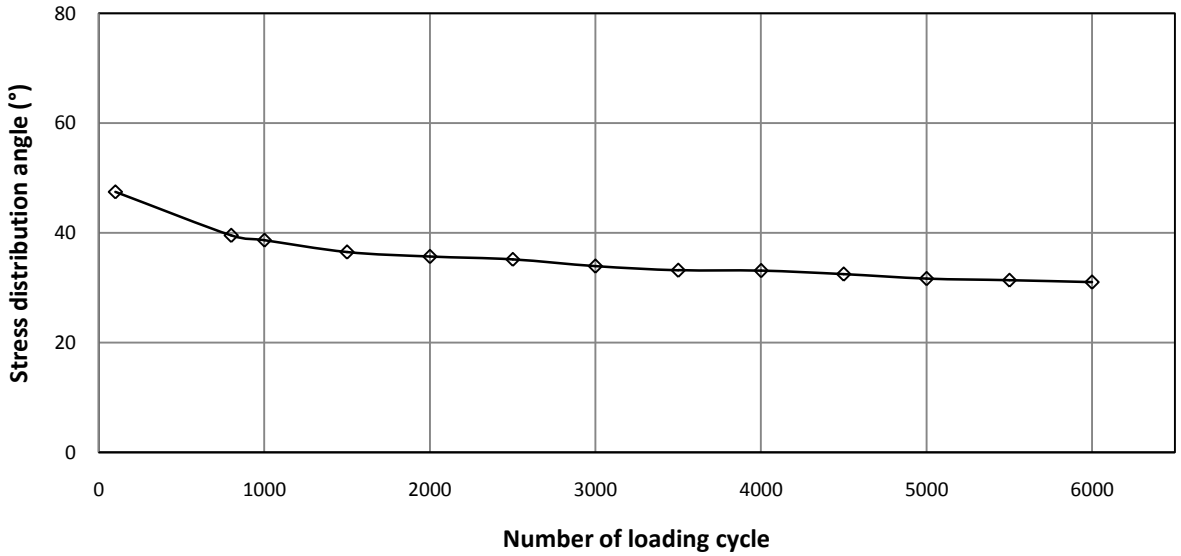

Figure 4.35 The stress distribution angle versus number of loading cycle for 15 cm thick geocell-reinforced RAP base section

4.3.5 23 cm thick geocell-reinforced RAP base section

The CBR profile of the test section obtained from the DCP tests is shown in Figure 4.36. The locations of the DCP tests, L1, L2, L3, and L4, were randomly distributed inside the test box. The average CBR profile was obtained by averaging the CBR values from the four curves at the same depth. The average CBR values of the subgrade and base estimated by the vane shear tests and DCP tests are presented in Table 4.4. The average CBR value of the subgrade obtained from the vane shear tests was 5.1 %. Similarly, the average CBR values of the subgrade and the RAP base obtained from the DCP tests were 5.9 % and 10.7 % respectively. The test results indicated that the CBR value of the subgrade from the DCP tests is higher than that by the vane shear tests.

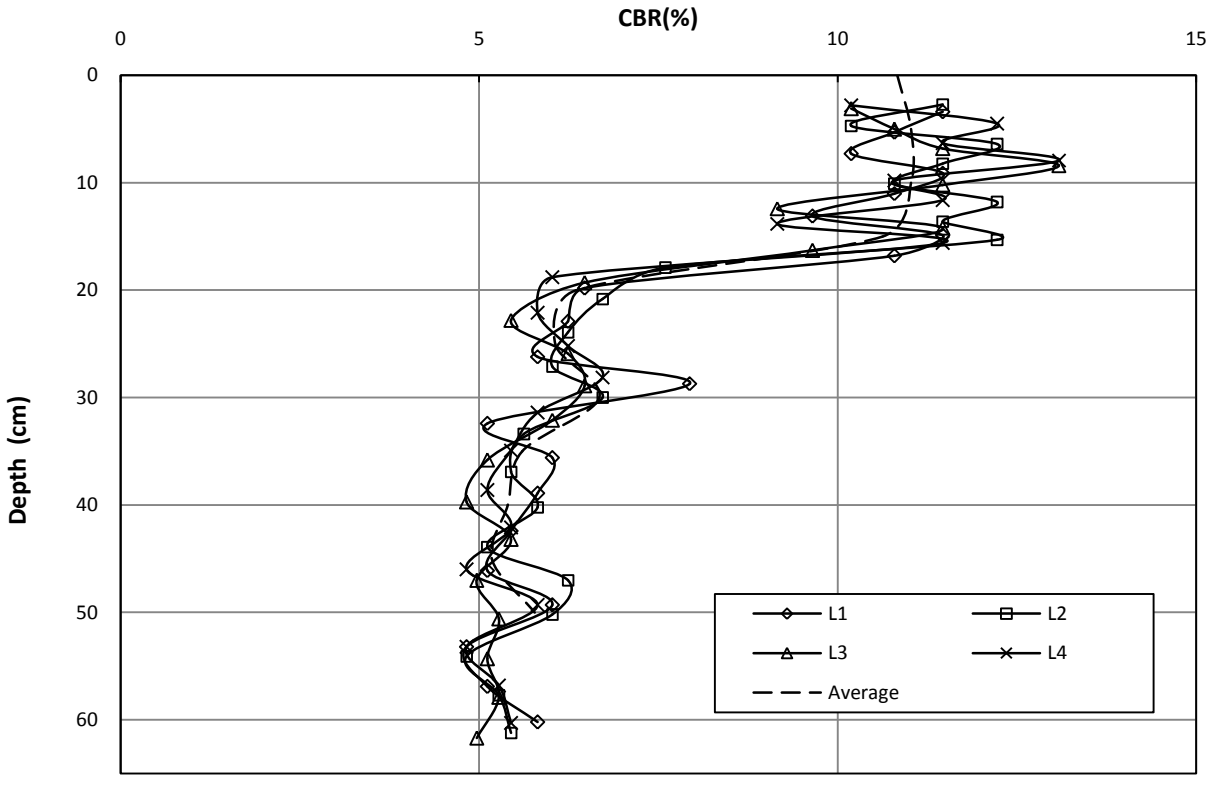

Figure 4.36 CBR profile obtained from DCP tests for the 23 cm thick geocell-reinforced RAP base section before the test

Table 4.4 The average CBR values of subgrade and base from vane shear test and DCP tests

Test method	CBR Value (%)						
	Subgrade at different locations						Base Layer
Vane Shear Test	1	2	3	4	5	Average	-
	5.1	4.6	5.1	5.7	5.3	5.1	
DCP Test	5.9						10.7

The calculated dynamic deformation moduli (E_{vd}) of the subgrade, base and HMA surface versus the size of the loading plate of the instrument from the LWD tests result are shown in Figure 4.37. The test results show that the E_{vd} values decreased from the HMA surface, the RAP base to the subgrade.

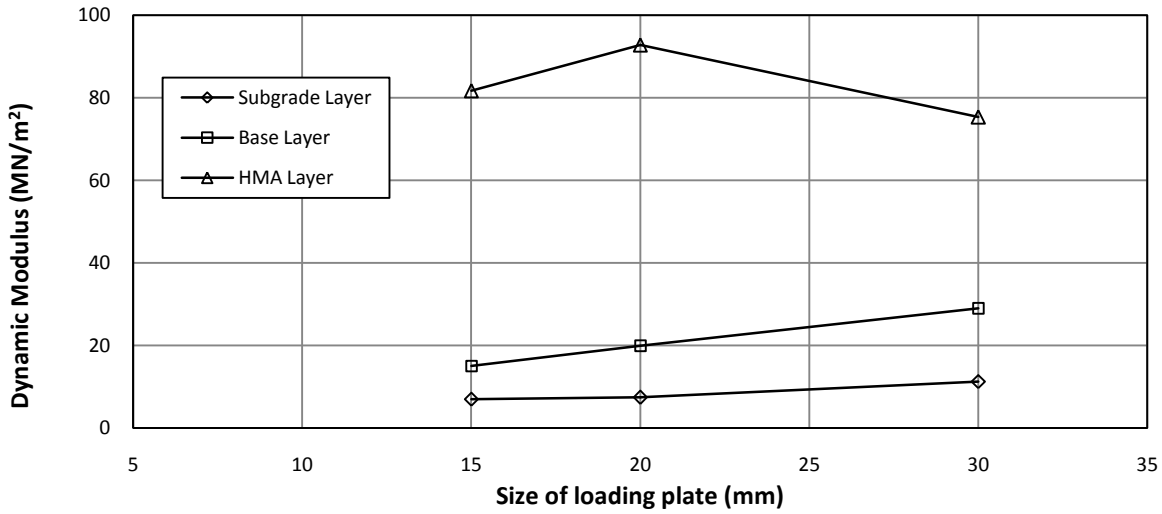

Figure 4.37 The calculated dynamic deformation modulus versus size of loading plate for the 23 cm thick geocell-reinforced RAP base section

The profiles of the HMA surfaces as shown in Fig. 4.38 were measured from the reference beam before and after the cyclic plate load test. It shows that a depression (equivalent to rutting under traffic) developed under the loading plate and some heaving occurred away from the loading plate after the test.

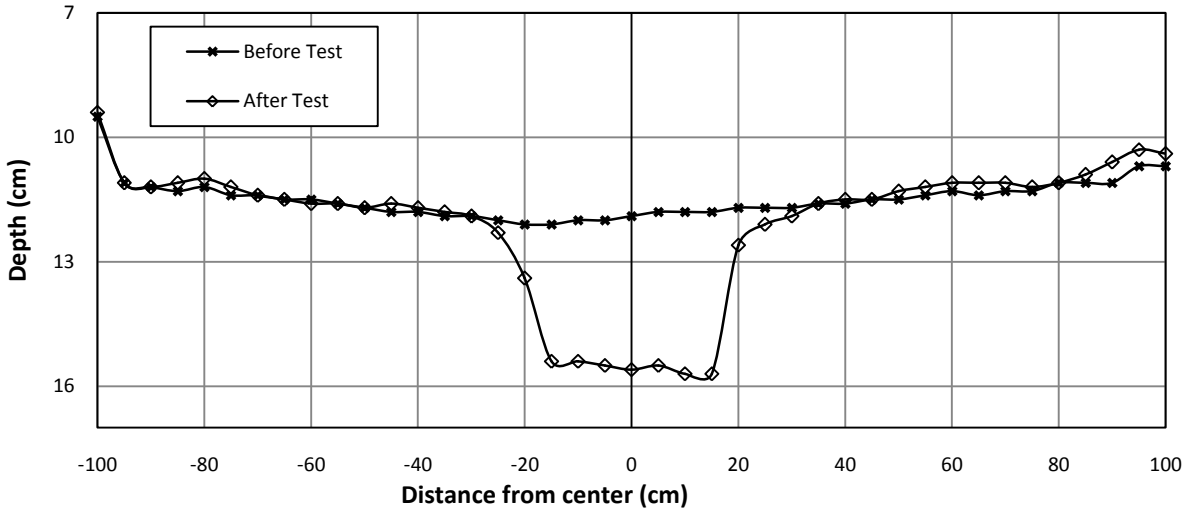

Figure 4.38 Profiles of the HMA surface before and after the test for the 23 cm thick geocell-reinforced RAP base section

The permanent deformation was obtained after unloading of each cycle. Figure 4.39 presents the measured permanent deformations of the pavement at the surface, at the top of the base, and at the top of the subgrade. The difference in the permanent deformations between the HMA surface and the base is the compression of the HMA surface while that between the base and the subgrade is the compression of the base course. The surface deformations at different distances from the center were obtained by the displacement transducers. It is shown that the surface permanent deformation was higher at the center and decreased at the distances of 25, and 50 cm away from the center. The elastic deformation (i.e., the rebound during the unloading of each cycle) is higher at the beginning of loading and then decreased slightly at a small rate until the end of the test as shown in Figure 4.40. The elastic deformation was much smaller than the permanent deformation and was less than 10% of the permanent deformation at the end of the test.

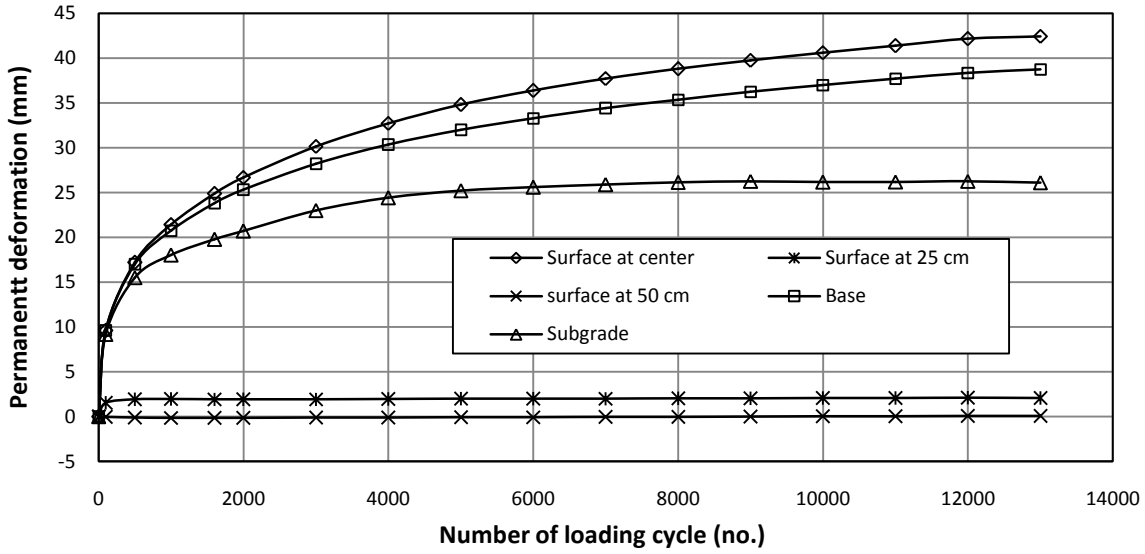

Figure 4.39 The permanent deformation versus number of loading cycle for the 23 cm thick geocell-reinforced RAP base section

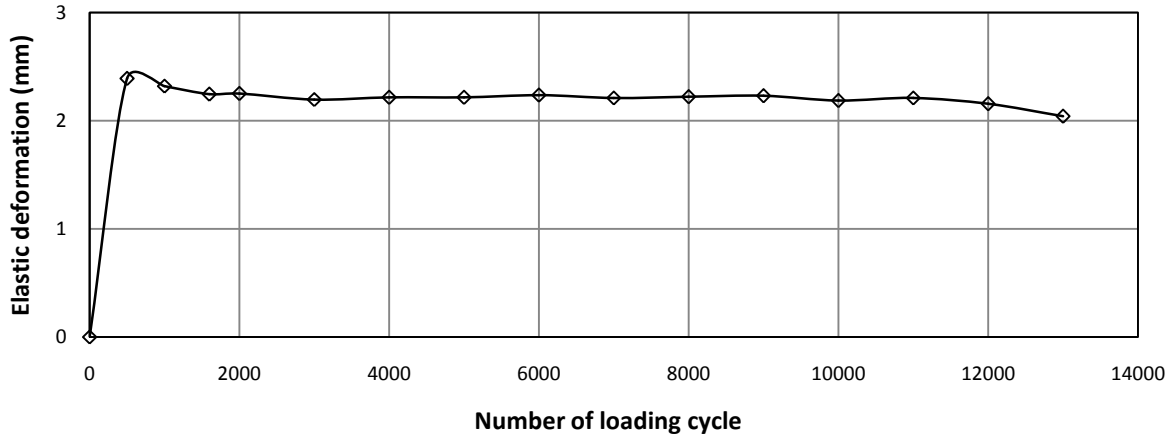

Figure 4.40 The elastic deformation versus number of loading cycle for the 23 cm thick geocell-reinforced RAP base section

Figure 4.41 shows the measured maximum strains on the geocell wall at different locations during the cyclic plate load test. The maximum strains were recorded manually during the test. It is shown that the tensile strains developed at gages GH1B, GH2, and GH3 while the compressive strains occurred at GH1T and GV1 respectively. Compressive strain developed at the beginning up to 3000 cycles and changed to tensile strain at GV2 up to the end of the test.

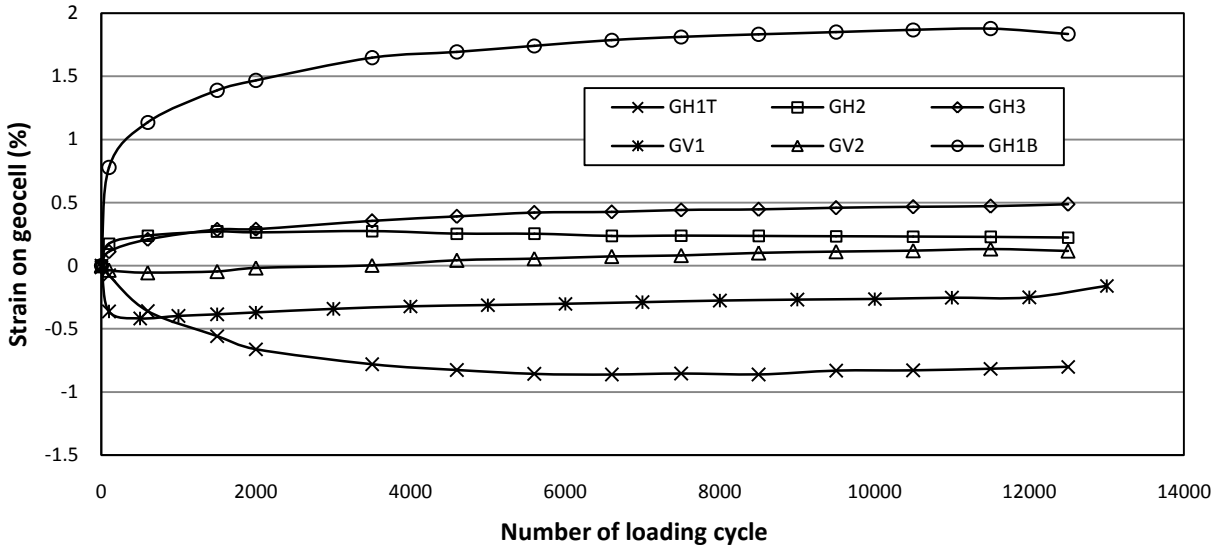

Figure 4.41 The measured strains on the geocell wall in different locations for the 23 cm thick geocell-reinforced RAP base section

The strains at the bottom of the HMA surface were measured by the pavement strain gauges at distances 0, 12.5, 25, 50, and 75 cm away from center as shown in Fig. 4.42. In this research, the strain is positive under tension and negative at compression. The bottom of the HMA surface at 0 and 25 cm from the center were under tension while 50 and 75 cm from center was under compression up to the end of the test. However, there was tension up to 3400 cycle and changed to compression up to the end of the test at a distance 12.5 cm from center.

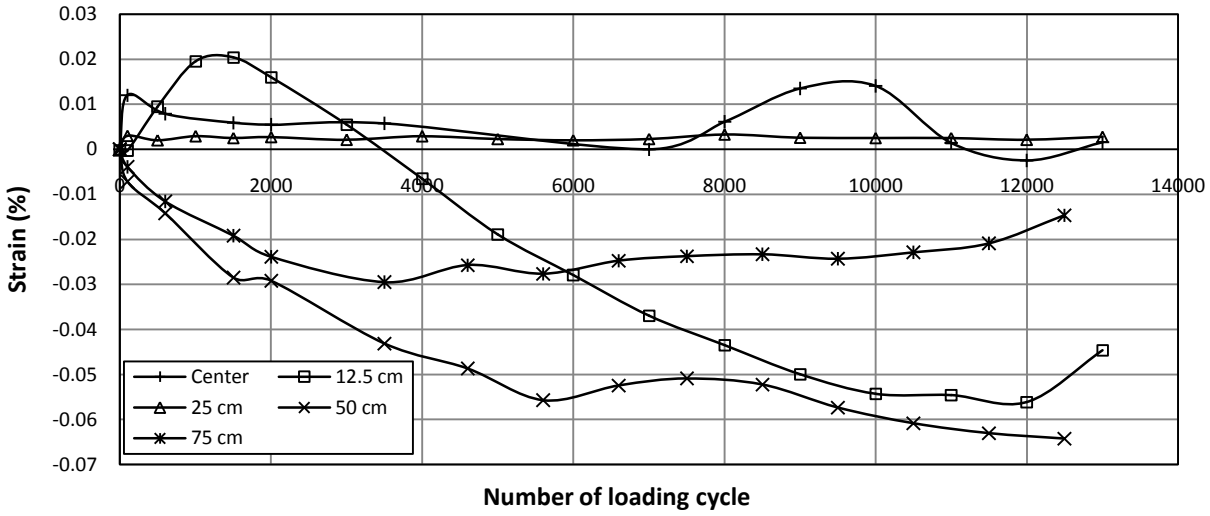

Figure 4.42 The strain at the bottom of the HMA surface versus the number of loading cycle for the 23 cm thick geocell-reinforced RAP base section

Figure 4.43 shows the measured vertical stresses at the interface between subgrade and base at five locations (center, 12.5, 25, 50, and 75 cm away from the center) versus the number of loading cycles. It is shown that vertical stress is higher at a distance 12.5 cm than at the center and decrease at the distances 25 cm, and 50 cm away from the center. The vertical stress at the distance of 75 cm away from the center is almost zero. As discussed earlier, the vertical stress at the center was used to calculate the stress distribution angle. The stress distribution angle versus the number of loading cycle is shown in Fig. 4.44. The stress distribution angle decreased with an increase of the load cycle in small rate up to the end of the test.

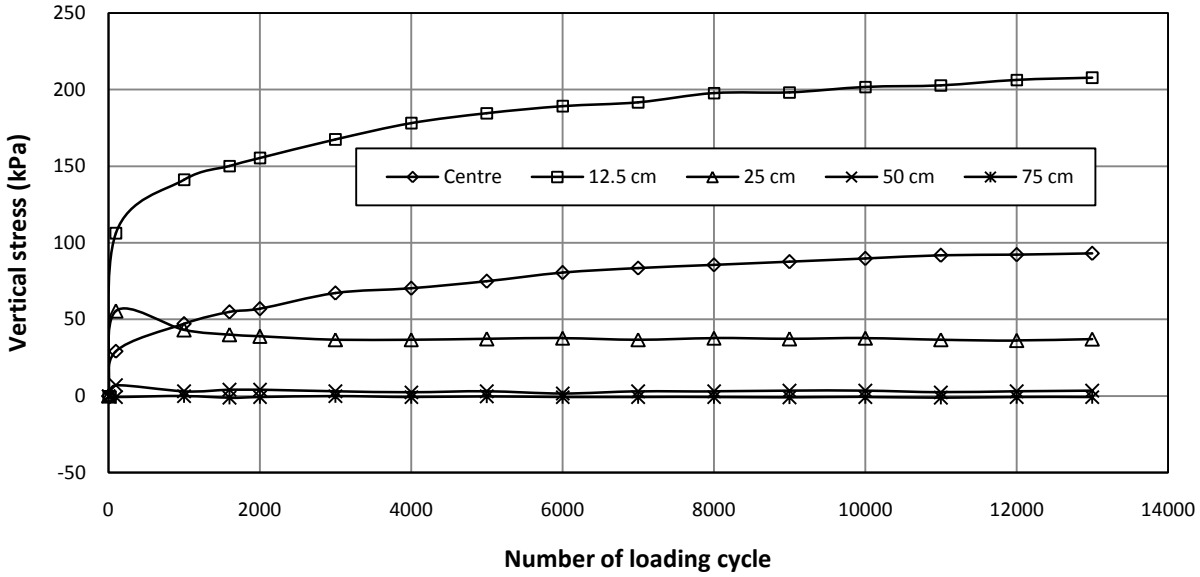

Figure 4.43 The vertical stress at the interface between subgrade and base versus the number of loading cycle for the 23 cm thick geocell-reinforced RAP base section

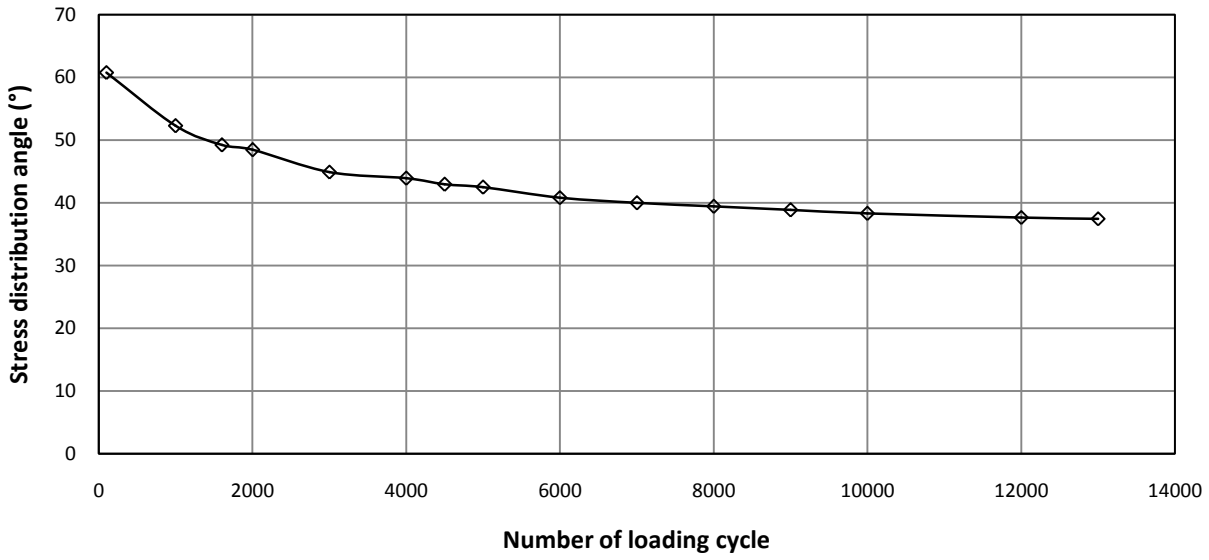

Figure 4.44 The stress distribution angle versus number of loading cycle for 23 cm thick geocell-reinforced RAP base section

4.3.6 30 cm thick unreinforced RAP base section

The CBR profile of the test section obtained from the DCP tests is shown in Figure 4.45. The locations of the DCP tests, L1, L2, L3, and L4, were randomly distributed inside the test box. The average CBR profile was obtained by averaging the CBR values from the four curves at the same depth. The average CBR values of the subgrade and base estimated by the vane shear tests and DCP tests are presented in Table 4.5. The average CBR value of the subgrade obtained from the vane shear tests was 5.1 %. Similarly, the average CBR values of the subgrade and the RAP base obtained from the DCP tests were 5.6 % and 9.9 % respectively. The test results indicated that the CBR value of the subgrade from the DCP tests is higher than that by the vane shear tests.

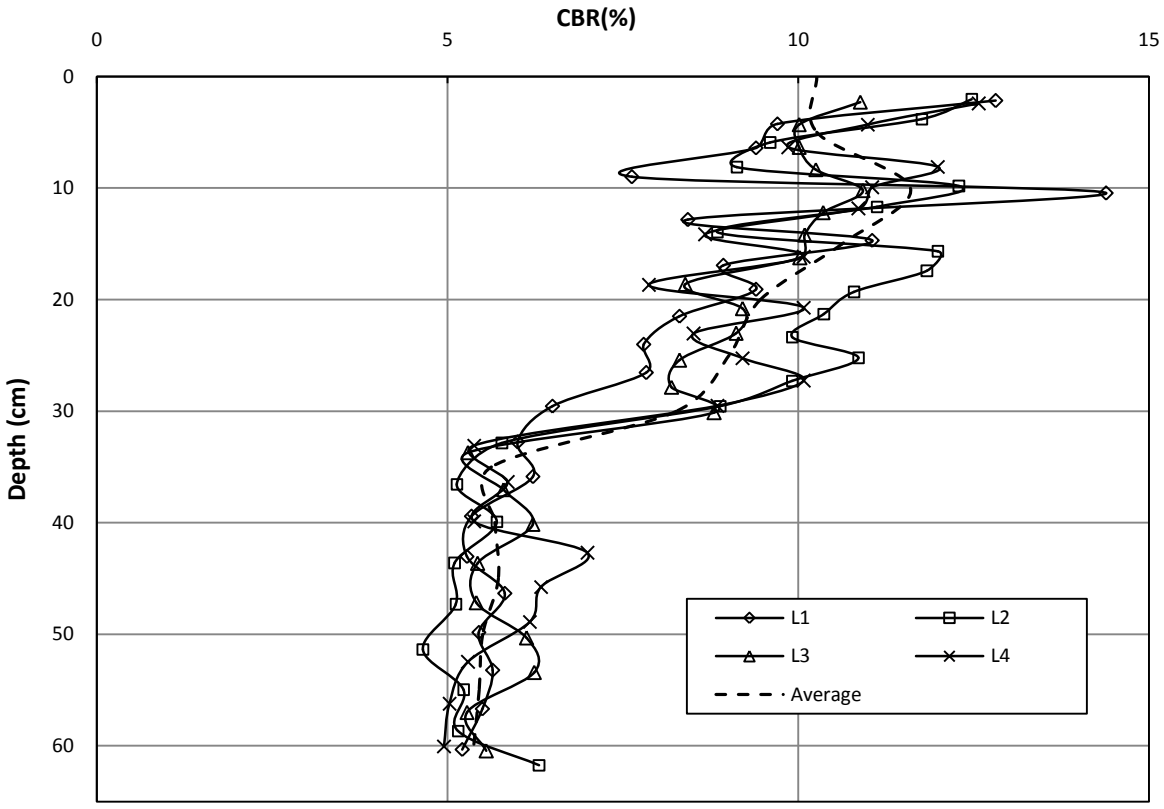

Figure 4.45 The CBR profile obtained from the DCP tests for the 30 cm thick unreinforced RAP base section

Table 4.5 The average CBR values of subgrade and base from the vane shear tests and DCP tests

Test method	CBR Value (%)						
	Subgrade at different locations						Base Layer
Vane Shear Test	1	2	3	4	5	Average	-
	5.1	5.1	5.7	4.6	5.3	5.1	
DCP Test	5.6						9.9

The calculated dynamic deformation moduli (E_{vd}) of the subgrade, base and HMA surface versus the size of the loading plate of the instrument from the LWD tests result are shown in Figure 4.46. The test results show that the E_{vd} values decreased from the HMA surface, the RAP base to the subgrade.

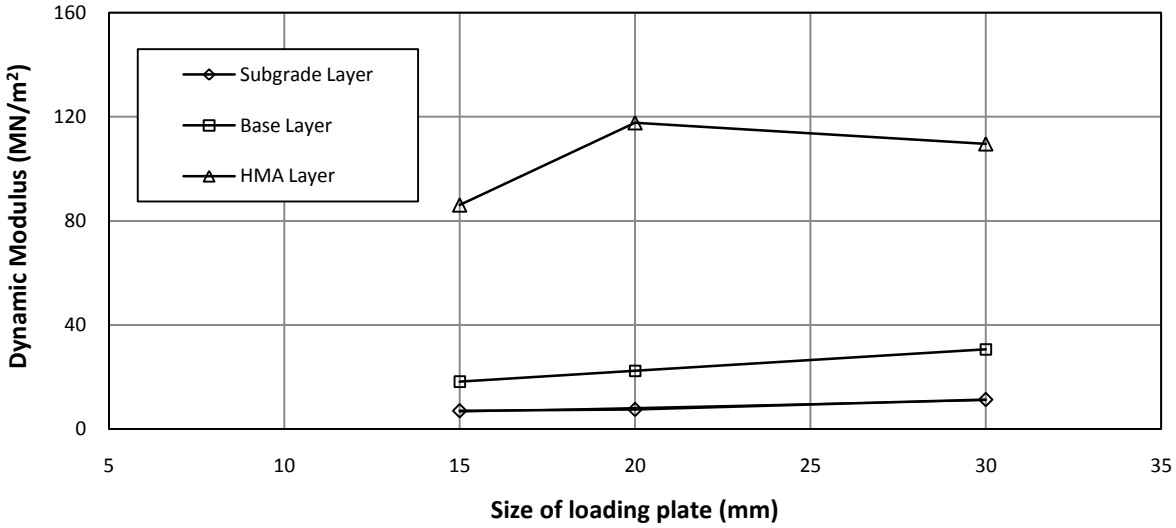

Figure 4.46 The calculated dynamic deformation modulus versus the size of loading plate for the 30 cm thick unreinforced RAP base section

The profiles of the HMA surfaces as shown in Fig. 4.47 were measured from the reference beam before and after the cyclic plate load test. It shows that a depression (equivalent to rutting under traffic) developed under the loading plate and some heaving occurred away from the loading plate after the test.

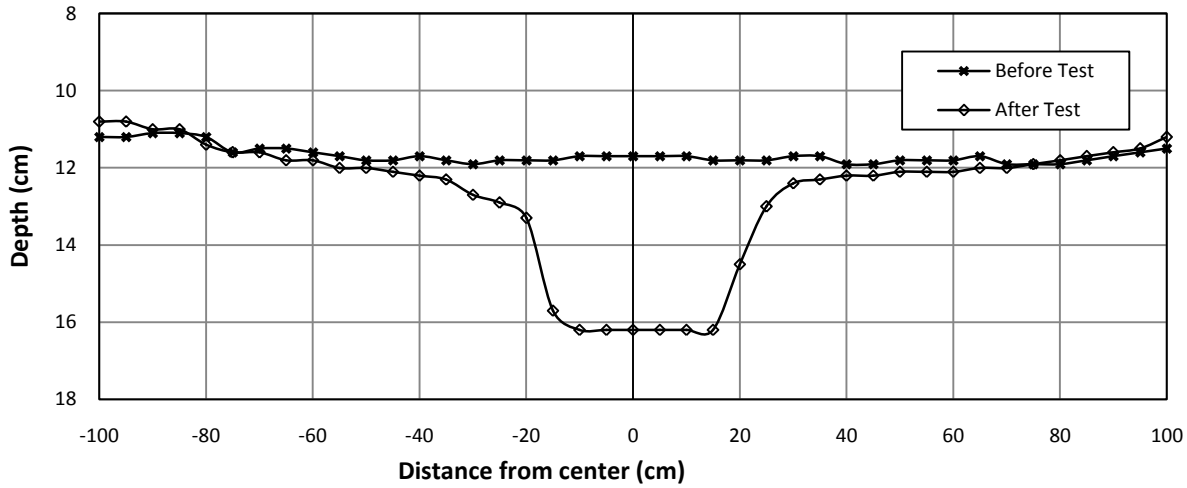

Figure 4.47 Profiles of the HMA surface before and after the test for the 30 cm thick unreinforced RAP base section

The permanent deformation was obtained after unloading of each cycle. Figure 4.48 presents the measured permanent deformations of the pavement at the surface, at the top of the base, and at the top of the subgrade. The difference in the permanent deformations between the HMA surface and the base is the compression of the HMA surface while that between the base and the subgrade is the compression of the base course. At the end of the test, the permanent deformation of the subgrade was approximately 50% of the total permanent deformation. The surface deformations at different distances from the center were obtained by the displacement transducers while the deformations at the top of the base and subgrade were obtained by the tell tales. It is shown that the surface permanent deformation was higher at the center and decreased at the distances of 25, and 50 cm away from the center. The elastic deformation (i.e., the rebound during the unloading of each cycle) as shown in Fig. 4.49 increased up to 200 cycles of loading and then decreased slightly at a small rate until the end of the test. The elastic deformation was much smaller than the permanent deformation and was less than 10% of the permanent deformation at the end of the test.

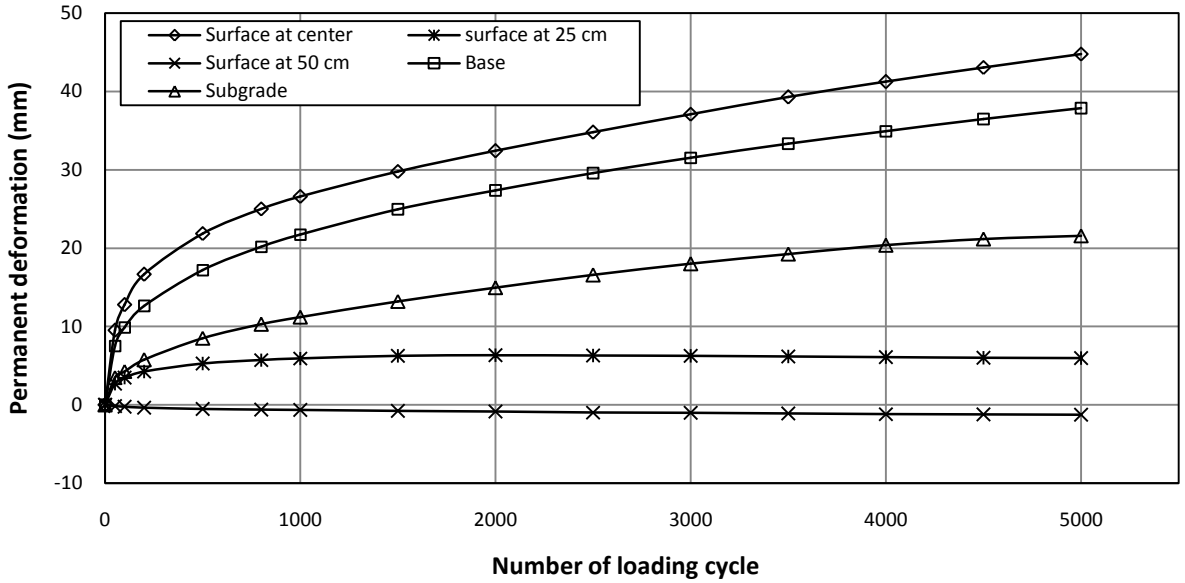

Figure 4.48 The permanent deformation versus the number of loading cycle for the 30 cm thick unreinforced RAP base section

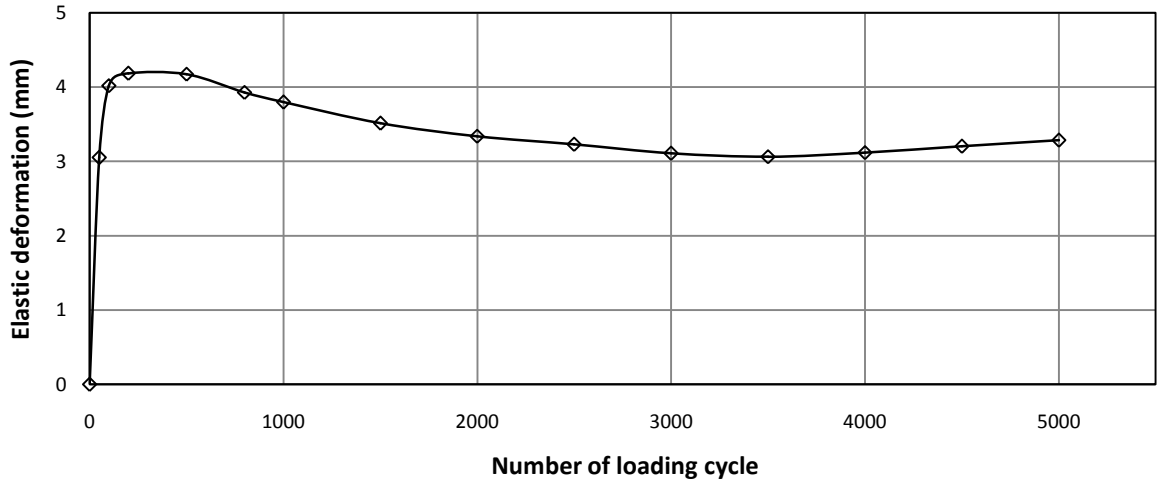

Figure 4.49 The elastic deformation versus the number of loading cycle for the 30 cm thick unreinforced RAP base section

The strains at the bottom of the HMA surface were measured by the pavement strain gauges at the center and 12.5 cm away from the center as shown in Fig. 4.50. In this research, the strain is positive under tension and negative at compression. The bottom of the HMA surface at the center was under compression from the beginning up to 3200 cycles and then became

under tension up to the end of the test even though the magnitude of the strain was small. However, the tensile strain developed at the bottom of the HMA surface at the distance of 12.5 cm away from the center.

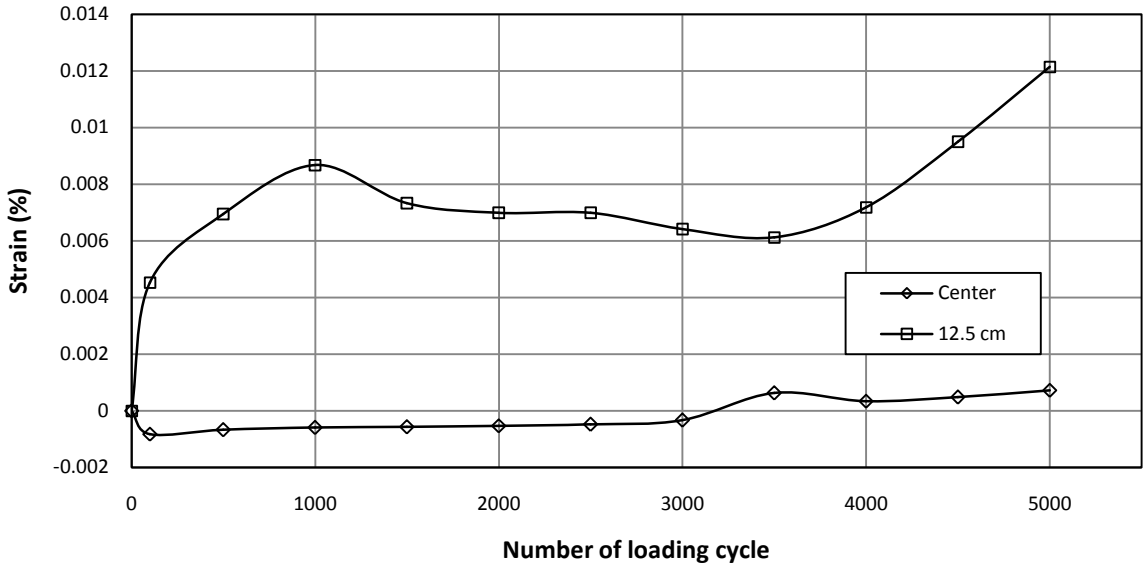

Figure 4.50 The strain at the bottom of the HMA surface versus the number of loading cycle for the 30 cm thick unreinforced RAP base section

Figure 4.51 shows the measured vertical stresses at the interface between subgrade and base at five locations (center, 12.5, 25, 50, and 75 cm away from the center) versus the number of loading cycles. It is shown that the vertical stresses at the center or close to the center were much higher than those away from the center. The vertical stress at the distance of 75 cm away from the center is almost zero. As discussed earlier, the vertical stress at the center was used to calculate the stress distribution angle. The stress distribution angle versus the number of loading cycle is shown in Fig. 4.52. The stress distribution angle decreased with an increase of the load cycle and remained almost the same after 50 loading cycles.

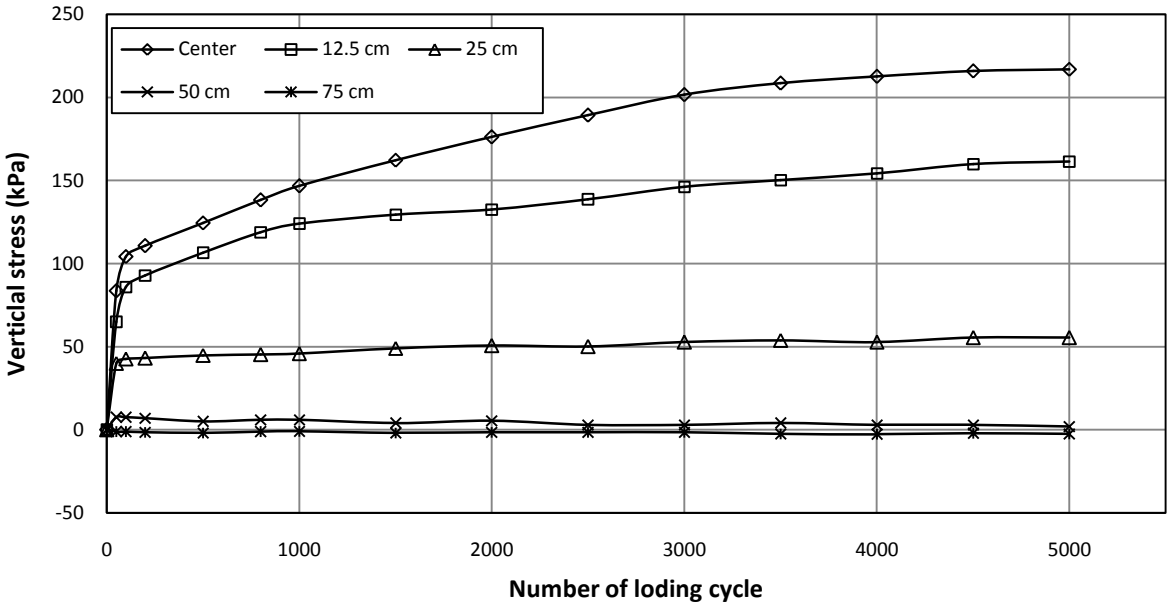

Figure 4.51 The vertical stress at the interface between subgrade and base versus the number of loading cycle for the 30 cm thick unreinforced RAP base section

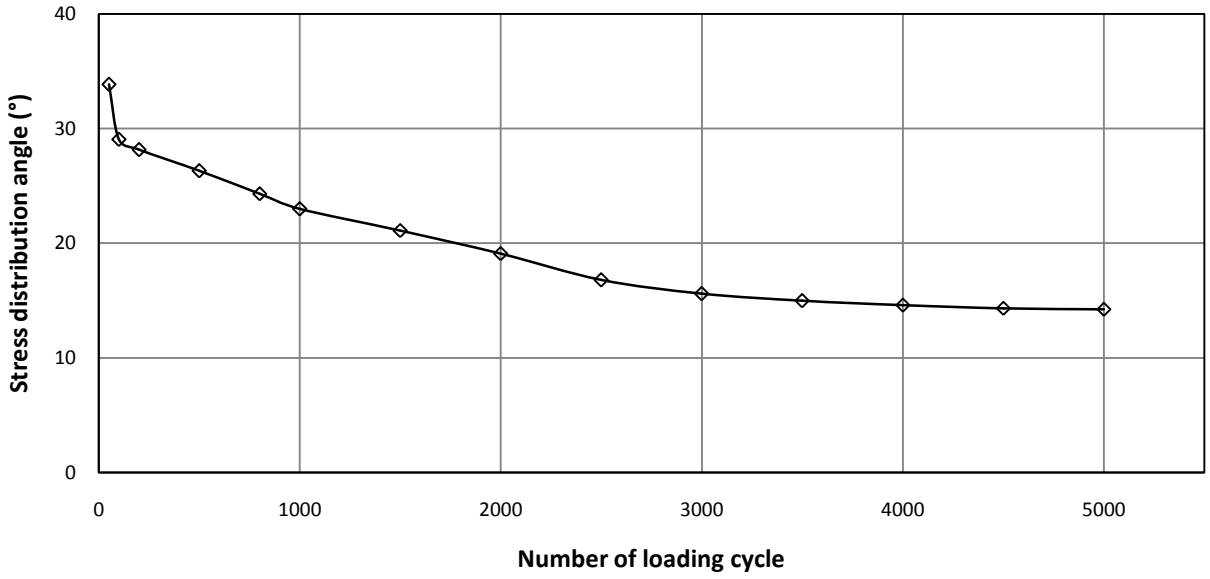

Figure 4.52 The stress distribution angle versus the number of loading cycle for the 30 cm thick unreinforced RAP base section

4.3.7 30 cm thick geocell-reinforced RAP base section

The CBR profile of the test section obtained from the DCP tests is shown in Figure 4.53. The locations of the DCP tests, L1, L2, L3, and L4, were randomly distributed inside the test box. The average CBR profile was obtained by averaging the CBR values from the four curves at the same depth. The average CBR values of the subgrade and base estimated by the vane shear tests and DCP tests are presented in Table 4.6. The average CBR value of the subgrade obtained from the vane shear tests was 5.3 %. Similarly, the average CBR values of the subgrade and the RAP base obtained from the DCP tests were 6.1 % and 8.9 % respectively. The test results indicated that the CBR value of the subgrade from the DCP tests is higher than that by the vane shear tests.

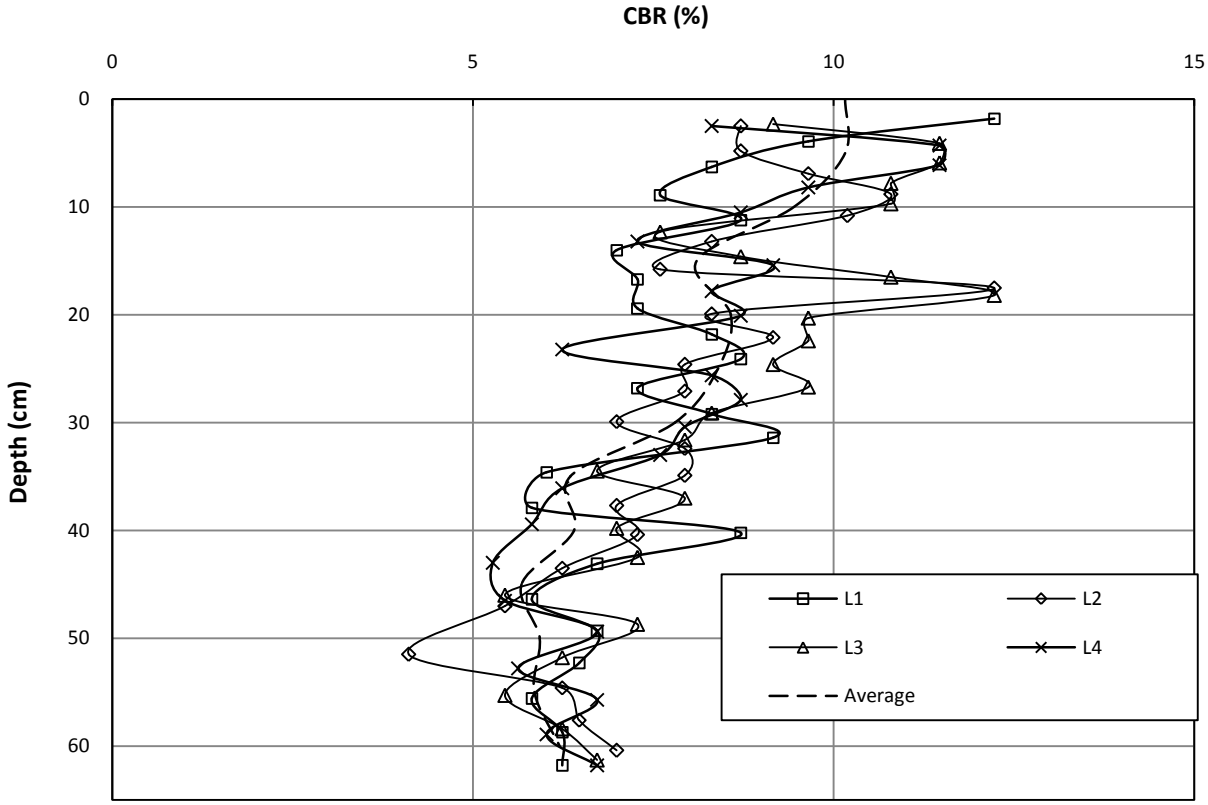

Figure 4.53 CBR profile obtained from DCP tests for the 30 cm thick geocell-reinforced RAP base section before the test

Table 4.6 The average CBR values of subgrade and base from vane shear test and DCP tests

Test method	CBR Value (%)						
	Subgrade at different locations						Base Layer
Vane Shear Test	1	2	3	4	5	Average	-
	5.4	5.6	4.8	5.1	5.5	5.3	
DCP Test	6.1						8.9

The calculated dynamic deformation moduli (E_{vd}) of the subgrade, base and HMA surface versus the size of the loading plate of the instrument from the LWD tests result are shown in Figure 4.54. The test results show that the E_{vd} values decreased from the HMA surface, the RAP base to the subgrade.

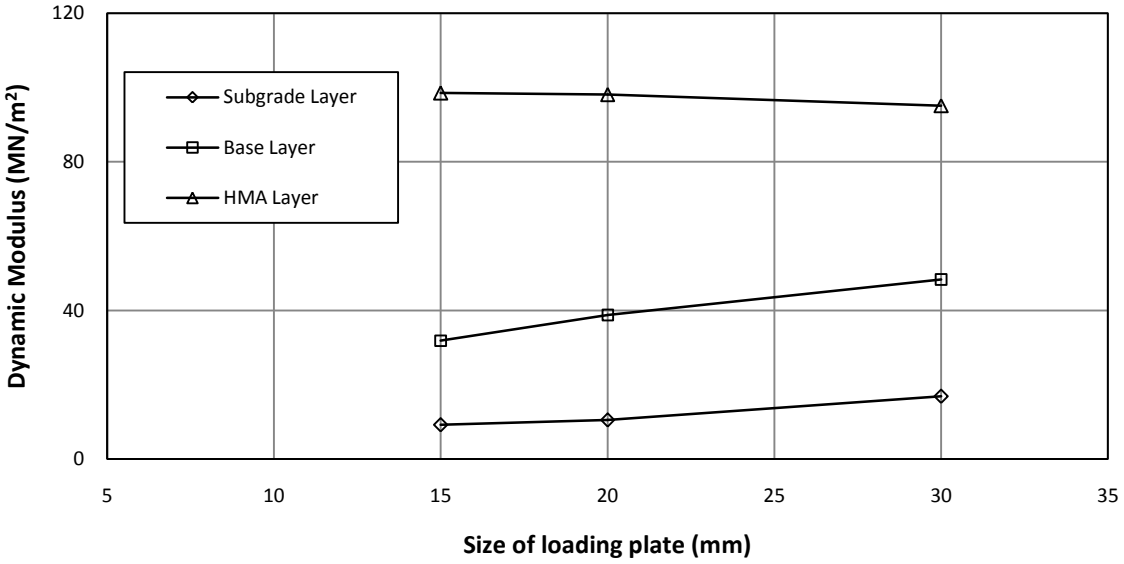

Figure 4.54 The calculated dynamic deformation modulus versus size of loading plate for the 30 cm thick geocell-reinforced RAP base section

The profiles of the HMA surfaces as shown in Fig. 4.55 were measured from the reference beam before and after the cyclic plate load test. It shows that a depression (equivalent

to rutting under traffic) developed under the loading plate and some heaving occurred away from the loading plate after the test.

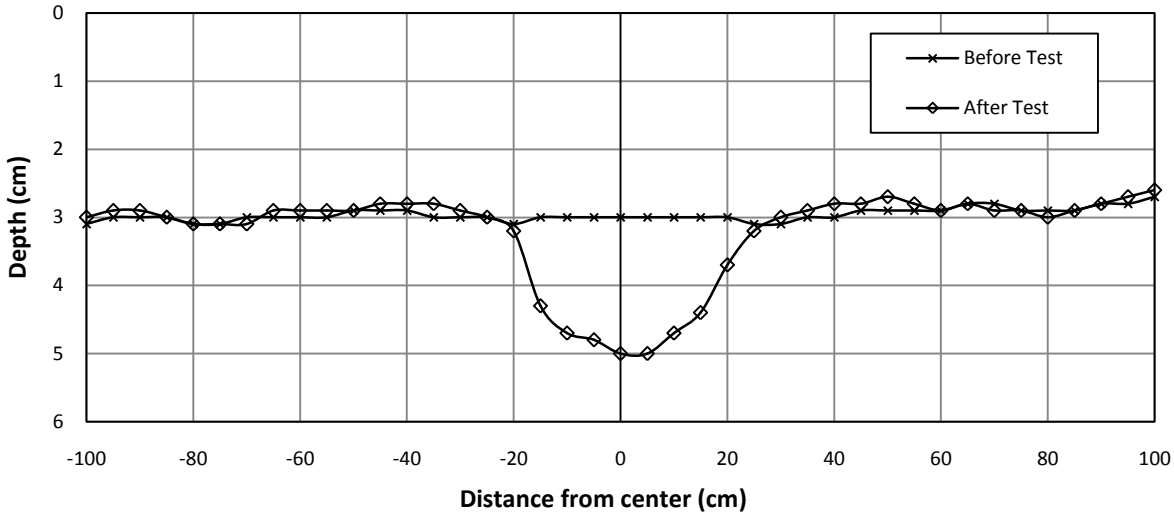

Figure 4.55 Profiles of the HMA surface before and after the test for the 30 cm thick geocell-reinforced RAP base section

The permanent deformation was obtained after unloading of each cycle. Figure 4.56 presents the measured permanent deformations of the pavement at the surface, at the top of the base, and at the top of the subgrade. The surface deformations at different distances from the center were obtained by the displacement transducers. It is shown that the surface permanent deformation was higher at the center and decreased at the distances of 2, 50, and 75 cm away from the center. However, the permanent deformation at 50 and 75 cm away from center were very lower than center. The elastic deformation (i.e., the rebound during the unloading of each cycle) is higher at the beginning of loading and then decreased slightly at a small rate until the end of the test as shown in Figure 4.57. The elastic deformation was much smaller than the permanent deformation and was less than 10% of the permanent deformation at the end of the test.

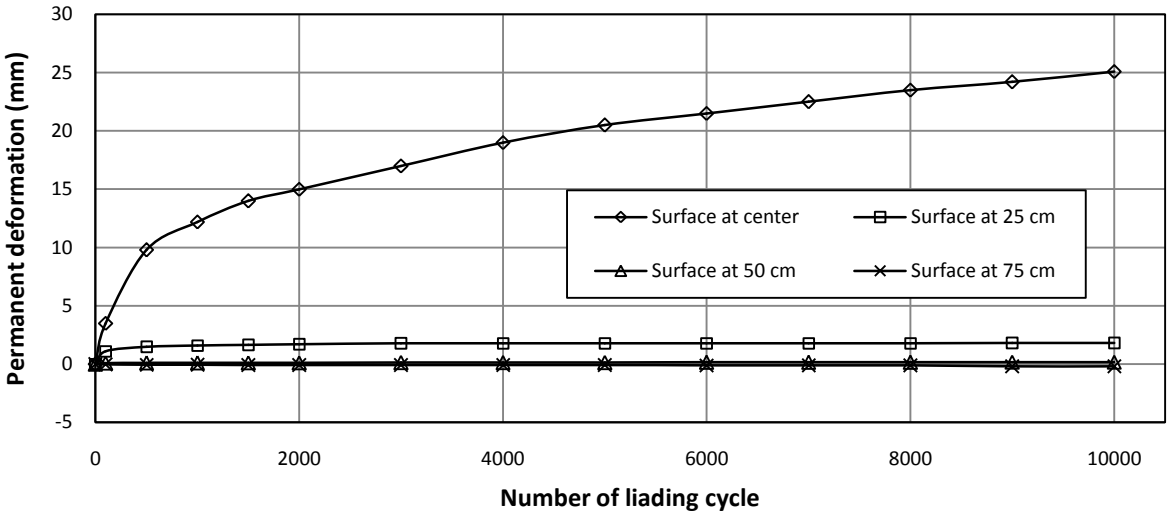

Figure 4.56 The permanent deformation versus number of loading cycle for the 30 cm thick geocell-reinforced RAP base section

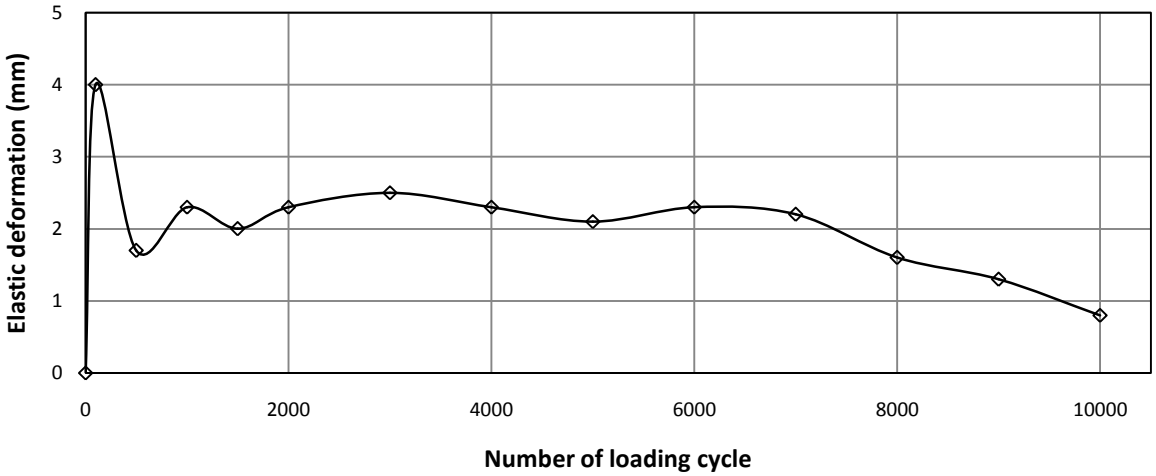

Figure 4.57 The elastic deformation versus number of loading cycle for the 30 cm thick geocell-reinforced RAP base section

Figures 4.58 and 4.59 shows the measured maximum strains on the top geocell and bottom geocell wall at different locations during the cyclic plate load test. The maximum strains were recorded manually during the test. For top geocell, it is shown that the tensile strains developed at all of horizontal strain gauges GH1T, GH2, and GH3 while the compressive strains occurred at strain gauges GV1 and GV2 respectively. The strain gauge GH1B of the top geocell

was broken during preparation of RAP base. For bottom geocell, it is shown that the tensile strains developed at all of horizontal strain gauges GH1T, GH2, and GH3 while the compressive strains occurred at strain gauges GV1 and GV2 respectively. Compressive strain with very small magnitude developed in strain gauge GH1B in bottom geocell.

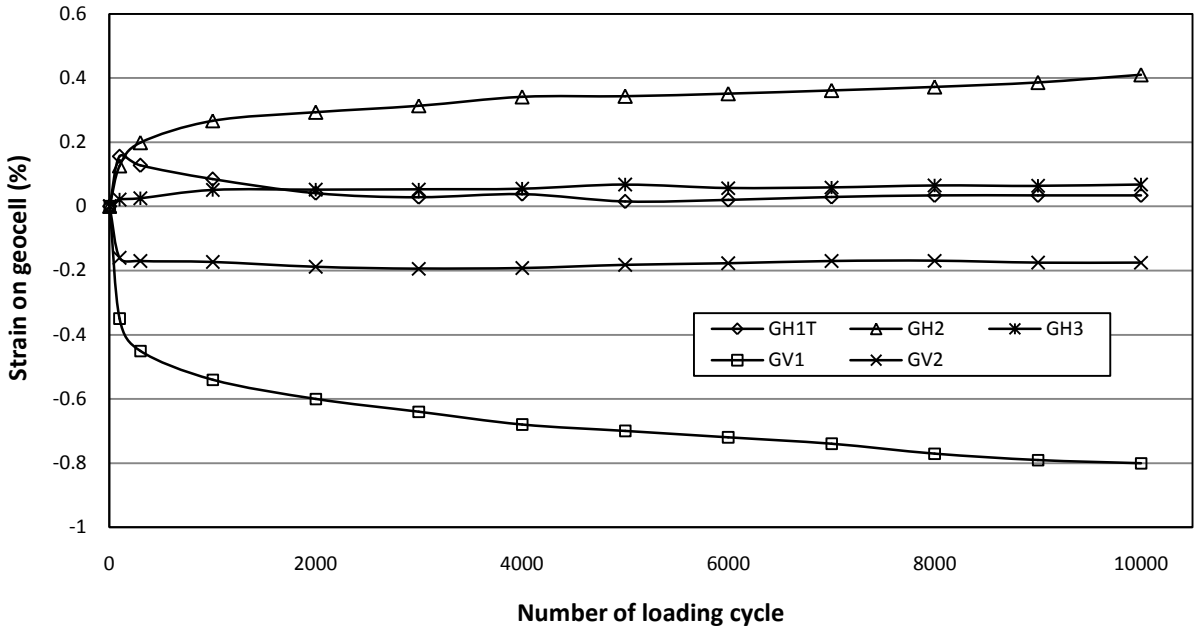

Figure 4.58 The measured strains on the geocell wall in different locations for the 30 cm thick geocell-reinforced RAP base section (top geocell)

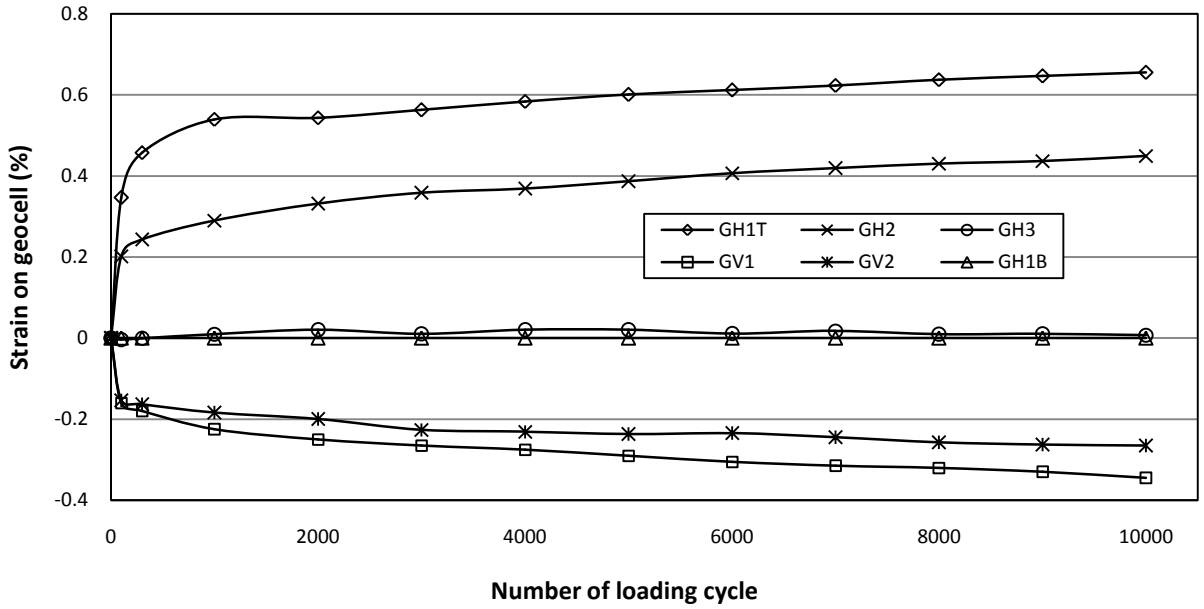

Figure 4.59 The measured strains on the geocell wall in different locations for the 30 cm thick geocell-reinforced RAP base section (bottom geocell)

The strains at the bottom of the HMA surface were measured by the pavement strain gauges at distances 0, 12.5, 25, 50, and 75 cm away from center as shown in Fig. 4.60. In this research, the strain is positive under tension and negative at compression. The bottom of the HMA surface at 0, 12.5, 25, and 75 cm from the center were under compression. The bottom of the HMA surface at 50 cm from center was under tension up to 1800 cycle and changed to compression up to the end of the test.

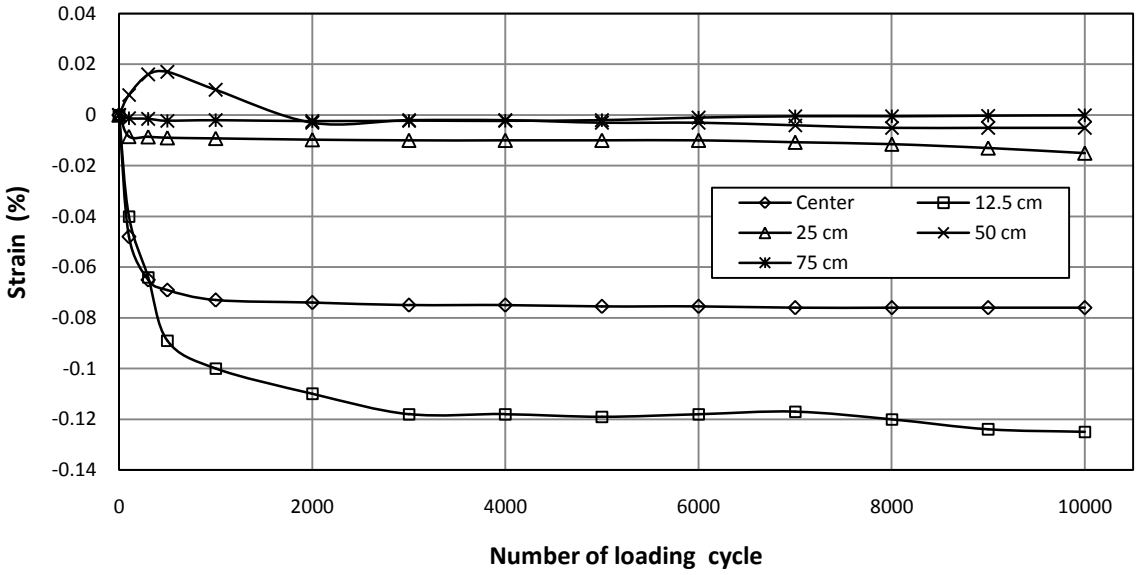

Figure 4.60 The strain at the bottom of the HMA surface versus the number of loading cycle for the 30 cm thick geocell-reinforced RAP base section

Figure 4.61 shows the measured vertical stresses at the interface between subgrade and base at five locations (center, 12.5, 25, 50, and 75 cm away from the center) versus the number of loading cycles. It is shown that vertical stress at center or close to the center were much higher than those away from center. The vertical stress at the distance of 75 cm away from the center was negative indicated heave at that location. As discussed earlier, the vertical stress at the center was used to calculate the stress distribution angle. The stress distribution angle versus the number of loading cycle is shown in Fig. 4.62. The stress distribution angle decreased with an increase of the load cycle in small rate up to the end of the test.

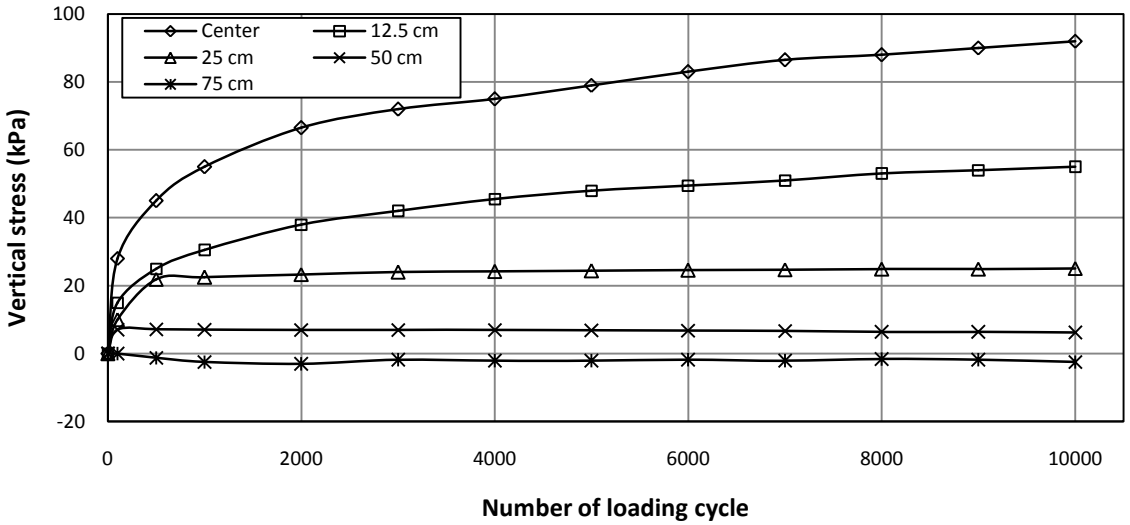

Figure 4.61 The vertical stress at the interface between subgrade and base versus the number of loading cycle for the 30 cm thick geocell-reinforced RAP base section

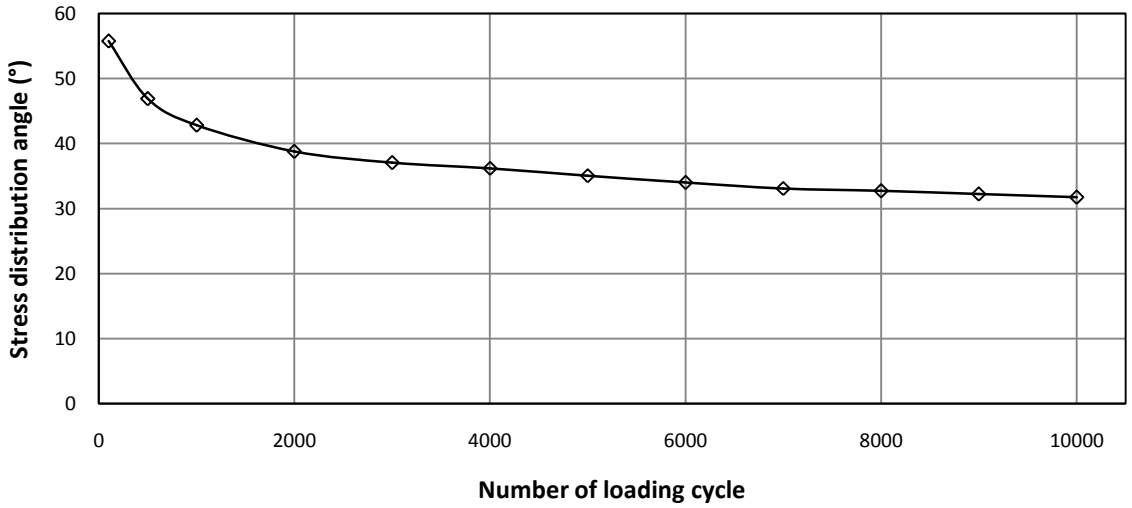

Figure 4.62 The stress distribution angle versus number of loading cycle for 30 cm thick geocell-reinforced RAP base section

4.4 Analysis of Test Data

Six cyclic plate load tests were conducted following the same construction (except the test section with the harder subgrade) and testing procedures on unreinforced and geocell-reinforced pavements with RAP bases in the large geotechnical testing box. The test data for all the experiments are analyzed together in this section in terms of subgrade and base CBR values, dynamic deformation moduli, percent of air voids of the HMA surface, permanent deformations, elastic deformations, strains at the bottom of the HMA, and strains on the geocells, vertical stresses at the interface between subgrade and RAP base, and stress distribution angles.

4.4.1 CBR values of subgrade and base course

Figure 4.63 presents the average CBR profiles of all six test sections from the DCP tests in the subgrade and the bases. It is shown that all the test sections had consistent average CBR profiles except the 15 cm thick geocell-reinforced RAP base section with the hard subgrade as discussed earlier.

The test results in Table 4.7 indicate that the average CBR values of the subgrade obtained from the DCP tests were higher than those obtained from the vane shear tests. The reasons for the higher CBR results from the DCP tests were additional compaction of the subgrade during the preparation of RAP bases and the DCP tests performed at 24 hours after the preparation of the base layer.

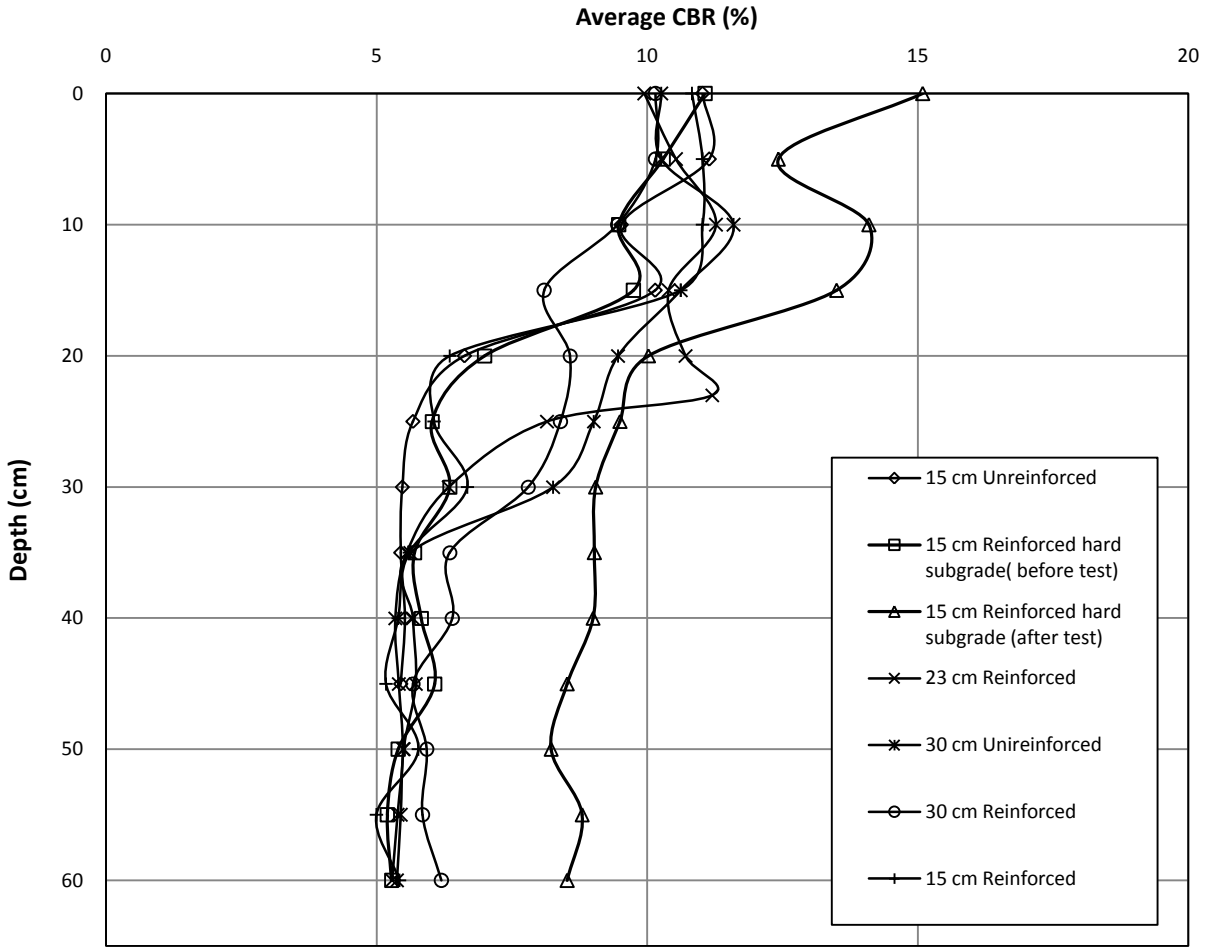

Figure 4.63 The average CBR profiles obtained from the DCP tests

Table 4.7 Average CBR value of test sections from vane shear test and DCP test

Base Thickness (cm)	Reinforcement		CBR (%)		Remarks
		Vane shear	DCP		
		Subgrade	Subgrade	Base	-
15	Unreinforced	4.9	5.7	10.5	-
15	Reinforced (hard subgrade)	5.5	5.9	10.2	Before test
		-	9.0	13.8	After test
15	Reinforced	5.1	5.7	10.9	-
23	Reinforced	5.1	5.9	10.7	-
30	Unreinforced	5.1	5.6	9.9	-
30	Reinforced	5.3	6.1	8.9	-

4.4.2 Dynamic deformation moduli of subgrade, base, and HMA surface

The LWD tests were conducted on the subgrade, the base, and the HMA surface in all the test sections using three loading plates of 15, 20, and 30 cm in diameter at six locations in each test section. The dynamic deformation moduli (E_{vd}) obtained from the LWD tests are presented in Table 4.8.

Table 4.8 Dynamic deformation moduli of the test sections

Base Thickness (cm)	Reinforcement	Dynamic Deformation Modulus (MN/m^2)								
		Subgrade			Combined base and subgrade layers			Combined HMA, base and subgrade layers		
		15 cm	20 cm	30 cm	15 cm	20 cm	30 cm	15 cm	20 cm	30 cm
15	Unreinforced	4.7	4.9	6.8	10.6	15.7	17.2	56.0	66.3	51.5
15	Reinforced (hard subgrade)	11.0	12.2	17.1	21.5	28.8	35.2	96.4	201.9	104.1
15	Reinforced	14.1	20.0	29.1	16.4	19.9	26.1	81.1	98.1	82.7
23	Reinforced	7.0	7.4	11.3	15.0	19.9	28.9	81.7	92.7	75.3
30	Unreinforced	8.2	7.7	9.3	18.1	22.4	30.6	86.0	117.7	109.6
30	Reinforced	9.2	10.5	16.9	31.9	38.8	48.3	98.6	98.1	95.2

The E_{vd} values of the subgrade and the base increased with an increase of the size of the loading plate for most of the tests. However, the E_{vd} values of the HMA surface were the highest in most of the test sections when the 20 cm loading plate was used. The E_{vd} values decreased from the HMA surface, the RAP base to the subgrade in all the test sections.

4.4.3 Percent of air void in the HMA surface

Percent of air void (V_a) is an important physical property of compacted dense and open HMA which is used to correlate with its performance. This parameter affects the overall stability and durability of the pavement. Lower percent of air void in the mixture can cause excessive

rutting of the pavement due to plastic flow. However, higher percent of air void provides more permeable surface to the air and water, which can result in a higher rate of oxidation of asphalt binder and ultimately premature cracking or raveling of the HMA surface. The bulk specific gravity (G_{BS}) and the theoretical maximum specific gravity (G_{MS}) of the HMA samples obtained by the core cutter were determined in the laboratory and are provided in Table 4.9. The percents of air void of the samples were then calculated using Eq. (3.3) and are presented in Table 4.9.

Table 4.9 Percent of air void of the HMA samples

Base Thickness (cm)	15	15	15	23	30	30
Reinforcement	Unreinforced	Reinforced (hard subgrade)	Reinforced	Reinforced	Unreinforced	Reinforced
Bulk Specific Gravity	2.09	2.18	2.08	2.14	2.15	2.16
Maximum Theoretical Specific Gravity	2.26	2.33	2.23	2.31	2.31	2.30
Percent of Air Void (%)	7.64	6.59	6.81	7.01	7.18	6.08

The percents of air void of the HMA samples ranged from 6.08 to 7.64 %, which show relatively consistent density of the HMA surfaces in all the test sections. It is shown that the test section with hard subgrade and base had the lower percent of air void. The reinforced test sections had lower percent of air void than the unreinforced test sections. These results indicate that hard subgrade and/or base courses (including geocell-reinforced bases) helped the compaction and resulted in denser HMA surfaces.

4.4.4 Permanent deformation on the HMA surface

Figure 4.64 shows the permanent deformations on the HMA surface at the center versus the number of loading cycles for all six test sections. It is shown that the permanent deformation increased at a higher rate at the beginning and then increased at a reduced rate after a certain number of loading cycles. The unreinforced base sections had higher rates of the increase in the permanent deformations than the geocell-reinforced sections. The thinner base sections had higher rates of the increase in the permanent deformations than the thicker base sections. In addition, the test section with hard subgrade and base course had a lower rate of the increase in the permanent deformations. Figure 4.64 also shows that the 15 cm thick geocell-reinforced base section had an equivalent or even better performance than the 30 cm thick unreinforced base section.

The surface permanent deformation of 25 mm is often used as a criterion for a tolerable deformation of a pavement. The number of loading cycles at the 25 mm permanent deformation in each test is presented in Table 4.10. It is shown that the 15 cm thick reinforced base section with hard subgrade and base and the 30 cm thick geocell-reinforced base section had the largest number of load cycles. The 15 cm thick unreinforced base section has the smallest number of load cycles. The improvement of the pavement performance can be defined as the traffic benefit ratio (TRB) at the same pavement thickness reaching the same surface permanent deformation of 25 mm at the center. Table 4.10 shows that the geocell-reinforced base sections have the TBR values of 10 and 12.5 for 15 and 30 cm thick RAP base section. This result demonstrates the benefit of geocell confinement of RAP bases.

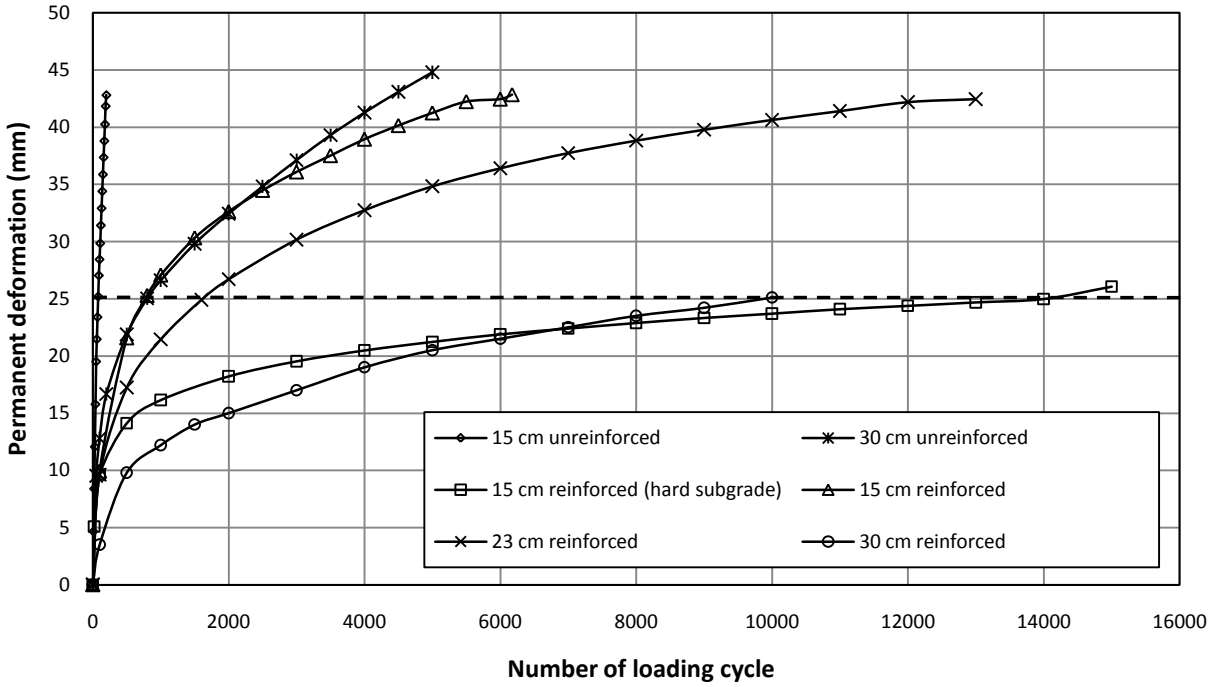

Figure 4.64 The surface permanent deformation at the center versus the number of loading cycle

Table 4.10 Number of loading cycles at 25 mm surface permanent deformation at the center

Base thickness (cm)	Number of loading cycle		Traffic Benefit Ratio (TBR)
	Unreinforced	Reinforced	
15	80	750	10
15 (hard subgrade)	-	14000	-
23	-	1600	-
30	800	10000	12.5

Figure 4.65 presents the distributions of surface permanent deformations at difference distances to the center when the permanent deformation at the center was 25 mm. It is shown that all test sections had similar distributions, i.e., the permanent deformation decreased with an increase of the distance.

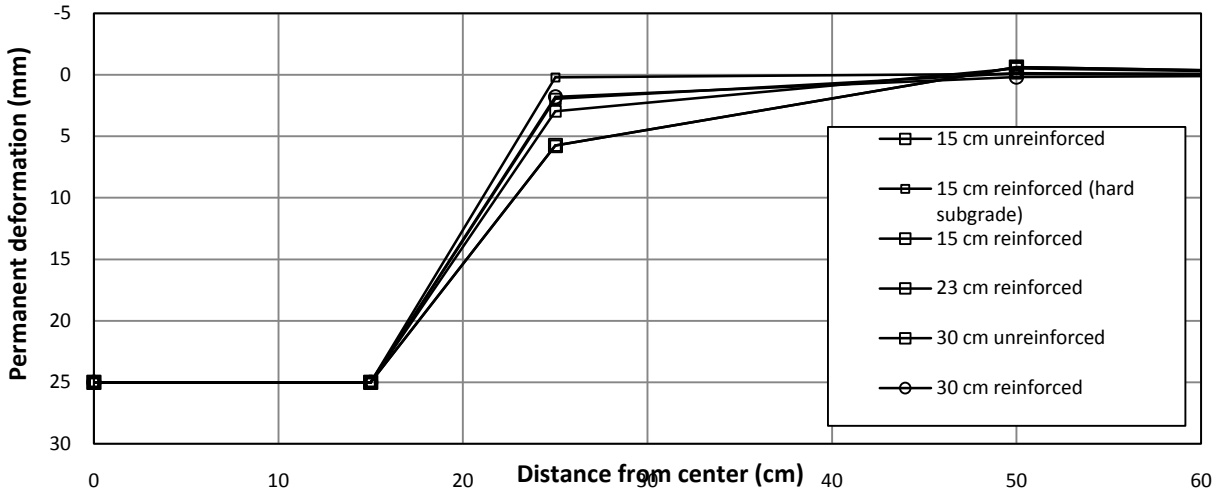

Figure 4.65 Distributions of surface permanent deformations at the 25 mm deformation at the center

4.4.5 Elastic deformation at the surface of HMA layer

Elastic deformation is the surface rebound of the pavement when the applied load was unloaded from 40 kN to 0.5 kN. The percent of elastic deformation is defined as the percent of the elastic deformation to the total deformation in each load cycle. Figure 4.66 shows the percent of elastic deformation varied with the number of load cycles. The general trend is that the percent of elastic deformation increased with the number of load cycles.

The elastic deformation and percent of elastic deformation at the 25 mm permanent deformation at the center are presented in Table 4.11. It is shown that the percent of elastic deformation ranged from 55 to 92%.

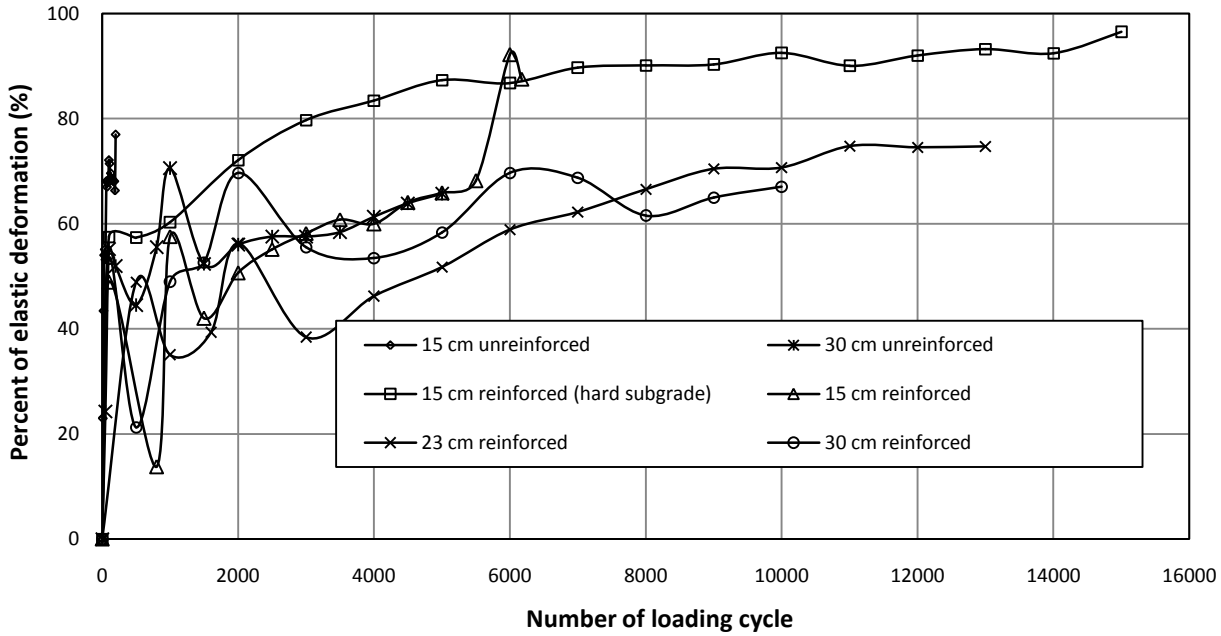

Figure 4.66 The percentage of elastic deformation versus the number of loading cycle

Table 4.11 Elastic deformation and percentage of elastic deformation at 25 mm permanent deformation at the center

Test	15 cm	15 cm (hard subgrade)	15 cm	23 cm	30 cm	30 cm
Reinforcement	Unreinforced	Reinforced	Reinforced	Reinforced	Unreinforced	Reinforced
Elastic deformation (mm)	3.87	1.96	2.40	2.24	2.93	0.80
Percentage of elastic deformation (%)	68	92	67	82	55	57

4.4.6 Permanent deformations of pavement layers

Tell tales were used to measure the deformations on the top of the subgrade and the base course for all the test sections except the 15 cm thick geocell-reinforced base section (hard subgrade) and the 30 cm thick geocell-reinforced base section. The compression of the HMA surface was determined by subtracting the measured deformation on the top of the RAP base

from the measured deformation on the HMA surface at the center of the loading plate. Similarly, the compression of the RAP base was determined by subtracting the deformation on the top of the subgrade from the deformation on the top of the RAP base at the center under the loading plate. The vertical compressions of the HMA surface, the RAP base (unreinforced or geocell-reinforced), and subgrade with the number of loading cycles are shown in Figures 4.67, 4.68, and 4.69 respectively. The vertical compressions of these layers at the 25 mm permanent deformation at the center are shown in Table 4.12.

Figure 4.67 shows that the compressions of the HMA surfaces in the two unreinforced RAP base sections were much higher than those in the reinforced base sections. Two explanations for this result are: (1) the density of the HMA surfaces in the unreinforced base sections was lower than that in the reinforced base sections and (2) the HMA surfaces in the unreinforced base sections carried more concentrated stresses than those in the reinforced base sections because the base courses in the unreinforced base sections were weaker and softer than those in the reinforced base sections.

Figure 4.68 also shows that the compressions in the unreinforced bases were higher than those in the geocell-reinforced bases. The lower compressions in the reinforced bases can be easily explained that the geocell-reinforced bases had higher stiffness than that in the unreinforced bases.

Lastly, Table 4.12 shows that the compression of the subgrade in the reinforced base sections at the same surface permanent deformation of 25 mm at the center was much higher than that in the unreinforced base sections. Due to the larger stress distribution angles in the

reinforced base sections, the influence depths in the reinforced base sections were larger than those in the unreinforced base sections. Therefore, the contribution of the subgrade compression to the total surface permanent deformation became more significant in the reinforced base sections. However, Figure 4.69 shows that at the same number of load cycles, the magnitude of the subgrade compression decreased from the 15 cm thick unreinforced base section, the 15 cm thick reinforced base section, the 23 cm thick reinforced base section, and the 30 cm thick unreinforced base section. The fastest increase of the subgrade compression in the 15 cm unreinforced base section was because the test section was fast approaching to the failure. The slowest increase of the subgrade compression in the 30 cm thick unreinforced base section was because of the largest thickness of this section.

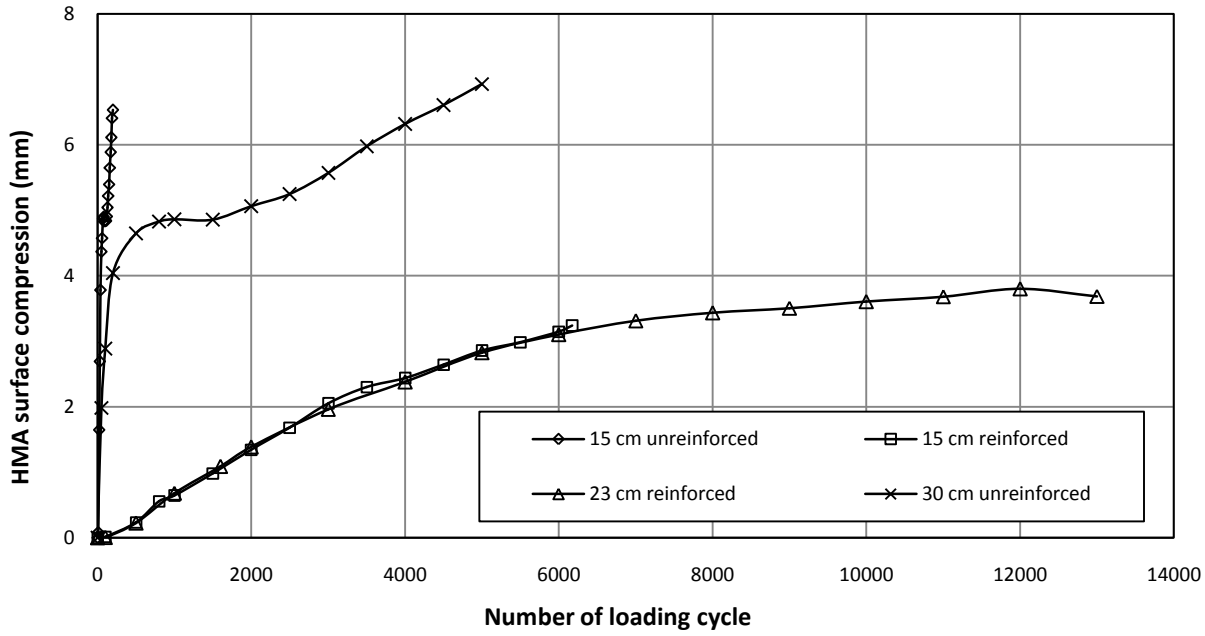

Figure 4.67 Vertical compression of the HMA surface versus the number of loading cycle

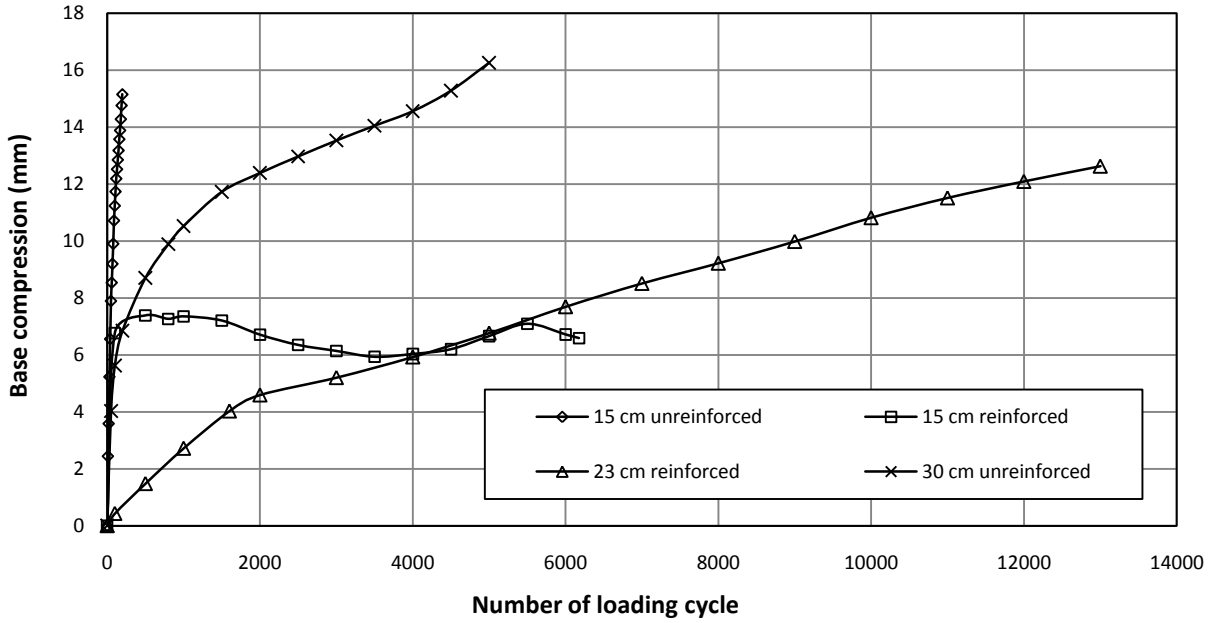

Figure 4.68 Vertical compression of the RAP base versus the number of loading cycle

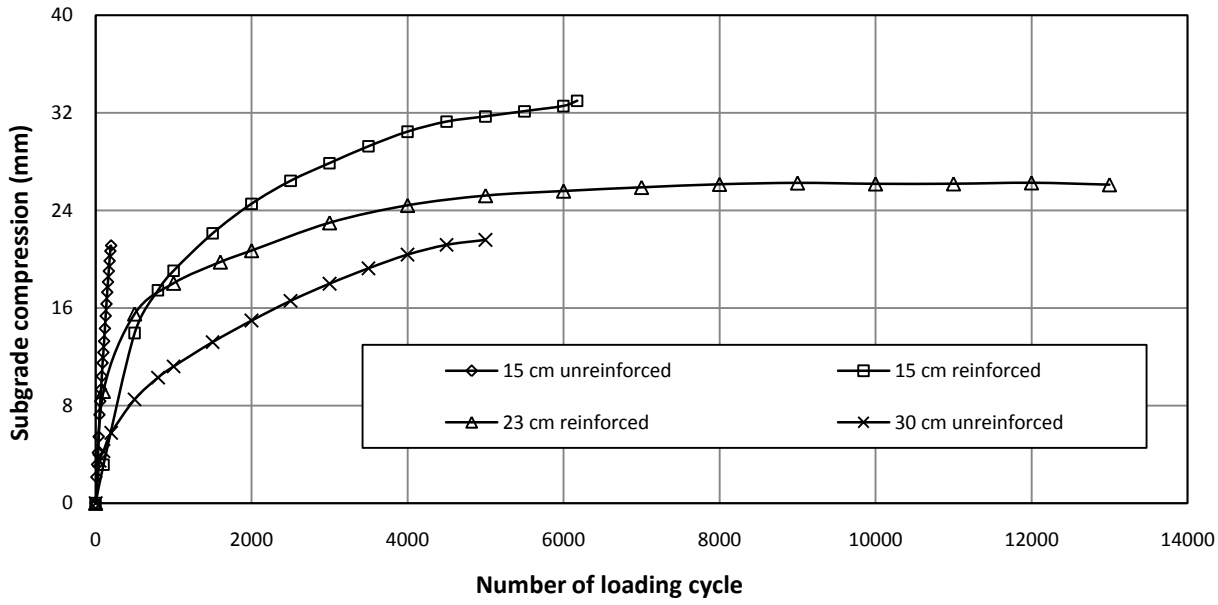

Figure 4.69 Vertical compression of subgrade layer versus number of loading cycle

Table 4.12 Vertical compressions of the HMA surface, base, and subgrade at 25 mm permanent deformation at the center

Test	15 cm	15 cm	23 cm	30 cm
Reinforcement	Unreinforced	Reinforced	Reinforced	Reinforced
HMA compression(mm)	4.80	0.52	1.12	4.82
Base compression (mm)	9.80	7.30	4.06	9.88
Subgrade compression (mm)	10.40	17.18	19.82	10.30

4.4.7 Maximum Strain on the geocell

Tensile strain, compressive strain, and tensile strain were developed at the top gages, middle gages and bottom gages of the geocell wall respectively for almost all of the experiments. However, there was compressive strain at the top gauge of central geocell for 23 cm thick geocell-reinforced RAP base section and at the bottom gage of central geocell at lower layer for 30 cm thick geocell-reinforced RAP base section. The magnitude of strain was higher for geocell at center and lower for geocell at distances 25 cm and 50 cm away from center respectively. Table 4.13 shows the maximum tensile and compressive strain developed on geocell.

Table 4.13 Maximum strain on geocell wall

Base thickness (cm)	Geocell height (cm)	Strain (%)	
		Tension	Compression
15	10	0.49	0.63
15 (hard subgrade)	10	0.25	0.44
23	15	1.88	0.86
30 (top geocell)	10	0.41	0.80
31 (bottom geocell)	10	0.66	0.35

4.4.8 Maximum strain at the bottom of the HMA surface

Figure 4.70 shows the strains at the bottom of the HMA surfaces at the center under the loading plate increased with the number of loading cycle. Tensile strains developed at the bottom of the HMA surfaces in the 15 cm thick unreinforced base section, the 15 cm thick geocell-reinforced base sections (normal and hard subgrade), and the 23 cm thick geocell-reinforced base section. However, there was also no strain developed at the bottom of the HMA surface at the center under the loading plate in the 30 cm thick unreinforced base section.

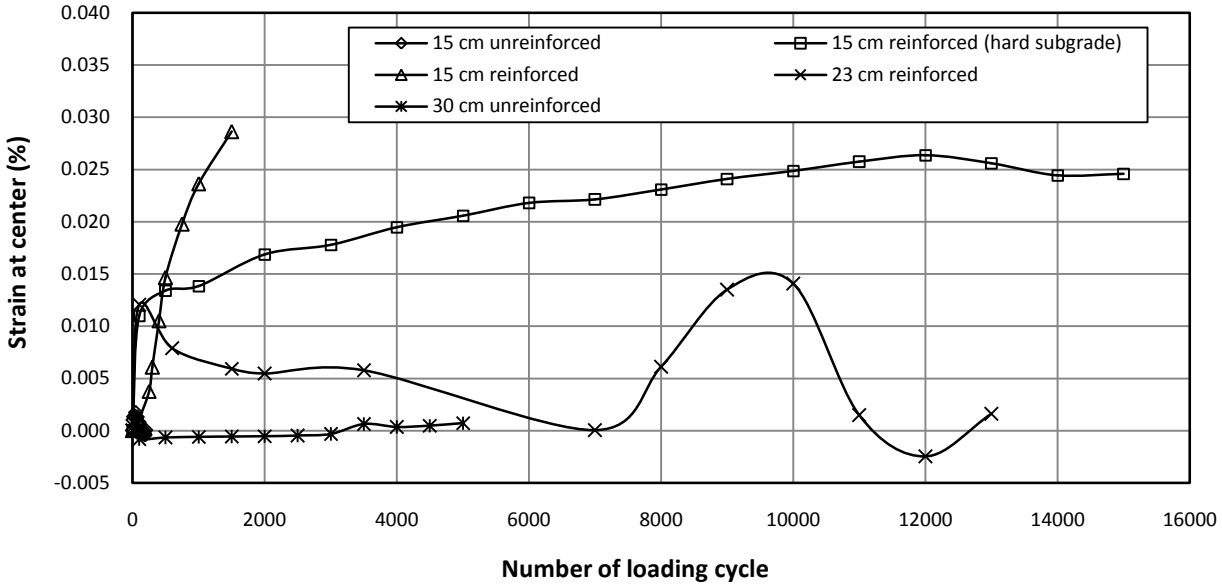

Figure 4.70 Strain at the bottom of the HMA surface versus the number of loading cycle

4.4.9 Vertical stress at the interface between subgrade and base

The vertical stresses at the interface between subgrade and RAP base at the center under the loading plate versus the number of loading cycle are shown in Figure 4.71.

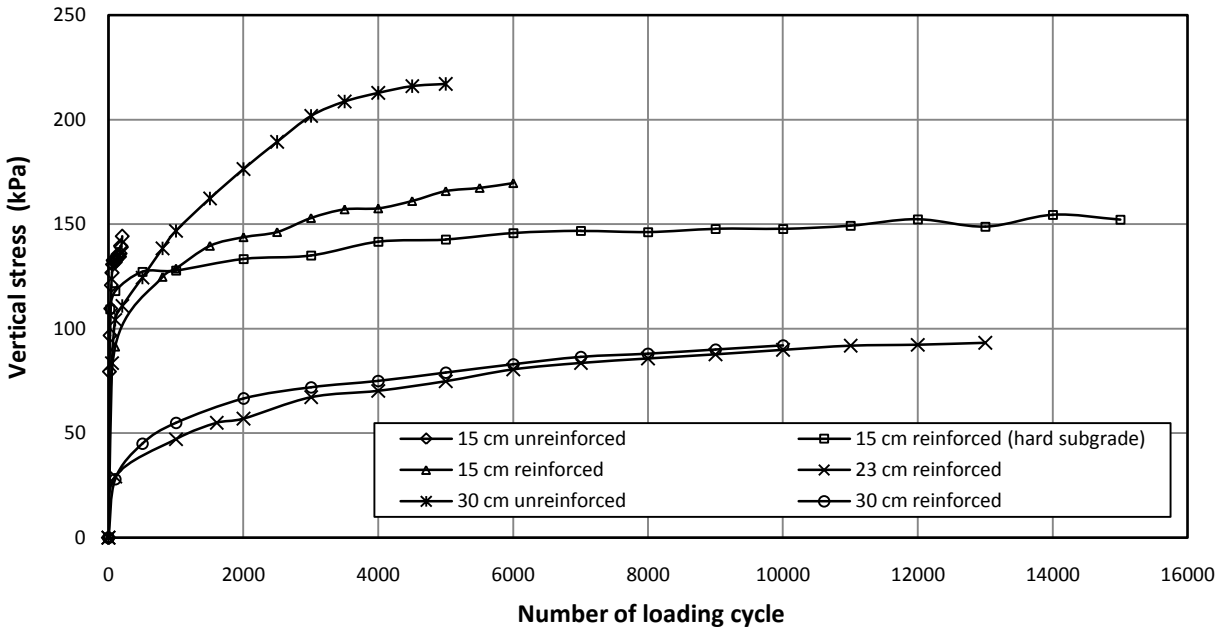

Figure 4.71 Vertical stress at the interface between subgrade and RAP base versus the number of loading cycle at the center

The vertical stresses at the interface between subgrade and RAP base increased with the number of load cycles, firstly at a faster rate and then at a slower rate. The vertical stresses in both unreinforced base sections increased faster than those in all the reinforced base sections. The vertical stresses in the 23 and 30 cm thick geocell-reinforced base sections were close, but much lower than the 15 cm thick geocell-reinforced base sections (normal and hard subgrade). The comparison of the vertical stresses in the 30 cm thick unreinforced and geocell-reinforced base sections shows that the reinforced section had the vertical stress less than half what the unreinforced section had. This comparison demonstrates the benefit of the geocell confinement.

The distributions of the vertical stresses at the interface between subgrade and RAP base in all the test sections are shown in Fig. 4.72. The maximum vertical stresses developed at the center and the magnitude of the vertical stresses decreased with an increase of the distance.

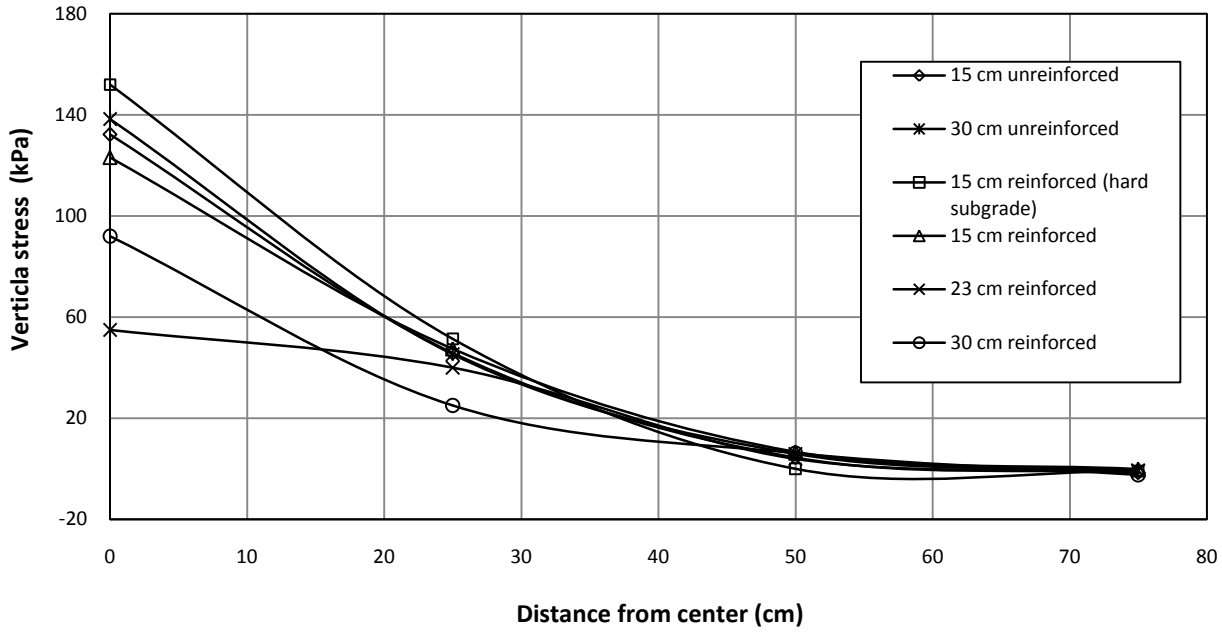

Figure 4.72 Distribution of the vertical stresses at the interface between subgrade and RAP base versus the number of loading cycle at 25 mm surface permanent deformation at the center

4.4.10 Stress distribution angle

Figure 4.73 shows the stress distribution angles decreased with an increase of the number of load cycles. The geocell-reinforced base sections had the higher stress distribution angles than the unreinforced base sections. This result demonstrates the benefit of geocell confinement on increasing the stiffness of the base courses so that the stress distribution angles were enlarged.

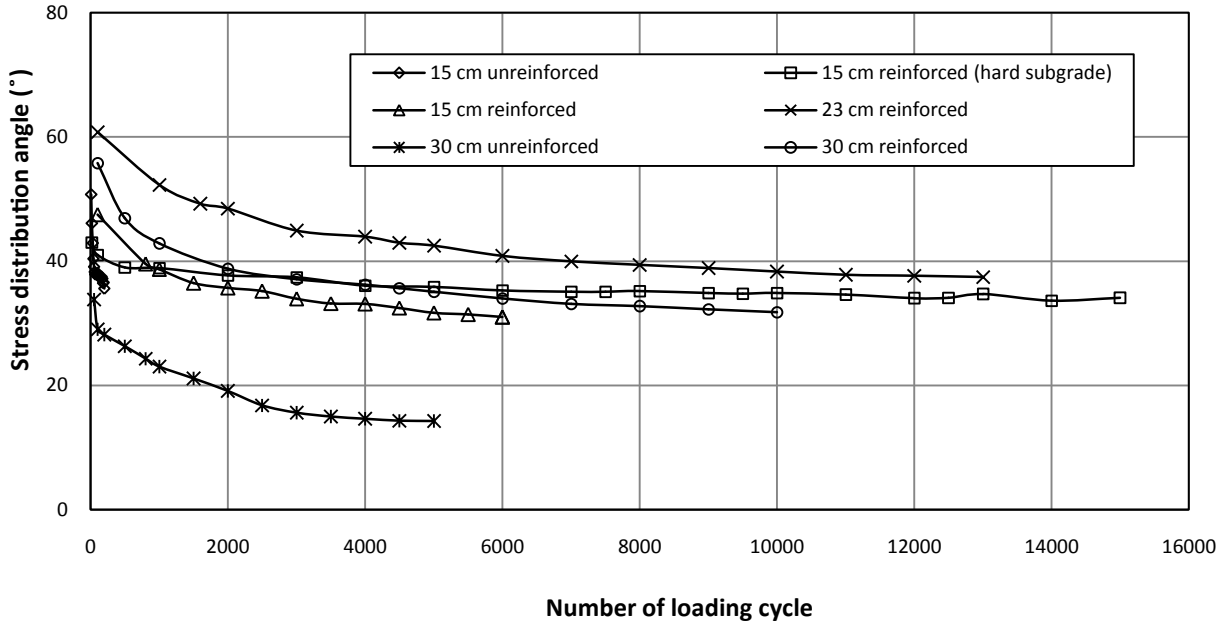

Figure 4.73 Stress distribution angle versus the number of loading cycle

4.5 Summary of Results

The geocell confinement, the increase of base thickness, and the increase of subgrade CBR significantly improved the performance of the pavement. The geocell-reinforced RAP bases behaved like semi-rigid mattresses, which resulted in the distribution of the vertical stresses to wider areas. The geocell-reinforced RAP bases had higher percent of elastic deformation, lower compression of HMA and RAP base, and more compression contributed by subgrade as compared with unreinforced RAP base sections.

CHAPTER FIVE

CONCLUSIONS AND RECOMMENDATIONS

The experimental work was carried out on unreinforced and geocell-reinforced flexible pavements with recycled asphalt pavement (RAP) bases under cyclic loading in the large geotechnical testing box at the University of Kansas. Six experiments were carried out by varying the thickness of the base course without or with geocell confinement.

5.1 Conclusions

Based on the test results, the following conclusions can be drawn:

1. Vane shear test, dynamic cone penetration test, and light weight deflectometer test were effective methods for quality control for subgrade, base course, and hot mix asphalt (HMA) surface during the preparation of test sections.
2. The novel polymeric alloy (NPA) geocell reinforcement significantly reduced the permanent deformation of the flexible pavement and increased the pavement life of the same thickness by 10 times.
3. The thinner geocell-reinforced base section had equivalent performance to the thicker unreinforced base section. In this study, the 15 cm thick geocell-reinforced RAP base was equivalent to the 30 cm thick unreinforced RAP base.
4. The geocell confinement increased the stiffness of the base course and reduced the compression of the base course.
5. The geocell-reinforced RAP bases provided a solid foundation for better compaction of the HMA surface and resulted in lower percent of air void in the HMA surface.

6. The subgrade contributed to most of the total permanent deformation, followed by the RAP base and the HMA surface.
7. The geocell-reinforced base acted as a semi-rigid mattress foundation, which distributed the applied load to a wider area on the subgrade with higher stress distribution angle and resulted in lower compression of subgrade, RAP base and HMA surface layers compared with unreinforced base sections.

5.2 Recommendations

This experimental study of the geocell-reinforced flexible pavement with RAP base is the beginning of the research on the geocell technology for flexible pavement applications. The experimental results from this study can be used as a basis for numerical modeling and development of a design method in the future.

The following work should be carried out to further advance the geocell technology for flexible pavement applications:

1. Investigate the effects of subgrade CBR and HMA thickness on the pavement performance;
2. Develop a method to quantify the benefit of geocell confinement;
3. Verify the cyclic plate load test results with moving wheel load tests; and
4. Develop the design method for geocell-reinforced flexible pavements with RAP bases.

REFERENCES

American Society for Testing and Materials (ASTM D2573 – 08). "Standard Test Methods for Field Vane Shear Test in Cohesive Soil".

American Society for Testing and Materials (ASTM D3203). "Standard Test Method for Percent Air Voids in Compacted Dense and Open Bituminous Paving Mixture".

American Society for Testing and Materials (ASTM D4439). "Standard Terminology for Geosynthetics".

American Society for Testing and Materials (ASTM D6951 – 09). "Standard Test Methods for Use of the Dynamic Cone penetrometer in Shallow Pavement Applications".

Alam, T. B., Abdelrahman, M., and Scharm, S. A. (2009). "Laboratory characteristics of Recycled Asphalt Pavement as a base layer." *International Journal of Pavement Engineering, Vol. 11, No. 2, 123-131.*

Al-Quadi, I.L., Carpenter, S., Roberts, G., Ozer, H., and Aurangzeb, Q. (2009). "Determination of usable residual asphalt binder in RAP (ICT-R27-11)." *Transportation Research Record ICT-09-031.*

Attia, M., and Abdelrahman, M. (2010). "Modeling the effect of moisture on resilient modulus of untreated Reclaimed Asphalt Pavement." *Journal of the Transportation Research Board, No. 2167, Transportation Research Board of the National Academics, Washington, D. C., pp. 30-40.*

Audery, C. (2011). "Reclaimed Asphalt Pavement in Asphalt Mixtures: State of Practice." *U.S. Department of Transportation, Federal Highway Administration, Research, Development, and Technology, Turner-Fairbank Highway Research Center, Publication No. FHWA-HRT-11-021.*

Becham, W.K. and Mills, W.H. (1935). “Cotton-fabric reinforced roads.” *Engineering NewsRecord,* Oct. 3, 453-455.

Bennert, T. and Maher, A. (2005). "The development of a performance specification for granular base and subbase materials.” *Dept. of Civil & Environmental Engineering, Center for Advanced Infrastructure & Transportation (CAIT), Rutgers, The State University, Piscatawav, NJ 08854-8014.*

Berthelot, C., Haichert, R., Podborochynski, D., Wandzura, C., Taylor, B., and Guenther, D. (2010). "Mechanistic laboratory evaluation and field construction of recycled concrete materials for use in road substructures." *Journal of the Transportation Research Board, No. 2167, Transportation Research Board of the National Academics, Washington, D. C., pp. 41-52.*

Collin, J.G., Kinney, T.C. and Fu, X. (1996). "Full scale highway load test of flexible pavement systems with geogrid reinforced base course." *Geosynthetics International, Vol. 3, NO. 4, pp. 537-549.*

Dash, S. K., Sireesh, S., and Sitharam, T. G. (2003). "Model studies on circular footing supported on geocell reinforced sand underlain by soft clay." *Geotextiles and Geomembranes 21 (2003) 197-219.*

Emersleben, A. and Meyer, M. (2008). "The use of geocells in road construction over soft soil: vertical stress and falling weight deflectometer measurement.” *Institute of Geotechnical Engineering, Technology University of Clausthal, EuroGeo4 – Edinburgh, Paper number 132.*

Emersleben, A. and Meyer, M. (2010). "The influence of hoop stresses and earth resistance on the reinforcement mechanism of single and multiple geocells. *"Institute of Geotechnical*

Engineering and Mine Surveying, Clausthal University of Technology, Erzstrasse, 9th International Confrerence on Geosynthetics, Brazil, 2010.

Giroud, J.P. and Han, J. (2004). "Design method for geogrid-reinforced unpaved roads – Part I: theoretical development." ASCE *Journal of Geotechnical and Geoenvironmental Engineering*, 130(8), 776-786.

Giroud, J.P. and Han, J. (2004). "Design method for geogrid-reinforced unpaved roads – Part II: calibration and verification." ASCE *Journal of Geotechnical and Geoenvironmental Engineering*, 130(8), 787-797.

"Geosynthetic." (*eNotes. - Retrieved July 15, 2011)* *http://www.enotes.com/topic/Geosynthetic#Geocells*

Hass, R., Walls, J. and Carroll, R.G. (1988). "Geogrid Reinforcement of Granular Bases in Flexible Pavements." *Transportation Research record 1188, pp. 19-27.*

Han, J., Pokharel, S.K., Yang, X., Manandhar, C., Leshchinsky, D., Halahmi, I., and Parsons, R.L. (2011). "Performance of geocell-reinforced RAP bases over weak subgrade under full-scale moving wheel loads." *Journal of Materials in Civil Engineering*, ASCE, 23(11).

Keif, O. and Rajagopal, K. (2008). "Three dimensional cellular confinement system contribution to structural pavement reinforcement." *Geosynthetics India '08 Seminar, Hyderabad, India.*

Kim, W., Labuz, J.F., and Dai, S. (2005). "Resilient modulus of base course containing Recycled Asphalt Pavement." *Transportation Research Board of National Academics, Washington, D. C., 2007, pp 27-35, DOI: 10.3141/2005-04.*

Kerisel, J. (1985). “The History of Geotechnical Engineering up until 1700, Golden Jubilee Book on History of Geomechanics”. Procedings of the 11th International Conference on Soil Mechanics and Foundation Engineering, 1985, 11-12.

Koch, S., and Ksaibati, K. (2010). "Performance of Recycled Asphalt Pavement in gravel roads." *Department of Civil and Architectural Engineering, University of Wyomimg.*

Latha, G. M., Rajgopal, K., and Krishnaswamy, N. R. (2006). "Experimental and theoritical investigations on geocell-supported embankments." *International Journal of Geomechanics, ASCE, January/February 2006.*

Mohamed, A. and Magdy, A. (2010). “Modelling the effect of moisture on resilient modulus of untreated reclaimed asphalt pavement.” Journal of Transportation Research Board, No. 2167, Transportation Board of the National Academics, Washington, D.C., 2010, pp. 30-40

Mokwa, R. L., and Peebles, C. S. (2005). "Evaluation of the engineering characteristics of RAP/Aggrerage blends.” *The State of Montana Department of Transportation, FHWA/MT -05-008/8117-24.*

Pokharel, S. K. (2010). Experimental study on Geocell-Reinforced Bases under Static and Dynamic loadings. PhD dissertation, CEAE Department, the University of Kansas.

Pokharel, S. K., Han, J., Parsons, R. L., and Qian, Y., Leshchinsky, D., and Halahmi, I.(2009a). "Experimental study on bearing capaity of geocell-reinforced bases." *Eight International Conference on Bearing Capacity of Roads, Railways, and Airfields, University of Illinois at Urbana-Champaign, Champaign, Illinois, USA.*

Pokharel, S. K., Han, J., Leshchinsky, D., Parsons, R. L., and Halahmi, I. (2009b). "Experimental evaluation of influence factor for single geocell-reinforced sand." *U.S. Transportation Research Board (TRB) 88th Annual Meeting, Washington, D. C.*

R.D. HOLTZ (1990). "Design and construction of geosynthetically reinforced embankments on very soft soils." *Performance of reinforced soil structure: Proceedings of the International Reinforced Soil Conference Organized by the British Geotechnical Society, Glasgow.*

Reclaiming Roads – Vol. 73 . No. 5 – Public Roads (FHWA-HRT-10-001)

http://www.fhwa.dot.gov/publications/publicroads/10mar/06.cfm

"Reclaimed Asphalt pavement in Asphalt Mixtures: State of Practice", (FHWA-HRT-11-021) http://www.fhwa.dot.gov/publications/research/infrastructure/pavements/11021/index.cfm

Singh, V. K., Prasad, A., and Arrawal, R.K. (2007). " Effect of soil confinement on ultimate bearing capacity of square footing under eccentric-inclined load." *The Electronic Journal of Geotechnical Engineering, Vol. 12, Bund. E*

Sitharam, T. G., Srilakshmi, G., and Sireesh, S. (2006). "Numerical modeling of geocell reinforced sand beds using FLAC3D." *4th International Conference in FLAC3D, Spain.*

Chang, T., Chang. C., Chien, T., and Pai, S. (2009). "Bearing capacity and dynamic properties of sandy soil with confinement of geocells" . *Chinese Journal of Geotechnical Engineering, Vol. 31, No. 12*

Thakur, J. K. (2011). Experimental study on Geocell-Reinforced Recycled Asphalt Pavement (RAP) Bases under Static and Cyclic Loadings. Master's Thesis, CEAE Department, the University of Kansas.

"User Guidelines for Byproducts and Secondary Use Materials in Pavement Construction (2008): Reclaimed Asphalt Pavement." *U.S. Department of Transportation, Federal Highway Administration, Publication Number: FHWA-RD-97-148. (Retrieved July 20, 2011 from www.recycledmaterials.org/tools/uguidelines/index.asp).*

Webster, S.L. (1992). "Geogrid reinforced base courses for flexible pavements for light aircraft: Test section construction, Behavior under traffic, Laboratory tests, and Design criteria." *Technical Report GL-93-6, ASAE Waterways Experiment Station, Vicksburg, Mississippi, USA, 86 p.*

Yang, X.M. (2010). "Numerical Analysis of Geocell-reinforced Granular Soils under Static and Repeated Loads". Ph. D. Dissertation, the University of Kansas.

Yuu, J., Han, J., Rosen, A., Parsons, R.L., and Leshchinsky, D. (2008). "Technical review of geocell-reinforced base courses over weak subgrade." *The First Pan American Geosynthetics Conference and Exhibition, Cancun, Mexico.*